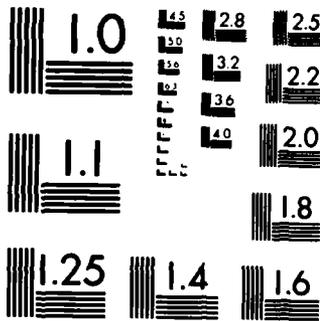END

FILMED

DTIC

MICROCOPY RESOLUTION TEST CHART
NATIONAL BUREAU OF STANDARDS-1963-A

AFOSR-TR. 85-0167

AD-A151 212

FINAL REPORT TO THE
AIR FORCE OFFICE OF SCIENTIFIC RESEARCH

on

WIND TUNNEL WALL INTERFERENCE

Grant AFOSR-82-0158
From 1 April 1982 to 31 March 1983

Submitted by

D. B. Bliss
Assistant Professor
Principal Investigator
and
P.-J. Lu
Graduate Research Assistant

Department of Mechanical and Aerospace Engineering
Princeton University
Princeton, New Jersey

April 1984

DTIC
ELEC
MAR 13 1985

DTIC FILE COPY

85 02 26 006

TABLE OF CONTENTS

PAGE

REPORT DOCUMENTATION PAGE	READ INSTRUCTIONS BEFORE COMPLETING FORM

1. REPORT NUMBER	2. GOVT ACCESSION NO.	3. RECIPIENT'S CATALOG NUMBER
AFOSR·TR· 85 - 0 167	AD-A151 212	

4. TITLE *(and Subtitle)*	5. TYPE OF REPORT & PERIOD COVERED
Wind Tunnel Wall Interference	Final 1 April 82 - 31 March 83
	6. PERFORMING ORG. REPORT NUMBER

7. AUTHOR(s)	8. CONTRACT OR GRANT NUMBER(s)
D. B. Bliss P.-J. Lu	AFOSR 82-0158

9. PERFORMING ORGANIZATION NAME AND ADDRESS	10. PROGRAM ELEMENT, PROJECT, TASK AREA & WORK UNIT NUMBERS
Princeton University Mechanical & Aerospace Engineering Department Princeton, NJ 08544	2307A1 61102F

11. CONTROLLING OFFICE NAME AND ADDRESS	12. REPORT DATE
Air Force Office of Scientific Research/NA Bldg. 410 Bolling Air Force Base, DC 20332	April 1984
	13. NUMBER OF PAGES

14. MONITORING AGENCY NAME & ADDRESS*(if different from Controlling Office)*	15. SECURITY CLASS. *(of this report)*
	UNCLASSIFIED
	15a. DECLASSIFICATION/DOWNGRADING SCHEDULE

16. DISTRIBUTION STATEMENT *(of this Report)*

Approved for public release;
distribution unlimited.

17. DISTRIBUTION STATEMENT *(of the abstract entered in Block 20, if different from Report)*

Approved for public release; distribution unlimited

18. SUPPLEMENTARY NOTES

19. KEY WORDS *(Continue on reverse side if necessary and identify by block number)*

Wind Tunnel Wall Interference
Slotted Walls
Porous Walls   Slot Aerodynamics
Ventilated Walls   Lifting Surface Theory

20. ABSTRACT *(Continue on reverse side if necessary and identify by block number)*

Research was conducted to understand the behavior of isolated holes and slots in wind tunnel walls. The aerodynamic characteristics of these individual wall elements can be used to help understand the behavior of walls with multiple perforations. Potential flow analysis similar to that employed in the kernal function approach to lifting surface theory was used to determine the pressure differential versus flowrate relationship for various hole planforms in high speed subsonic flow. The effect of an imposed pressure gradient was also

DD FORM 1473 EDITION OF 1 NOV 65 IS OBSOLETE

analyzed. Good agreement with slender-body theory results was obtained for low aspect ratio planforms. Although the finite hole problem resembles the lifting wing problem, there are significant differences: the pressure differential is known and the free surface shape is unknown; the Kutta condition is applied to the hole leading edge; and there are no wake effects in the hole out-flow problem. The analysis was extended to include the effect of an inviscid rotational power law boundary layer over the hole by using a 'shear flow aerodynamics' kernel function. The effect of the boundary layer was determined for transverse slots and holes with various planform shapes. The presence of a wall boundary layer tends to reduce the flow resistance coefficient, and, since the layer thickness may be comparable to the hole size, the effect is reasonably strong. The spatial behavior of the shear flow kernel function also suggests that the presence of a boundary layer will reduce mutual interference effects between adjacent holes.

A-1

(1.0)

Introduction

This report summarizes the achievements of a one year program conducted at Princeton University under AFOSR sponsorship. To a certain extent this report represents a continuation of a previous 5 year program that studied a number of topics related to wind tunnel wall interference. The present effort focused on the aerodynamics of an isolated hole in the wind tunnel wall. This problem is not only of interest in its own right but, as the previous research demonstrated, it is also the basic building block for the determination of the average boundary condition for a wall covered with holes. The basic approach is to determine the behavior of a hole using a lifting surface type computer code. This method was inspired by an analogy observed between a 2-D lifting wing and the free surface problem for a 2-D slot in a wall. As an significant refinement, the effect of a power law boundary layer has been included through the use of a "shear flow aerodynamics" kernel function. The primary problems analyzed in this report are therefore

- 2-D and 3-D potential flow over an isolated hole, including the effect of an imposed pressure gradient.

- 2-D and 3-D shear flow aerodynamics over an isolated hole.

Most of the remainder of this document provides a detail report on the results of this work. The next section provides a list of publications and participating personnel.

(2.0)

Publications and Professional Personnel

(2.1) Professional Personnel

The professional personnel associated with the research effort were Professor D.B. Bliss and Mr. P.-J. Lu, graduate assistant.

(2.1) Publications

The following publications are in preparation:

"Potential Flow over an Isolated Hole in a Wind Tunnel Wall," (to be submitted to the AIAA J.), P.-J. Lu and D.B. Bliss.

"Application of Shear Flow Aerodynamics to Ventilated Wind Tunnel Walls," (to be submitted to the AIAA J.), P.-J. Lu and D.B. Bliss.

"Aerodynamic Behavior of Ventilated Wind Tunnel Walls," Princeton Ph.D. Dissertation to be completed in 1984, P.-J. Lu.

(3.0)

Research Activities

The reseach during the past year focused on the local analysis of an isolated hole in a wind tunnel wall. Such holes are the elements which make up a perforated wall. The purpose of this local analysis is to develop theoretical models to examine the inner structure of the fluid flow around an isolated hole. In subsequent sections the cases of inviscid irrotational (potential) and rotational (shear) flows over isolated holes will be discussed. The pressure gradient effect in the potential flow case is also considered. For convenience sake, the terminology used to describe the flow over a 2D transverse slot and a 3D finite hole is leaking-slot and leaking-hole theory, respectively. These local analyses will justify the functional relationship between the pressure differential and average flow deflection angle across a hole, and give analytic values of the flow resistance constant K_h.

(3.1) Potential Analysis

To date, potential flow has been assumed in every analytical investigation of ventilated wind tunnel walls. For longitudinally slotted walls, experiments show that viscous effects are not that important. The fluid flow and interference effects are principally due to potential flow aerodynamic phenomena. However, for perforated walls, viscous/boundary layer effects are by no means negligible. On the

contrary, many experiments suggest they are very important. The present potential flow analysis, which necessarily excludes viscous/boundary layer effects, is undertaken in order to get a theoretical model which gives a clear understanding of the most fundamental aspect of perforated wall flow, namely, the momentum deflection of the oncoming stream across the hole. Potential flow results are basically valid for large holes, i.e., the cases when the hole diameter is much larger than the boundary layer thickness. This potential flow treatment is only a first step in the theoretical approach to understand the physics of perforated wall flows and is a necessary undertaking prior to the more complicated boundary layer analysis discussed later.

(3.1.1) Leaking-Slot Theory

Consider a transversely slotted wall, Fig.(3-1a), with negligible wall thickness separating two different streams, one in uniform motion and the other at rest. The static pressure differential across this slot is assumed so small that small perturbation techniques can be applied, i.e. the free surface deflection is small compared to the slot length. Fig.(3-1a) depicts this slot flow, as well as the coordinate system location. The half slot width and free stream velocity are used as the normalization quantities.

The equation of motion is,

$$(1 - M_\infty) \phi_{xx} + \phi_{zt} = 0$$

(3-1)

The boundary conditions are:

a) On the wall, fore and aft of the slot region, $w = \partial\phi/\partial z$ and over the slot region, $p = p_a$ holds.

b) ϕ and $\nabla\phi$ vanish in the far field.

c) At the leading edge of the slot, the Kutta condition is satisfied, i.e., $w=0$ at $x=-1$.

(3-2)

The boundary conditions as specified are valid only for the out-flow case. To date, no theoretical analysis has been developed to treat the in-flow problem. In the in-flow case, the flow is sucked into the high speed stream from the plenum chamber. This process involves many effects beyond the scope of simple potential flow analysis. For instance, a wake flow usually will be generated after the flow passes around the sharp trailing edge. Moreover, even without consideration of the viscous effects, the sucked-in flow would form a low speed zone downstream between the wall and the high speed main stream. The location of the dividing slip streamline between the high and low speed zones is not known in advance, therefore, the boundary condition (3-2a) is no longer applicable for eqn(3-1). A reasonable solution to this potential in-flow problem must consider two flows with different stagnation pressures having static pressures that must match on the slip streamline and satisfy individually the appropriate boundary conditions. This in-flow problem is not treated in the present work, and only on the out-

flow problem is considered from here on.

Maeder[1] discovered the analogy between the 2D lifting airfoil and
leaking-slot flow in the early fifties. In the almost thirty years
since the discovery of the 2D analogy, the 3D hole problem has not been
solved analytically. The approach to be presented here is different
from Maeder's, and it is particularly helpful because it can be readily
extended to the 3D case described later.

If we examine the governing equation and boundary conditions of the
2D lifting airfoil and leaking-slot flows, the analogy is immediately
apparent. The comparison is illustrated in Fig.(3-1b). Since both
$p(=-2\phi_x)$ and w $(=\phi_z)$ satisfy the Laplace-type eqn(3-1), switching the
roles of p and w and reversing the streamwise coordinate will transform
the lifting problem into the slot problem, or vice versa. The analogy
states,

$$p_L(x) = w_s(x) \tag{3-3}$$

where subscripts L and s denote lifting and slot respectively.

To prove eqn(3-3) more formally, let us start from the integral
equation form which is deduced from the differential equation (3-1)
subject to the boundary conditions (3-2), except for the Kutta
condition. The integral equation, which can be found in many
texts[2,3,4], states that,

$$\phi_x = \oint_{-1}^{+1} \frac{1}{\pi(x-\xi)} \frac{w(\xi)}{\beta} d\xi \quad (z=0, -1 \le x \le 1) \tag{3-4}$$

The integral sign indicates that the Cauchy principal-value is taken for integration across the singular point x= ξ.

Note that eqn(3-4) holds true for both the thickness flow of airfoil theory and the leaking-slot flow, since the flows are symmetric for these two cases. The differences between them lie in the mathematics and the interpretation of the downwash distribution. For the thickness and slot flows, $w(\xi)$ stands for the surface slope distribution of the airfoil or the free streamline deflection, respectively. The former is given for a fixed airfoil configuration and the latter is what we want to determine in the slot problem. Mathematically, t' ...ickness problem is a direct problem, which means that by directly in~~grating the principal-value integral the pressure distribution on the airfoil can be determined. However, the slot flow is an indirect problem, because ϕ_x is known while $w(\xi)$ must be obtained by solving the singular integral equation together with the Kutta condition satisfied at the leading edge.

Recall that the integral equation for the 2D lifting problem is,

$$\frac{w_L(x)}{\beta} = \oint_{-1}^{+1} \frac{-1}{\pi(x-\xi)} \, \phi_{L_x}(\xi) \, d\xi \tag{3-5}$$

The inversion formula of eqn(3-5) has a variety of forms; the one being used here is from Ref.(5).

$$\phi_{L_x}(x) = -\frac{1}{\pi} \sqrt{\frac{1+x}{1-x}} \oint_{-1}^{+1} \sqrt{\frac{1-\xi}{1+\xi}} \, \frac{w_L(\xi)/\beta}{\xi - x} d\xi + \frac{C''}{\sqrt{1-x^2}} \tag{3-6a}$$

or,

$$\phi_{L_x}(x) = -\frac{1}{\pi}\sqrt{\frac{1-x}{1+x}}\oint_{-1}^{+1}\sqrt{\frac{1+\xi}{1-\xi}}\,\frac{w_L(\xi)/\beta}{\xi-x}\,d\xi + \frac{c'''}{\sqrt{1-x^2}} \qquad (3\text{-}6b)$$

Equations (3-6a,b) are two conjugate solutions to the singular integral equation (3-5). Eqn(3-6b) was adopted in lifting problem by letting c'''=0 to satisfy the Kutta condition at the trailing edge, whereas eqn(3-6a) was discarded since no physically compatible flow was found to be associated with it in the airfoil problem.

This technique developed for lifting airfoil theory can also apply to the slot equation (3-4) since it possesses the same kernel function. However, in the case of slot flow, we adopt eqn(3-6a) instead, since now the Kutta condition is specified at the leading edge. Therefore, $w(\xi)/\beta$ in eqn(3-4) is given by

$$\frac{w(x)}{\beta} = \frac{1}{\pi}\sqrt{\frac{1+x}{1-x}}\oint_{-1}^{+1}\sqrt{\frac{1-\xi}{1+\xi}}\,\frac{\phi_x(\xi)}{\xi-x}\,d\xi \qquad (3\text{-}7)$$

For constant plenum chamber pressure, ϕ_x is constant over the slot area, namely,

$$\phi_x = -\frac{1}{2}\,\frac{P_b-P_\infty}{q} \equiv \frac{1}{2}\,\Delta P/q$$

where, $\Delta P \equiv (P_\infty - p_a)/q$ ($\Delta P > 0$ for out-flow)   (3-8)

Substituting the above pressure differential into eqn(3-7) yields,

$$\frac{w(x)}{\beta} = -\frac{1}{2}\,\frac{\Delta P}{q}\sqrt{\frac{1+x}{1-x}} \qquad (3\text{-}9)$$

in which the integral identity

ventilated wall behavior because there are fundamental differences in the nature of these fluid flows.

(3.1.3) Pressure Gradient Effect on Slot and Hole Flows

The pressure gradient along a tunnel wall can very often reflect the degree of interference between wall and model. For instance, if a very low blockage-ratio model, say less than one percent, is installed in a tunnel, the wall pressure gradient will be very small. However, for larger models, especially ones in transonic flow with a supersonic bubble intersecting the tunnel walls, very irregular pressure distributions are seen, and under this situation, it is known that severe wall and model interference occurs.

Suppose the hole in a tunnel wall is no longer considered as an idealized point, but has finite dimensions. A pressure gradient will be experienced as the hole is exposed in a non-uniform flow. It is desirable to see how this pressure gradient affects the fluid flow around the hole. As usual, we start our study from the 2D transverse slot.

The downwash-pressure disturbance relation was already derived in eqn(3-7) for a slot with constant imposed pressure,

$$\frac{w(x)}{\beta} = \frac{1}{\pi} \sqrt{\frac{1+x}{1-x}} \oint_{-1}^{+1} \sqrt{\frac{1-\xi}{1+\xi}} \; \frac{\phi_x(\xi)}{\xi - x} \, d\xi \qquad \text{(c.f. 3-7)}$$

interference effects are negligible. Surprisingly, the potential leaking-hole theory result fits very well with the experimental data for smaller holes. However, since information on the boundary layer was not provided, it can only be regarded as a coincidence.

Owing to the lack of reliable experimental data, justification of the validity of the leaking-hole theory can only be performed indirectly. Bliss[12] utilized slender-body theory to study longitudinal slots analytically. He found that for certain slot shape, called D.B.B.'s analytical shape, the exact solution can be found. This analytical shape is shown in Fig.(3-10). This particular shape was used for the hole planform, and the finite hole computer program was run for different aspect ratios to check whether these two theories agree at low aspect ratio. The result is plotted in Fig.(3-11), and the agreement is encouraging.

At this stage, the properties and general features of the finite hole in the tunnel wall can be summarized as follows.

1) The resistance coefficient K_h ($= 1/C_{Q_\rho}$) decreases as the aspect ratio of hole decreases.

2) The resistance coefficient K_h increases in proportion to $1/\beta$ ($\beta = \sqrt{1-M^2}$) as free stream Mach number increases in subsonic flow.

3) The hole flow is a thickness problem even though there are some similarities between the corresponding flow variables for holes and lifting surfaces. Experience gained in airfoil studies should not be directly transferred to predict or explain

sectional distribution. However, near the tip the low and high aspect ratio cases show different tendencies. Generally speaking, the sectional flowrate increases more sharply around the tip region as the aspect ratio decreases.

Experimental data on the isolated hole problem is hard to find. Most experiments are associated with perforated walls, most of which are thick wall cases done in the fifties and sixties[10]. The data found for the isolated slot and hole was carried out by Maeder[1] and indirectly reproduced in Fig.(3-9) from Goethert[11]. These data were obtained from a 4 inch height test section wind tunnel, with a slot having 1 inch width and a hole 2.26 inch in diameter. First consider the upper plot in Fig.(3-9). The difference between potential theory and the experimental results can be seen. Boundary layer effect cannot be blamed because the dimensions of the slot and hole are deliberately chosen to be large to eliminate the boundary layer effect. Moreover, the boundary layer effect tends to decrease the slope of pressure coefficient versus deflection angle. This trend has been justified by other more carefully designed experiments in which boundary layer thickness was reported. The slot width is much larger than the wall thickness, so the edge effect is not likely to be important either. A similar trend also occurs for the single hole case shown on the lower plot, on which is shown our theoretical result $K_h = 1/C_{Q_\rho} = 1.003$. The reason for this trend is probably the relative dimensions of the tunnel cross section to the slot or hole size. For a one inch slot and 2.26 inch hole installed in a 4x4 square inch tunnel it is hard to imagine that the side walls and ceiling

divided by the free stream velocity to make it dimensionless. Since our theory is linear, therefore, C_{Q_P} is the reciprocal of the resistance coefficient K_h, i.e., $C_{Q_P}=1/K_h$. Fig.(3-6) shows its behavior in connection with the aspect ratio. Its trend of asymptotically approaching the 2D slot limiting case agrees with physical intuition. The computer program ceases to be valid for aspect ratios less than 0.25. The reason is not clear, but failure could be attributed to the inappropriate simulation of the preselected mode functions to the actual downwash, because these modes basically are designed for larger aspect ratio cases. The program also cannot handle shapes with aspect ratios greater than 3.5. This situation is probably due to increasing the number of spanwise control points which introduces more higher order polynomials that are oscillatory in character. This causes the associated influence matrix to become less well conditioned to inversion. A similar limitation with respect to aspect ratio range was also encountered in the kernel function method for wings. Nevertheless, the round hole case falls in the range of validity of this leaking-hole theory.

The Mach number dependence of C_{Q_P} is shown in Fig.(3-7). Its trend of decreasing (increasing for K_h) in proportion to $\beta(1/\beta$ for K_h) has long been observed in many experimental investigations.

Presented in Fig.(3-8) is the sectional volume flowrate coefficient, which is similar to the sectional lift coefficient of the finite wings. Three cases are studied, the round hole case has a very squared

various parameters were all performed with 9 control points. These control points are positioned at x=-0.5 ,0, 0.5 in the chordwise direction, and y=0.2, 0.5, 0.8 in the spanwise direction. Actually, this kind of control point distribution was suggested as the optimal collocation arrangement by Watkins et al. in their development of the kernel function method for lifting-surface theory.

A series of numerical experiments were carried out to examine the elliptical hole family. A primary concern, the round hole, is a special case of the ellipse with equal major and minor axes. The downwash distribution is shown in Fig.(3-4) for a round hole in incompressible flow. Three stations are selected to be the representatives for flow near the root chord, mid-span, and tip regions of a round hole. The distributions show similar behaviors to each other, but, deviate substantially from the 2D transverse slot result. Fig.(3-5) shows the downwash distribution for different aspect ratio* holes. Roughly speaking, the basic shape of the downwash is magnified uniformly along the slot as the aspect ratio decreases. In other words, low aspect ratio holes are more effective in allowing fluid to pass through.

Fig.'s (3-6) to (3-9) examine the volume flowrate coefficient C_{Q_p} (C_Q at $\Delta p/q = 1$). The volume flowrate coefficient C_Q is defined as the volume of fluid flow passing across the hole per unit time per unit area, then

----

* The aspect ratio defined in the hole problem is the maximum span to chord ratio. Multiplying this result by π recovers the usual aspect ratio defined in the airfoil theory.

eqn's(3-20) and (3-21). This is the most difficult portion of the numerical simulation. To adapt the numerical scheme to the present hole problem, treatment of the singular integration must be modified. For the lifting-surface problem, a Mangler type singularity is encountered in the spanwise integration; however, for the hole problem, a Cauchy type singularity occurs in the chordwise integration. Experience gained from numerical lifting-surface theory indicates that proper handling of the singularity is crucial to the accuracy of the final results. Generally speaking, the quadrature scheme must be sufficiently accurate and must preserve the special character of the principal-value integration.

Guassian quadratures are adopted here for the numerical integration. In order to achieve high accuracy, the hole area was divided into six sub-regions, which are illustrated in Fig.(3-3). Each sub-region is confined within the nearest solid lines. Sub-region IV contains the control point(x,y) where singular behavior occurs, and considerable care must be taken (the Cauchy principal-value and the Hadamard finite part concept must be invoked). The location of the control point makes the aspect ratios of these sub-regions change vastly. In order to use the Guassian quadratures effectively, the order of the Guassian quadrature used must be adaptable to the variation of this aspect ratio change.

A computer program was thus developed to study the finite hole problem with 4,9,12 and 16 control points. The program results show that the 9 point case is already converged. Therefore, studies for

yields

$$\phi_x(x,y) = 2s \sum_n \sum_m a_{nm} \int_{-1}^{+1} G(\eta) \eta^m \sqrt{1-\eta^2} \, d\eta \qquad (3\text{-}20)$$

and,

$$G(\eta) = \oint_0^\pi \tilde{A}(x-\xi, y-\eta) \ell_n(\Theta) \sin\Theta \, d\Theta \qquad (3\text{-}21)$$

$$\tilde{A}(x-\xi, y-\eta) = \frac{1}{4\pi} \frac{x-\xi}{[(x-\xi)^2 + \beta^2 s^2 (y-\eta)^2]^{3/2}} \qquad (3\text{-}22)$$

in which, $s=\ell/b_0$, and all quantities are dimensionless.

The methods of solving for these unknown coefficients include: the collocation method which makes the pressure differential be satisfied exactly at a set of points; or the least-square method which approximately satisfies the pressure differential at a larger set of control points in the sense of least-square error. There is no concrete evidence to suggest that the more complicated and expensive least-square method is superior, therefore, we use the collocation method here.

If the hole shape is symmetric with respect to the mid-plane y=0, which is often the case, and the imposed pressure differential is also right-left symmetric, then the flow field will possess the same symmetry property. Under this circumstance, there is an advantage to distributing the control points only on half of the hole area and choosing only even power polynomial modes in eqn(3-17). This significantly reduces the computing effort.

The remaining problem is how to numerically evaluate the integrals in

The mode functions selected in the chordwise direction are in terms of the angular variable θ. These functions are

$$\tan \frac{\theta}{2}, \quad \sin\theta, \quad \sin 2\theta, \quad \cdots, \quad \sin n\theta, \cdots$$

The leading one, $\tan(\theta/2)$, takes care of the square-root singularity and vanishing behavior at the trailing and leading edges. The rest are regular over the region of interest and vanish at both ends.

The spanwise mode functions, however, are polynomials weighted by the factor $\sqrt{1-\eta^2}$ which accounts for the vanishing of downwash at the tip. These mode functions approach unity asymptotically at the symmetry plane $y=0$.

$$A_n(\eta) = \sqrt{1-\eta^2} \left(a_{no} + \eta a_{n1} + \cdots + \eta^m a_{nm} + \cdots \right)$$

$$= \sqrt{1-\eta^2} \sum_m \eta^m a_{nm} \tag{3-17}$$

Therefore, the unknown downwash distribution is expanded as,

$$\phi_z = \frac{b}{b_o} \sum_n \ell_n(\theta) A_n(\eta) \tag{3-18}$$

In the above, the chordwise modes are multiplied by a factor $4/2^{2n}(n>1)$ for convenience. The chordwise mode functions are

$$\ell_n(\theta) = \begin{cases} \tan \dfrac{\theta}{2} & (n=0) \\ \dfrac{4}{2^{2n}} \sin n\theta & (n \geq 1) \end{cases} \tag{3-19}$$

Substituting eqn's(3-18), (3-19), and (3-17) into the integral equation (3-13), and manipulating the non-dimensionlization factors, finally

the 2D slot flow problem. However, the tip behavior must be justified separately. Since the tip behavior is not singular, a loss of knowledge about its behavior causes no serious trouble in the present numerical analysis. The unknown coefficients of the downwash modes can adjust themselves to achieve the best fit of the boundary conditions. Based on this reasoning, Watkin's spanwise modes are adopted without modifying the weighting function, since this weighting function ensures that downwash vanishes at the tip which is required by the boundary condition.

Since the approach is based on Watkin's method, we adopt his notation and nondimensionlization. The new coordinate system is illustrated in Fig.(3-2). Two reference length scales are taken, one is the half root chord b_0 in the x-direction and the other is the maximum half span ℓ in the y-direction. Thus, the (x,y) or (ξ,η) coordinates of the hole fall within the range, $[-1, 1]$. An angular chordwise variable θ was defined also which allows the use of sin $(n\theta)$ mode functions in the chordwise direction. The θ variable is defined as :

$$\xi = \xi_m - \frac{b}{b_0} \cos\theta \qquad 0 \leq \theta \leq \pi \qquad (3\text{-}16\text{a})$$

where,

$$\xi_m = (\xi_{te} - \xi_{le})/2 \qquad (3\text{-}16\text{b})$$

$$b/b_0 = (\xi_{te} + \xi_{le})/2 \qquad (3\text{-}16\text{c})$$

The functions $\xi_{le}(\eta)$, $\xi_m(\eta)$ and $\xi_{te}(\eta)$ represent the equations of the leading edge, midchord line, and trailing edge, respectively.

basically the kernel function method approach, which was developed in 1959 by NASA researchers, Watkins et al.[9]. Of course, some modification must be done to adapt this method to the present leaking-hole problem.

First of all, we expand the unkown function ϕ_z into a series of preselected mode functions with arbitrary coefficients to be determined,

$$\phi_z(\xi,\eta) = \sum_i \Phi_i(\xi)\Theta_i(\eta)$$

Each function $\Phi_i(\xi)$ must satisfy the Kutta condition at the leading edge, otherwise the solution will not be unique. This spanwise mode functions $\Theta_i(\eta)$ must vanish at the side edge, or tip, of the hole. Whether this series converges and how many terms it takes to converge within certain satisfactory error bounds, depends strongly on the choice of mode functions. Generally speaking, the more we know about the behavior of ϕ_z at the edges of the planform, the fewer the number of mode functions that are required for the series to converge. This is because the fluid flow changes abruptly at the edges where the discontinuity in the boundary condition occurs. For lifting surfaces, the pressure distribution usually behaves in proportion to $\varepsilon^{-\frac{1}{2}}$, $\varepsilon^{\frac{1}{2}}$, and $\varepsilon^{\frac{1}{4}}$ at the leading, trailing, and side edges, respectively, where ε is the distance to the edge. These behaviors near the edges have been obtained from the study of simple cases such as a flat plate at angle of attack and the elliptic planform of lifting-line theory. In regard to the hole problem, leading and trailing edge behaviors were determined in

Eqn(3-14) can be arrived at by many methods, such as a Green's Function approach or integral transforms. The derivation is not performed here, since in the subsequent shear flow analysis a complete integral transform method will be presented, and this potential flow is just a limiting case. By observation, we know eqn(3-13) is in correct form.

Physically, this integral equation can be interpreted as follows: $2\phi_z$ is the source strength distribution (a factor 2 is needed because sources are located on the wall), and the kernel function $A(x-\xi,y-\eta)$ represents ϕ_x induced at point(x,y) by a point source located at (ξ,η). Note that equation (3-14) also holds for the airfoil thickness problem.

The integral equation is again a singular one. A double bar across the integral sign denotes a second order singularity, which is of the Cauchy type rather than the Mangler type. This singularity happens when $y=\eta$, for then

$$A(x-\xi, 0) = -\frac{1}{4\pi} \frac{1}{(x-\xi)|x-\xi|} \qquad (3-15)$$

It can be seen that $A(x-\xi,0)$ is anti-symmetric and has a singularity of order ε^{-2} across the point $x=\xi$. It is this anti-symmetric property that makes the singularity of the Cauchy type. Therefore, the Cauchy principal-value is invoked for chordwise integration across this jump point.

Over the years great effort had been spent in the development of numerical lifting-surface theory[6,7,8]. The method used herein is

(3.1.2) Leaking-Hole Theory

For the finite hole problem, no analogy between leaking-hole and lifting-surface theories can be found. The reason for this is due to the wake of a lifting surface, which has no counterpart in the finite hole case. Making the problem three-dimensional introduces the spanwise coordinate and spanwise variables, such as the y-perturbation velocity ϕ_y. Across the wake of a lifting surface, ϕ_y takes a finite jump, and is anti-symmetric with respect to the z=0 plane. However, for the hole in a rigid plane wall, ϕ_y is continuous and symmetric across the z=0 plane. No mechanism in the leaking-hole problem can be found to match the role of the trailing vortex sheet in the lifting problem. Therefore, it is unlikely there will exist an analogy between these two flows. Thus, to solve the 3D hole problem, we have to directly deal with the boundary-value problem, and the understanding gained in the previous 2D investigation is very helpful.

As mentioned earlier, a hole can be replaced by distributed source/sink singularities which occupy the same hole area. Other types of singularities are excluded since they can not satisfy the boundary condition on the rigid wall. The integral relation connecting ϕ_x and ϕ_z is therefore

$$\phi_x(x,y) = \iint_S A(x-\xi, y-\eta)\ 2\phi_z(\xi,\eta)\ d\xi d\eta \qquad (3\text{-}14)$$

where,

$$A(x,y) = \frac{\partial}{\partial x}\left(\frac{-1}{4\pi r}\right)\Big|_{z=0} \quad , \quad r = \sqrt{x^2 + \beta^2(y^2 + z^2)}$$

the present me 'nd directly attacks the boundary-value problem by establishing and solving the associated integral equation. The advantages for the present method are that the physical picture is clearer, and the integral transform method can be extended to three-dimensional flows without fundamental difficulties.

What is learned from the leaking-slot(2D hole) theory can be summarized as follows :

1) The slot flow is a thickness problem; it takes exactly the same integral equation as the non-lifting problem of airfoil theory. The slot flow problem can be viewed as finding a suitable strength distribution of sources/sinks over the slot region which can sustain the pressure differential across the hole as well as satisfy the Kutta condition at the leading edge.

2) From a mathematical standpoint, slot flow is analogous to lifting flow. The techniques developed originally to solve the singular integral equation of the lifting problem can also apply to the slot flow problem.

3) The downwash distribution over the slot region has a square-root singularity at the trailing edge and vanishes in a square-root manner at the leading edge. Indeed, the slot downwash distribution is analogous to the airfoil pressure distribution, and the slot pressure distribution is analogous to the downwash on the airfoil surface.

$$I_1 = \oint_{-1}^{+1} \sqrt{\frac{1-\xi}{1+\xi}} \frac{d\xi}{\xi-x} = -\pi \quad \text{for } -1 \le x \le +1 \tag{3-10}$$

was used.

For a flat plate with angle of attack α, the pressure perturbation on the upper surface is,

$$\frac{P_L(x)}{q} = -\frac{2\alpha}{\beta} \sqrt{\frac{1-x}{1+x}} \tag{3-11}$$

By appropriately choosing the constants $\alpha, \beta, \Delta P$ and q, the analogy to eqn(3-3) can be established.

Integrating w(x) from eqn(3-9) over the slot area yields the volume flowrate across the slot,

$$Q = \int_{-1}^{+1} -w(x)\,dx = \frac{\pi\beta}{2} \frac{\Delta P}{q}$$

The mean downwash velocity across the slot can now be obtained by dividing Q by the slot width,

$$w_m = \frac{Q}{2} = \frac{\pi\beta}{4} \frac{\Delta P}{q}$$

or,

$$\frac{\Delta P}{q} = \frac{4}{\pi\beta} w_m \tag{3-12}$$

The flow resistance constant, $K_h = 4/\pi\beta$, of our analysis is the same that Maeder obtained. However, the approach is different. Maeder solved the incompressible flow problem by modifing the complex potential function to transform the 2D lifting problem into the slot problem, but

The total static pressure comprises three parts,

$$P = P_\infty + p_g + p \qquad (3\text{-}23)$$

where P_∞ is the free-stream pressure of the tunnel flow p_g is the pressure disturbance induced by the model and adjacent holes; and p is the pressure disturbance caused by the hole which is under discussion. For the inner slot flow, $P_\infty + p_g$ is regarded as the imposed static pressure infinitely far away, where p is considered to vanish. Moreover, p_g also satisfies the Laplace equation since it is derived from the tunnel flow. Therefore, eqn(3-7) still holds for the case of an applied pressure gradient. However, ϕ_x takes on another form and meaning over the slot region. Across the slot area the pressure matches with the ambient pressure p_a, hence

$$p_a = P = P_\infty + p_g + p$$

and,

$$p = p_b - P_\infty - p_g \qquad (3\text{-}24)$$

Assume that p_g is a linear function in the streamwise direction, say,

$$p_g(x) = \left.\frac{\partial P}{\partial x}\right|_{x=0} x \qquad (3\text{-}25)$$

Upon substitution of eqn(3-25) into eqn(3-24), ϕ_x on the slot can be derived,

$$\phi_x = -\frac{1}{2}\frac{p}{q} = \frac{1}{2}\frac{\Delta P}{q}\left(1 + \frac{1}{\Delta P}\left.\frac{\partial P}{\partial x}\right|_0 x \right) \qquad (3\text{-}26)$$

where,

$$\Delta P \equiv P_\infty - P_b \tag{3-27}$$

An analytic expression for the downwash distribution can be obtained by inserting eqn(3-26) into eqn(3-7), together with the following integral identities,

$$I_1 = \oint_{-1}^{+1} \sqrt{\frac{1-\xi}{1+\xi}} \; \frac{d\xi}{\xi - x} = -\pi \qquad -1 < x < 1 \tag{3-9}$$

$$I_2 = \oint_{-1}^{+1} \sqrt{\frac{1-\xi}{1+\xi}} \; \frac{\xi \, d\xi}{\xi - x} = \pi(1-x) \qquad -1 < x < 1 \tag{3-28}$$

Thus, the downwash distribution becomes,

$$\frac{w(x)}{\beta} = -\frac{1}{2} \frac{\Delta P}{q} \sqrt{\frac{1+x}{1-x}} \left[1 - \frac{1}{\Delta P} \frac{\partial P}{\partial x}\Big|_0 (1-x) \right] \qquad -1 < x < 1 \tag{3-29}$$

The volume flowrate, found by integrating $w(x)$ over the slot region, is given by

$$\frac{Q}{\beta} = \int_{-1}^{+1} \frac{-w(x)}{\beta} \, dx = \frac{\pi}{2} \frac{\Delta P}{q} \left[1 - \frac{1}{2} \frac{1}{\Delta P} \frac{\partial P}{\partial x}\Big|_0 \right] \tag{3-30}$$

Averaging the volume flowrate by dividing it by the slot width, 2, and rewriting in dimensional form, a modified $\Delta P/q$ versus w_m/U_∞ relationship which accounts for pressure gradient is obtained, (Here ΔP is the mean pressure differential across the hole and w_m/U_∞ is the averaged flow deflection angle)

$$\frac{\Delta P}{q} \left[1 - \frac{1}{4} \frac{d}{\Delta P} \frac{\partial P}{\partial x}\Big|_0 \right] = \frac{4}{\pi\beta} \frac{w_m}{U_\infty} \tag{3-31}$$

where d is the slot width.

Recently, Bliss[13] extended his slender-slot theory to take into account the pressure gradient effect. For his analytic shape with aspect

ratio 0.25 and $M_\infty = 0$, an equation form similar to the above 2D transverse slot relation, eqn(3-31), can be deduced with coefficients calculated correspondingly. The relation is,

$$\frac{\Delta P}{q} \left[1 - 0.232 \frac{\ell}{\Delta P} \frac{\partial P}{\partial x}\Big|_o \right] = 0.4785 \frac{w_m}{U_\infty} \tag{3-32}$$

in which, ℓ is the maximum slot length in the streamwise direction.

The same functional form can also apply to finite(3D) hole cases, with the left hand side pressure differential term of the integral equation(3-14) being replaced by eqn(3-26). The whole numerical algorithm stays unchanged. Therefore, the pressure gradient effect can easily be investigated by using the same constant pressure differential program. The results calculated by these three theories are plotted in Fig.(3-12). Slender slot theory breaks down for aspect ratios greater than about 0.3, for which the slenderness assumption is violated. The agreement is generally acceptable.

Fig.(3-13) shows the sectional volume flowrate distribution influenced by the presence of pressure gradient. The basic shape of the distribution seems not to be disturbed too much by reversing the sign of pressure gradient.

Since the above three theories are all linear, the effect of volume flowrate change due to the presence of pressure gradient can be analyzed in a more convenient manner. First, let us begin with eqn(3-31), the 2D transverse slot case. Listed below are the 2D slot relations with and without pressure gradient,

$$\frac{\Delta P}{q} \left[1 - \frac{1}{4} \frac{d}{\Delta P} \frac{\partial P}{\partial x} \Big|_o \right] = \frac{4}{\pi \beta} \frac{w_n}{U_\infty}$$

$$\frac{\Delta P}{q} = \frac{4}{\pi \beta} \left(\frac{w_n}{U_\infty} \right)_c \tag{3-31}$$

where ΔP can be viewed as the average pressure differential over the slot, and the subscript c denotes the constant pressure case. Subtracting these two equations yields

$$\frac{\Delta P}{q} \left[- \frac{1}{4} \frac{d}{\Delta P} \frac{\partial P}{\partial x} \Big|_o \right] = \frac{4}{\pi \beta} \Delta \left(\frac{w_n}{U_\infty} \right)$$

where, $\Delta \left(\frac{w_n}{U_\infty} \right) = \frac{w_n}{U_\infty} - \left(\frac{w_n}{U_\infty} \right)_c$, and therefore,

$$\Delta C_Q = - \frac{\pi \beta}{16} \frac{d}{\Delta P} \frac{\partial P}{\partial x} \Big|_o \tag{3-33}$$

Similar processes operate in the slender-slot and finite-hole theories. The influence of pressure gradient on the volume flowrate is the same for these three theories, i.e., the slopes are all of the same sign, as expected. However, the family of curves for finite holes does not fall in between the transverse and slender-slot theories. The reason is not clear, and needs further explanation. It would be especially desirable to compare with experimental results, should these become available in the future.

(3.2) Shear Flow Aerodynamics

Classical potential flow theory has proved to be extraordinarily useful in aeronautical engineering. Attempts had been made to extend the methods of inviscid flow analysis to more realistic flows which can account for the effect of a boundary layer, at least qualitatively.

Many researchers[14-22] have undertaken the development of methods to solve for small disturbances to an inviscid, parallel shear flow passing over a nearly plane surface. All these approaches are basically the same: the equations of motion are derived by taking small perturbations to the Euler equations with the main shear stream profile assumed given. The role of viscosity is included only in that a mean shear flow profile has been established. Neglecting viscous effects is valid as long as they do not play an important role in the response of the shear flow to the disturbances of interest. This will be the case as long as convective effects on the rotational velocity field are dominant. Obviously, a certain amount of judgement is required to determine for which problems the method is applicable.

Shear flow aerodynamics is claimed to be valid for certain problems involving free turbulent wake and jet flows, as well as for turbulent boundary layer flows. Dowell[14], Ventres[15], Williams[16], and Chi[17] used the turbulent power law profiles as their main shear stream pattern. Lighthill[18], Weissinger[19], Homentcovschi and Barsony-Nagy[20], and Hanin[21,22] assumed no specific shear flow profiles in their theoretical models, except for requiring a non-vanishing main shear stream velocity and some integrability and smoothness conditions on the profile at rigid surfaces. Dowell, et al.[14-17] developed their model originally for the purpose of solving panel flutter problems in the presence of a wall boundary layer. They achieved considerable success in comparisons with experimental results[23] by using a power law profile. However, researchers who have applied shear flow models to

the aircraft lifting-surface problems have met with rather limited success. Two major criticisms can be made of the use of the power law profile for wings. First, on the wing of an aircraft, there always exists a finite extent of laminar boundary layer starting from the leading edge region which can not be modelled by a turbulent power law profile; second, the boundary layer thickness is not constant along the wing. (The case of slowly varying thickness has been treated by Chi[17], although the analysis is considerably more complex.) Application of this type of shear flow aerodynamics is therefore restricted to control surfaces for which the boundary layer has already been fully developed on the main wing. The smaller chord lengths of control surfaces provide less chance for the boundary layer thickness to vary significantly. Lighthill's approach[18], as adopted by Barsony-Nagy and Hanin et al.[21,22], was to study the aerodynamics of wings in a sheared wind, a jet, or a wake. The approach provides much flexibility in selecting the appropriate shear flow profile. However, the difficulty in deriving the kernel functions is increased, and thus the whole analysis relies heavily on numerical means which in general are complex and expensive.

A perforated tunnel wall boundary layer is a mixed combination of wall turbulent and free turbulent boundary layer flows. For the case of zero porosity (a completely closed wall) the flow is entirely wall turbulence; for unity porosity (fully open wall) it is free turbulence. Since the aim of the analysis is to analyze boundary layer effects on low porosity walls, it is natural to adopt the shear flow model of

Dowell, et al.. The aforementioned two drawbacks of this model become unimportant for the present application. In a wind tunnel test section the wall boundary layer is usually a fully-developed turbulent flow, and the layer thickness may be nearly constant, or at least slowly varying throughout the test section. It is the combined contributions of inertia, wall shear stress, momentum diffusion by viscosity, and boundary layer suction due to leakage through the holes which result in the equilibrium, constant boundary layer thickness power law profile. The boundary layer effect on a leaking-hole is therefore ideally suited for the methods of shear flow analysis. The boundary layer is well established before encountering a hole, and the hole size and boundary layer thickness may be comparable. This means that the layer structure cannot be greatly altered by its brief encounter with the hole. Viscous effects act only in the formation of a free shear layer at the free surface over the hole, but this shear layer thickness will be small compared to the overall boundary layer thickness. The deflection of the flow into the plenum chamber is therefore regarded as the bending of streamlines to counterbalance the vertical pressure differential. Viscosity dominates only when this pressure differential does not exist, or is very small.

In order to keep the analysis as clear as possible, a method developed by Ventres[15] is considered here to analyze the boundary layer effect on the transverse slot and finite hole flows. We will first review Ventres' approach, then add the necessary modifications to adapt this method to the hole problem.

(3.2.1) Basic Shear Flow Analysis

Ventres[15] considered a steady, incompressible, parallel shear flow as depicted in Fig.(3-15). The surface, $z=f(x,y)$, creates a small perturbation from the initially parallel shear flow $u=U(z)$, $v=w=0$. The function $U(z)$ is constant for $z>\delta$, so that the shear layer is limited to the region $0<z<\delta$ adjacent to the surface.

The momentum and continuity equations for the fluid flow are

$$u \cdot u_x + v\, u_y + w\, u_z + (1/\rho)\, p_x = 0$$

$$u\, v_x + v\, v_y + w\, v_z + (1/\rho)\, p_y = 0$$

$$u\, w_x + v\, w_y + w\, w_z + (1/\rho)\, p_z = 0$$

$$u_x + v_y + w_z = 0$$

$$(3\text{-}34 \ a,b,c,d)$$

Let u', v', w' be the perturbation velocity components, and let p' be the perturbation pressure. Then the total velocity and pressure are

$$u = U(z) + u'$$

$$v = v'$$

$$w = w'$$

$$p = P_\infty + p'$$

$$(3\text{-}35 \ a,b,c,d)$$

Inserting eqn's (3-35 a-d) into eqn's (3-34 a-d), and retaining only the lowest order terms yields,

$$U u_x' + w'(dU/dz) + (1/\rho) p_x' = 0$$

$$U v_x' + (1/\rho) p_y' = 0$$

$$U w_x' + (1/\rho) p_z' = 0$$

$$u_x' + v_y' + w_z' = 0$$

A single equation for the perturbation pressure p (the prime is now dropped for convenience) can be derived by eliminating the velocity perturbations between the equations.

$$\nabla^2 p - (2/U)(dU/dz) p_z = 0 \tag{3-36}$$

where ∇^2 is the Laplacian operator. The Fourier transform technique is used here to solve the boundary-value problem. The Fourier transform pair is defined as,

$$p^* = \frac{1}{2\pi} \iint_{-\infty}^{+\infty} p \, e^{-i(k_1 x + k_2 y)} \, dx \, dy$$

$$p = \frac{1}{2\pi} \iint_{-\infty}^{+\infty} p^* \, e^{i(k_1 x + k_2 y)} \, dk_1 \, dk_2 \tag{3-37}$$

By applying this transform to eqn(3-36), an ordinary differential equation is obtained,

$$\frac{d^2 p^*}{dz^2} - (2/U)(dU/dz)\frac{dp^*}{dz} - (k_1^2 + k_2^2) p^* = 0 \tag{3-38}$$

The variable coefficient in front of the second term vanishes for $z > \delta$, where the initial flow velocity is constant.

Specifying a 1/n power law for the shear flow velocity profile,

$$U(z) = U_1 (z/\delta)^{1/n} \qquad z < \delta$$

$$= U_1 \qquad z > \delta$$

(3-39)

and applying it to eqn(3-38) gives

$$\frac{d^2 p^*}{dz^2} - \frac{2}{nz} \frac{dp^*}{dz} - R^2 p^* = 0$$

$$R \equiv (k_1^2 + k_2^2)^{1/2}$$

(3-40)

Eqn(3-40) can be transformed into a recognizable Bessel equation by the following transformations of the dependent and independent variables,

$$p^* = \lambda^\nu g(\lambda)$$

$$\lambda \equiv Rz$$

(3-41)

where, $\nu = 1/2 + 1/n$. The transformed equation reads,

$$\frac{d^2 g}{d\lambda^2} + \frac{1}{\lambda} \frac{dg}{d\lambda} - \left[\left(\frac{\nu^2}{\lambda^2} \right) + 1 \right] g = 0$$

(3-42)

The general solution to eqn(3-42) is,

$$g = A I_\nu (Rz) + B I_{-\nu} (Rz)$$

(3-43)

in which, I_ν is the Bessel function of the second kind of order ν. The unknown coefficients A and B are determined by the boundary conditions imposed on the surface and at the outer edge of the shear layer. The boundary condition for the outer edge of the shear layer is obtained by noting that eqn(3-40) reduces to

$$\frac{d^2 p^*}{dz^2} - R^2 p^* = 0 \qquad \text{for} \quad z > \delta$$

Solutions to this equation have the form,

$$p^* = e^{Rz}, \quad e^{-Rz}$$

Only the second one is bounded as $z \to \infty$. Therefore, for $z > \delta$, p^* satisfies the equation

$$\frac{dp^*}{dz} + R p^* = 0 \tag{3-44}$$

We shall employ this relation as the boundary condition at $z = \delta$.

Note that both the shear flow profile, eqn(3-39,) and the equation of motion, eqn(3-36) do not apply on the surface. The profile does not apply because the shear flow model is not valid within the laminar sublayer. The equation of motion is not applicable because it is not permissible to take perturbations around a vanishing base quantity. The inner boundary condition should be specified at the outer edge of the laminar sublayer. Here we denote the height of the sublayer by $z = z_0$, and from the z-momentum equation,

$$\left. \frac{\partial p}{\partial z} \right|_{z=z_0} = -\rho U \left. \frac{\partial w}{\partial x} \right|_{z=z_0}$$

where,

$$\left. w \right|_{z=z_0} = \left. U \right|_{z=z_0} \frac{\partial f}{\partial x}$$

or,

$$\left. \frac{\partial p}{\partial z} \right|_{z=z_0} = -\rho U_1^2 (z_0/\delta)^{2/n} \frac{\partial^2 f}{\partial x^2} \tag{3-45}$$

The Fourier transform of this boundary condition is,

$$\frac{dp^*}{dz}\bigg|_{z=z_0} = -\rho U_1^2 (z_0/\delta)^{2/n} \, ik_1 \left(\frac{\partial f}{\partial x}\right)^* \tag{3-46}$$

Using the outer boundary condition, eqn(3-44), will eliminate one unknown coefficient, and the general solution becomes,

$$p^* = (Rz)^\nu A \left[I_\nu(Rz) - L(\delta R) I_{-\nu}(Rz) \right] \tag{3-47}$$

where,

$$L(\delta R) = \frac{I_\nu(\delta R) + I_{\nu-1}(\delta R)}{I_{-\nu}(\delta R) + I_{1-\nu}(\delta R)} \tag{3-48}$$

By imposing the inner boundary condition and using the recurrence relation for Bessel functions, it can be found that,

$$\frac{1}{\rho U_1^2}\frac{dp^*}{dz}\bigg|_{z=z_0} = AR(Rz_0)^\nu \left[I_{\nu-1}(Rz_0) - L(\delta R) I_{-\nu+1}(Rz_0) \right]$$
$$= (z_0/\delta)^{2/n} \, ik_1 \left(\partial f/\partial x\right)^* \tag{3-49}$$

Since the thickness of the laminar sublayer is usually very thin, $z_0 \ll \delta$, the terms in the square bracket of eqn(3-49) can be expanded in a Taylor series. Note that,

$$I_\nu(z) \sim \left(\tfrac{1}{2}z\right)^\nu / \Gamma(\nu+1) \qquad \nu \neq -1, -2, \cdots \qquad , z \ll 1$$

By taking the limit of $z_0 \to 0$ in eqn(3-49), the constant A can be determined,

$$A = \frac{\Gamma(\nu)}{2^\nu} \frac{1}{R} \left(\frac{2}{\delta R}\right)^{2/n} ik_1 \left(\frac{\partial f}{\partial x}\right)^* \tag{3-50}$$

Analogously, we let z in eqn(3-47) approach zero to seek a relation connecting p* and $(\partial f/\partial x)^*$ on the surface,

$$p^* = A^* \left[U_1 (\partial f/\partial x)^* \right]$$

$$A^* (k,\delta, k_2\delta) = \frac{\Gamma(1+\nu)}{\nu\Gamma(1-\nu)} \left(\frac{ik_1}{R}\right)\left(\frac{2}{\delta R}\right)^{2/n} L(\delta R)$$

$$L(\delta R) = \frac{I_\nu(\delta R) + I_{\nu-1}(\delta R)}{I_{-\nu}(\delta R) + I_{1-\nu}(\delta R)}$$

$$(3-51\ a,b,c)$$

By inverting this Fourier transformed relation and using the convolution theorem, the pressure on a surface of infinite extent with an arbitrary perturbation contour can be established. The integral region becomes finite if we further utilize the specific symmetric/anti-symmetric property of the lifting or thickness problem. Ventres treated the lifting case by inverting $1/A^*$ to obtain the lifting kernel function. He then solved the lifting case numerically using an approach similar to Watkin's method. The present interest is to solve the problem of a hole on a plane rigid surface, which is a thickness problem. Therefore, from here on we proceed to solve the integral equation pertaining to this case.

(3.2.2) Shear Flow Leaking-Slot Theory

The two dimensional integral equation can be obtained by setting the y-direction wavenumber $k_2 = 0$ in the 3D equations. The 2D transformed equations thus derived are of the form

$$p^* = A^* (\partial f/\partial x)^*$$

$$A^*(|k_1|\delta) = \frac{\Gamma(1+\nu)}{\nu\Gamma(1-\nu)} \left(i\frac{k_1}{|k_1|}\right)\left(\frac{2}{\delta|k_1|}\right)^{2/n} L(\delta|k_1|)$$

$$L(\delta|k_1|) = \frac{I_\nu(\delta|k_1|) + I_{\nu-1}(\delta|k_1|)}{I_{-\nu}(\delta|k_1|) + I_{1-\nu}(\delta|k_1|)}$$

$$(3\text{-}52\ a,b,c)$$

in which quantities are normalized by the potential flow velocity U_∞ and the half slot width.

To obtain the thickness kernel, $A(x)$, we must invert A^*. However, it cannot be inverted in the usual Fourier transform sense. According to Lighthill[24], the singular part of $A(x)$ can be obtained by inverting the asymptotic expansion of A^* for large k_1. The function $L(\delta|k_1|)$ approaches unity uniformly regardless of the parameter ν, therefore with the aid of the formula[25],

$$\int_0^\infty x^{-\nu} \sin(xy)\,dx = y^{\nu-1} \Gamma(1-\nu) \cos\left(\tfrac{1}{2}\nu\pi\right)$$

$$0 < Re\ \nu < 2$$

$$(3\text{-}53)$$

where the singular part of the kernel function is expressed as,

$$A_s(x) = \frac{1}{\sqrt{2\pi}} \int_{-\infty}^{+\infty} \frac{\Gamma(1+\nu)}{\nu\Gamma(1-\nu)} \frac{ik_1}{|k_1|}\left(\frac{2}{\delta|k_1|}\right)^{2/n} e^{ik_1 x}\,dk_1$$

$$= \frac{-1}{\sqrt{2\pi}} \int_{-\infty}^{+\infty} \frac{2\Gamma(1+\nu)}{\nu\Gamma(1-\nu)}\left(\frac{2}{\delta k_1}\right)^{2/n} \sin k_1 x\,dk_1$$

$A_s(x)$ then takes the form,

important characteristic that differentiates the hole from the slot (Another important characteristic is the swept leading and trailing edges). It is shown in Fig.(3-28) that the velocity defect of the shear profile tends to enlarge this difference. A similar trend is also found for the boundary layer thickness effect on the sectional volume flowrate as illustrated in Fig.(3-29). This diagram also reveals the powerful influence of boundary layer thickness on the volume flowrate across the hole.

Fig.(3-30) demonstrates the boundary layer thickness effect on the volume flowrate. The simulation was performed for a 1/7 power law profile with pressure differential $\Delta p/q = 0.1$, and with δ normalized by the hole radius. A similar trend is observed by comparing with the slot case, Fig.(3-24). A dent in the curve occurs around $\delta=0.5$ for the hole. A check of the convergence of the program was done for this range of δ, and it appears this behavior is not due to numerical error. This special feature was not observed in the 2D case. The reason for this behavior may be related to an effect of the finite width of the hole and the complicated nature of the flow near the side edges.

Since the presence of the boundary layer magnifies the deflection of the oncoming stream into the hole, it is desirable to see at what thickness value the boundary layer would make the flow violate the small perturbation assumption. A test was carried out for the 1/7 power law profile shear flow with $\Delta p/q=0.1$. Since it is known that the largest deflection of the flow always occurs at the trailing edge of the hole, a

the potential case, but it is still of the Cauchy type. The singular integration involved in the solution method has the form,

$$I \sim \oint \frac{dx}{x \, |x|^{1-2/n}} \qquad (3\text{-}74)$$

It can be resolved by the method discussed in the potential flow with slight modifications.

Watkin's method is again employed to solve this singular integral equation. The mode functions are borrowed from the potential case without regard for their inappropriate representation of the edge behaviors. The numerical simulation was performed for two shapes, the round hole, and D.B.B's analytic shape. The latter can be regarded as a more nearly square hole.

The important C_p versus w_m/U_∞ behavior is illustrated in Fig.(3-26). As in the slot flow case, the curves are slightly non-linear and boundary layer shows a strong effect in changing the C_p versus w_m/U_∞ characteristic.

Fig.(3-27) shows the influence of shear profile on the volume flowrate across the hole. As compared to the 2D case of Fig.(3-18), the finite hole is more profoundly affected. This is probably due to the finite span effect which distinguishes the hole from the slot. This explanation is confirmed in the next figure.

The sectional volume flowrate is a convenient quantity for making comparisons between 2D and 3D cases. The finite lateral span is the most

approximately twice the boundary layer thickness. For thin boundary layer cases, $\delta/d \ll 1$, the averaged perforated wall condition only needs modification of its resistance constant k_h; the streamline curvature term will remain largely unaffected because the boundary layer effect is not likely to extend far enough.

According to Lighthill[24] the kernel function behavior in the larger distance $r \gg 1$ can be deduced from the behavior of its Fourier transformed counterpart for small $R = \sqrt{k_1^2 + k_2^2} \ll 1$. A^* for $R \ll 1$ is found to be,

$$A^* \sim \frac{i h_1}{R} \left[1 + \frac{1-2\nu}{\nu(1-\nu)} \frac{\delta R}{2} + O(\delta^2 R^2) \right] \qquad R \ll 1 \qquad (3\text{-}71)$$

Since,

$$\int_0^\infty J_0(Rr)\, dR = \frac{1}{r}$$

$$\int_0^\infty R\, J_0(Rr)\, dR = \frac{2}{r^2} \qquad\qquad (3\text{-}72)$$

We have

$$A \sim \frac{\partial}{\partial x} \left[\frac{1}{r} + \frac{1-2\nu}{\nu(1-\nu)} \frac{\delta}{r^2} + \cdots \right] \qquad r \gg 1 \qquad (3\text{-}73)$$

Eqn(3-73) justifies that for $r \gg \delta^{\frac{1}{2}}$, the shear kernel function A decays at the same rate as the potential kernel. Based on the numerical data exhibited in Fig.(3-25) and the far field analysis, in later numerical calculations the shear kernel is replaced by the potential kernel for $r/\delta > 2$. This simplification saves a lot computing effort.

The singular behavior of the present kernel is weaker than that of

the use of

$$\frac{\partial r}{\partial x} = \frac{x}{r}$$

$$\frac{d}{dz} J_0(z) = - J_1(z)$$

we can obtain a more numerically suitable form for δA_r, namely,

$$\delta A_r = \frac{-x}{\delta r} \int_0^\infty \frac{\Gamma(1+\nu)}{\nu \Gamma(1-\nu)} \left(\frac{2}{u}\right)^{2\nu} [L(u)-1]\, u\, J_1\left(u\frac{r}{\delta}\right) du \tag{3-69}$$

We can now conclude that the integral equation for 3D hole in shear flow is,

$$p(x,y) = \frac{1}{2\pi} \iint_S A(x-\xi, y-\eta) \frac{\partial f}{\partial \xi}(\xi,\eta)\, d\xi d\eta$$

$$A(x,y) = A_s(x,y) + A_r(x,y) \tag{3-70}$$

in which, A_s and A_r are defined in eqn's(3-67) and (3-69), respectively.

Because of the fundamental importance of the kernel function, we evaluate and plot the kernel in Fig.(3-25). The potential kernel is plotted from the previous potential flow analysis. The implications of this kernel function behavior are the same as for the 2D transverse slot: mutual interaction between holes is weakened by the presence of the boundary layer, and the boundary layer effect does not extend very far. In fact, beyond a distance of approximately twice the boundary layer thickness, the shear and potential kernels are not significantly different and die out at the same asymptotic rate. This implies that the boundary layer effect is confined within a zone of radius

eqn(3-63) is radially symmetric. Upon using polar coordinates for (x,y) and (k_1, k_2), the Fourier transform turns into the form of a Hankel transform and it states,

$$A_s(x,y) = \frac{\Gamma(1+\nu)}{\nu \Gamma(1-\nu)} \left(\frac{2}{\delta}\right)^{2/n} \frac{\partial}{\partial x} \int_0^\infty R^{-2/n} J_0(Rr) \, dR$$

$$r \equiv (x^2 + y^2)^{1/2}$$

$$(3-64)$$

where J_0 is the Bessel function of the first kind of order zero. Since, from Watson[26],

$$\int_0^\infty t^\mu J_\nu(at) \, dt = \frac{2^\mu \Gamma\left(\frac{1}{2} + \frac{1}{2}\mu + \frac{1}{2}\nu\right)}{a^{\mu+1} \Gamma\left(\frac{1}{2} - \frac{1}{2}\mu + \frac{1}{2}\nu\right)} \qquad (3-65)$$

therefore,

$$\int_0^\infty R^{-2/n} J_0(rR) \, dR = \frac{2^{-2/n} \Gamma\left(\frac{1}{2} - \frac{1}{n}\right)}{r^{1-2/n} \Gamma\left(\frac{1}{2} + \frac{1}{n}\right)} \qquad (3-66)$$

and consequently,

$$A_s(x,y) = \frac{1}{\delta^{2/n}} \frac{\partial}{\partial x} \left(\frac{1}{r^{1-2/n}}\right) \qquad (3\text{-}67\text{ a})$$

or,

$$\delta A_s(x,y) = \frac{\partial}{\partial x} \left[\frac{1}{(r/\delta)^{1-2/n}}\right] \qquad (3\text{-}67\text{ b})$$

Likewise, the regular part can be deduced by inverse Fourier transforming $A^* - A_s^*$ (actually Hankel transforming in the polar coordinate). The regular part A_r takes the form,

$$\delta A_r(x,y) = \frac{\partial}{\partial x} \int_0^\infty \frac{\Gamma(1+\nu)}{\nu \Gamma(1-\nu)} \left(\frac{2}{u}\right)^{2/n} [L(u) - 1] J_0\left(u\frac{r}{\delta}\right) du \qquad (3-68)$$

The partial derivative $\partial/\partial x$ can be taken inside the integral sign. With

(3.2.3) Shear Flow Leaking-Hole Theory

To study the 3D finite hole problem in a shear flow, we must first obtain the integral equation. The Fourier transformed equation connecting the pressure differential and the free surface slope function is already available in eqn(3-51). As noted in the 2D case, the kernel function is not invertable in the usual Fourier transform sense because it is singular. Therefore, we split the kernel into regular and singular parts. The singular part is derived analytically, for which the finite part concept is invoked, The regular part is not analytically derivable but can be obtained through routine numerical means.

The singular part, A_s, can be obtained by Fourier inversion of the asymptotic expansion of A^*. Note that the asymptotic expansion of the Bessel function I_ν is even with respect to the index ν. Therefore, $L(\delta R) \to 1$ as $R \to \infty$ ($R = \sqrt{k_1^2 + k_2^2}$), and the asymptotic expansion of A^* for large R is,

$$A^*(\delta R) \sim \frac{\Gamma(1+\nu)}{\nu\Gamma(1-\nu)} \left(\frac{ik_1}{R}\right)\left(\frac{2}{\delta R}\right)^{2/n} \qquad R \gg 1 \tag{3-62}$$

Applying eqn(3-36) to invert eqn(3-62) yields,

$$A_s(x,y) = \frac{1}{2\pi} \frac{\partial}{\partial x} \iint\limits_{-\infty}^{+\infty} \frac{\Gamma(1+\nu)}{\nu\Gamma(1-\nu)} \left(\frac{1}{R}\right)\left(\frac{2}{\delta R}\right)^{2/n} \cdot e^{i(k_1 x + k_2 y)} \, dk_1 \, dk_2 \tag{3-63}$$

in which the finite part concept is used. Note that the integrand in

Here n is the normal coordinate, V is the flow velocity, and R is the radius of curvature of the streamline. For the same pressure differential across a slot, the boundary layer tends to slow down the flow velocity near the wall and slot. This will make the streamlines in the vicinity of the slot region curve more to produce the same normal pressure gradient, thus resulting in a larger deflection of the free surface. A larger boundary layer thickness and a more slowly varying shear flow profile will both tend to reduce the flow velocity near the slot. Therefore, the free surface deflections, based on the above reasoning, become larger. However, the effective shear stream velocity along the entrance plane is affected in the opposite manner. These two counteracting tendencies both contribute to the final volume flowrate through the slot. The boundary layer thickness is found to be the more influential factor, and this generally agrees with experimental observations.

Fig.(3-24) shows the effect of boundary layer thickness on the volume flowrate. Here the pressure differential is not too large, $\Delta p/q=0.1$, and 1/7 power law profile is employed in the shear flow model. Below $\delta=0.5$ the boundary layer and the effective shear velocity $U(z_{f.s.})$ nearly balance each other to stay close to the potential flow result. Beyond $\delta=0.5$, the boundary layer effect becomes increasingly dominant and C_Q increases steadily, and does not approach an asymptotic value within the small perturbation range.

Owing to the non-linear behavior of the C_p versus w_m/U_∞ curve, the rest of our examination of the characteristics of a slot in shear slow is performed with the pressure differential $\Delta p/q = 0.1$.

The free surface slope distribution and the slot entrance downwash distribution are shown in Fig's(3-20) and (3-21) for three shear flow profiles n=5,7, and 50. The n=50 case is very close to the potential flow result. The results show that the greater the velocity profile defect(smaller n), the larger the free surface deflection will be. However, the main stream velocity at the entrance plane, $U(z_{f.s.})$, is reduced for larger velocity profile defect to an even greater extent. These two opposite trends, when multiplied together to produce the downwash distribution on the entrance plane, reduce the difference between the boundary layer flow and potential flow. Therefore, $w(x,o)$ in Fig.(3-21) is seen to depart less from the potential flow result than does the free surface slope.

A similar situation occurs for a fixed shear profile shape, say n=7, when the boundary layer thickness is varied. Fig.'s(3-22) and (3-23) illustrate this behavior in detail. All these slot flow phenomena are associated with the momentum and velocity deficits introduced in by the boundary layer, and can be explained in the following way.

The inviscid flow momentum equation in the normal direction described by the intrinsic coordinate system is,

$$\frac{\partial p}{\partial n} = \rho \frac{V^2}{R} \tag{3-61}$$

Fig.(3-18) shows the volume flowrate coefficient C_Q at pressure differential $\Delta p/q=0.1$ for different profiles. In turbulent flow the index n ranges between $5<n<12$, depending on the Reynolds number of the flow. The most common case is n=7. The boundary layer thickness was set to be unity, which means the boundary layer thickness equals to half the slot width. The diagram indicates that C_Q is not too sensitive to the shear flow profile shape.

Fig.(3-19) shows the C_p versus w_m/U_∞ characteristic curves. The shear flow model is a 1/7 power law profile, and the boundary layer thickness is chosen as the parameter being varied. A strong influence of boundary layer thickness on the C_p versus w_m/U_∞ characteristics is seen. The family of curves are only slightly non-linear near the origin. As pointed out earlier, the present theoretical model may not be appropriate for a very small pressure differential, since real viscous effects would be as important as the pressure differential term is in this case. Experimentally obtained C_p versus w_m/U_∞ characteristics also show very irregular and fluctuating data distributed around the origin. Moreover, experimentists often claim little confidence in their data in this region. The trend of decreasing slope of the C_p versus $w_m U/_\infty$ curve with increasing boundary layer thickness exhibited in Fig.(3-19) is consistent with the experimented results for thick walls with normal or slanted holes[11]. Unfortunately, no experiments have been carried out for a single slot or hole in a thin wall. Therefore, detailed comparisons can not be made to test the theoretical model.

The singular behavior of the shear kernel is proportional to

$$A(x) \sim \frac{|x|^{2/n}}{x}$$

near the point x=0. A(x) is discontinuous at x=0, but it is integrable from both sides of this singular point. There is no need to invoke the Cauchy principal-value concept. Care has to be exercised in the integration to be sure not to jump across the singular point when it is contained in the region of integration.

The kernel function method presented in the previous potential hole problem is used here to solve the singular integral equation(3-56). We expand the unknown free surface slope function into a set of preselected mode functions,

$$\frac{df}{d\xi} = \sum_i a_i \phi_i(\xi) \tag{3-59}$$

where,

$$\phi_0(\xi) = \sqrt{\frac{1+\xi}{1-\xi}} \qquad (n=0)$$

$$\phi_n(\xi) = \frac{4}{2^{2n}} \sin n\theta \ , \quad \theta = \cos^{-1}\xi \qquad (n \geq 1) \tag{3-60}$$

The singular mode is borrowed from the potential slot flow result with some reservation since its behavior at the leading and trailing edges are not yet known. This kind of strategy was also employed by Ventres. The numerical results show that convergence is satisfactory for this selected set of mode functions.

to it. The mass flux going out of the control volume is

$$\rho \int_0^{f(x) + \frac{\partial f}{\partial x}\Delta x} u(x,z)\,dz$$

Using the law of mass conservation gives,

$$\int_0^{f(x)} u(x,z)\,dz + w(x,0)\Delta x = \int_0^{f(x) + \frac{\partial f}{\partial x}\Delta x} u(x,z)\,dz \tag{3-57}$$

The right-hand-side term can be approximated as,

$$R.H.S. = \int_0^{f(x)} + \int_{f(x)}^{f(x) + \frac{\partial f}{\partial x}\Delta x}$$

$$= \int_0^{f(x)} u(x,z)\,dz + \frac{\partial f}{\partial x}\Delta x \cdot u(z)\Big|_{z = f(x)} + H.O.T.$$

Therefore, by taking $\Delta x \rightarrow 0$, w is found to be

$$w(x,0) = \frac{\partial f}{\partial x} u(x,z)\Big|_{z = f(x)}$$

$$= \frac{\partial f}{\partial x}\left[U(z) + u'(x,z)\right]\Big|_{z = f(x)} \qquad (u' \ll U)$$

$$\approx U(z_{f.s.}) \frac{\partial f}{\partial x} \tag{3-58 a}$$

and

$$z_{f.s.} = \int_{-1}^{x} \frac{\partial f}{\partial \xi}\,d\xi \tag{3-58 b}$$

because $z_{f.s.} = 0$ at the leading edge $x = -1$.

Eqn(3-58) implies that the main shear stream profile as well as the height and slope of the deflected free surface all have an influence on the flowrate across the hole. The dependence of the entrance downwash on the free surface slope is in general non-linear, therefore, we cannot expect a linear relationship between C_p and w_m/U_∞ in the shear flow.

Ventres) as the downwash that would exist on the surface if the shear layer were absent. Furthermore, this normal velocity is specified on the z=0 mean plane instead of the real surface because only lowest order solution of the perturbartion theory is to be considered. However, in the slot flow problem, the variable specified as the boundary condition over the slot region is the pressure, not the surface slope. Similarly, because the deflection of the free surface is small, and only lowest order solution is sought, the pressure is specified on the slot entrance surface z=0. The role of df/dx in these two closely related problems should not be confused, as both of them involve the specification of a boundary condition in which some approximation is made. The function df/dx of the slot flow problem is related to the downwash distribution on the z=0 plane. However, this relation is obtained from considering the conservation of mass, not the flow tangency condition used in the airfoil problem.

Consider, in Fig.(3-17), a shear flow that slides along the free surface deflected down into the plenum chamber. The dashed lines represent a control volume, and the distance between the left and right control surfaces is Δx. The mass flux coming into this control volume from the left control surface is

$$\rho \int_0^{f(x)} u(x,z)\,dz$$

and from the top is,

$$\rho\, w(x,o)\, \Delta x$$

No mass flux goes across the bottom surface because the flow is tangent

wall would be attenuated by the presence of boundary layer. One implication of this behavior is that interference between neighboring holes is strongest in potential flow.

The integral equation for the 2D shear flow thickness problem can be determined by formally inverting eqn(3-52), and using the convolution theorem and the fact that (df/dx) vanishes outside the hole planform. Thus,

$$P(x) = \frac{1}{\sqrt{2\pi}} \oint_{-1}^{+1} A(x-\xi)\left[\frac{df(\xi)}{d\xi}\right] d\xi$$

$$A(x) = A_s(x) + A_r(x) \qquad\qquad (3\text{-}56)$$

where $A_s(x)$ and $A_r(x)$ are defined in eqn's (3-54) and (3-55).

Before proceeding to solve the integral equation, some care must be taken to differentiate between df/dx and the downwash distribution on the z=0 plane. In our slot problem, z=f(x) is the equation of the free surface which separates the tunnel flow from the stagnant plenum chamber. Along this free surface the static pressure of the flow matches with the plenum chamber pressure. Without invoking any basic fluid flow equations, such as the continuity or momentum, df/dx has no special meaning except that it is the free surface slope distribution function. For airfoil problems, df/dx is associated with the normal velocity on the wing surface through the use of a kinematic flow tangency condition. In potential flow, U_∞df/fx is this normal velocity, while in shear flow, the corresponding quantity is multiplied by the outer potential flow velocity to become U_1df/dx, and is explained (by

$$A_s(x) = -\sqrt{\frac{2}{\pi}} \frac{\Gamma(1+\nu)\,\Gamma(2-2\nu)}{\nu\,\Gamma(1-\nu)} \frac{1}{x} \left(\frac{2|x|}{\delta}\right)^{2/n} \cos(\pi/n) \qquad (3\text{-}54)$$

The regular part of the kernel can be obtained by inverting $A^*-A_s^*$, so that A_r takes the form,

$$A_r(x) = -\sqrt{\frac{2}{\pi}} \frac{\Gamma(1+\nu)}{\nu\,\Gamma(1-\nu)} \frac{1}{\delta} \int_0^\infty \left(\frac{2}{u}\right)^{2/n} [L(u)-1] \cdot \sin\left(u\frac{x}{\delta}\right) du$$

$$(3\text{-}55)$$

$A_r(x)$ must be calculated numerically. This is not too difficult because of the exponential decay property of ($L(u)-1$).

A check on the shear flow kernel can be performed by letting the power $n\to\infty$. Since by definition $\nu=1/2+1/n$, therefore $\nu\to1/2$ as $n\to\infty$. This makes the function L identically equal to 1, and therefore from eqn(3-55), $A_r(x)\to0$. The singular part and the kernel can easily be deduced,

$$A(x) = A_s(x) + A_r(x) = -\sqrt{\frac{2}{\pi}} \frac{1}{x} \qquad \text{for } n\to\infty$$

This recovers the familiar 2D thickness kernel of potential flow.

Fig.(3-16) shows the shear flow kernel. Because it is anti-symmetric with respect to the streamwise coordinate, only the positive part is plotted. It can be seen that shear flow kernels for different profile shapes are all enclosed within the envelope of the potential kernel. This reflects the fact that if we have a point impulse of volume flow injected into the shear stream, the induced pressure disturbance on the

plot was made to examine the flow deflection at the trailing edge. The largest deflection in Fig.(3-31) is found at the center-line trailing edge for the case $\delta=5.0$, and its value is about a quarter of the hole diameter in dimensional terms. Roughly speaking, this is just barely permissible for a small perturbation theory. Because the maximum flow deflection of a round hole is always found located at the center-line trailing edge, this suggests a way to determine the largest boundary layer thickness that would not violate the small perturbation assumption. Remember that the free surface deflection is linearly related to the pressure differential, hence $\Delta p/q$ is set to be 1 for convenience. The results of this investigation are shown in Fig.(3-32).

Figures(3-33) to (3-37) show the results for D.B.B.'s analytic shape. The C_p versus w_m/U_∞ characteristic curve, the shear flow profile defect and boundary layer thickness effects, the sectional volume flowrate, and the total volume flowrate increase with respect to the boundary layer thickness are examined and plotted. In all, they are generally similar to the round hole case. This implies that the shape of the opening has much less influence on the cross-flow than the hole aspect ratio and boundary layer effect.

The conclusions of the boundary layer effect on the transverse slot and hole can be summarized as follows:

1) The boundary layer tends to decrease the flow resistance constant $K_h (\propto 1/C_Q)$, and it does this very effectively.

2) The interference between neighboring holes, as indicated by the

disturbance induced by a unit strength source/sink, is strongest in potential flow. The boundary layer tends to suppress the mutual interference, but this suppression is likely to be localized within a zone of the order of its thickness.

3) For a real wall flow, how the streamline curvature coefficient is modified by the velocity and momentum deficits of the main stream shear flow needs further careful study, because the above two effects tend to compensate for each other.

REFERENCES

1. Maeder, P.F., "Investigation of the Boundary Condition at a Perforated Wall," Brown Univ., TR WT 9, May, 1953.

2. Ashley, H. and Landahl, M.T., "Aerodynamics of Wings and Bodies," Addison-Wesley, Mass., 1965.

3. Bisplinghoff, R.L., Ashley, H., and Halfman, R.L., "Aeroelasticity", Addison-Wesley, Mass., 1957.

4. Dowell, E.H. et. al., "A Modern Course in Aeroelasticity," Sijthoff & Noordhoff, Netherlands, 1978.

5. Tricomi, F.G. "Integral Equations," Interscience, p.180.

6. Ashley, H., Widnall, S., and Landahl, M.T., "New Directions in Lifting-Surface Theory," AIAA J., vol. 3, no. 1, Jan. 1965, pp.3-16.

7. Landahl, M.T., and Stark, V.J.E., "Numerical Lifting-Surface Theory Problems and Progress," AIAA J., vol. 6, Nov., 1968, pp. 2049-2060.

8. Ashley, H. and Rodden, W.P., "Wing-Body Aerodynamic Interaction," Annual Review of Fluid Mechanuics, vol. 4, 1972, pp. 431-472.

9. Watkins, C.E., Runyan, H.L. and Woolston, D.S., "A Systematic Kernel Function Procedure for Determining Aerodynamic Forces on Oscillating or Steady Finite Wings at Subsonic Speeds," NASA TR R-48, 1959.

10. Pindzola, M. and Chew, W.L., "A Summary of Perforated Wall Wind Tunnel Studies at the Arnold Enginering Development Center," AEDC-TR-60-9, August 1960.

11. Goethert, B.H., "Transonic Wind Tunnel Testing," Pergamon Press, 1961.

12. Bliss, D.B., "Aerodynamic Behavior of a Slender Slot in a Wind Tunnel Wall," AIAA Journal, Vol. 20, No. 9, Sep. 1982, pp. 1244-1252.

13. Bliss, D.B., "Pressure Gradient Effect on a Slender Slot in a Wind Tunnel Wall," (forthcoming, accepted by AIAA J.)

14. Dowell, E.H., "Generalized Aerodynamic Forces on a Flexible Plate Undergoing Transient Motion in a Shear Flow with an Application to Panel Flutter," AIAA J., vol. 9, May 1971, pp. 834-841.

15. Ventres, C.S., "Shear Flow Aerodynamics : Lifting Surface Theory,"

AIAA J., vol. 13, Sep. 1975, pp. 1183-1189.

16. Williams, M.H. et. al, "Aerodynamic Effects of Invicid Parallel Shear Flows," AIAA J., vol. 15, Aug. 1977, pp. 1159-1166.

17. Chi, M.R., "Unsteady Lifting Surface Theory in an Incompressible Shear Flow," Princeton Univ. AMS Rept. No. 1283, Oct. 1976.

18. Lighthill, M.J., "The Fundamental Solution for Small Steady Three-Dimensional Disturbances to a Two-Dimensional Parallel Shear Flow," Journal of Fluid Mecanics, vol. 3, Nov. 1957, pp. 113-144.

19. Weissinger, J., "Linearisierte Profiltheorie bei Ungleichformiger Anstromung, I, Unendlich Dunne Profile (Wirbel und Wirbelbelegungen)," Acta Mechanica, vol. 10, 1970, pp. 207-228.

20. Homentcovschi, D. and Barsong-Nagy, A., "A Linearized Theory of Three-Dimensional Airfoils in Nonuniform Flow," Acta Mechanica, vol. 24, 1976, pp. 63-86.

21. Hanin, M., and Barsony-Nagy, A., "Slender Wing Theory for a Nonuniform Stream," AIAA J., vol. 18, Apr. 1980, pp. 381-384.

22. Barsong-Nagy, A., and Hanin, M., "Aerodynamics of Wings in Subsonic Shear Flow," AIAA J., vol. 20, Apr. 1982, pp. 451-456.

23. Muhlstein, L., Gaspers, P.A., and Riddle, D.W., "An Experimental Study of the Influence of the Turbulent Boundary Layer on Panel Flutter," NASA TN-D-4486, March 1968.

24. Lighthill, M.J., "Introduction to Fourier Analysis and Generalized Functions," Cambridge Univ. Press, 1959.

25. Bateman, H. et al., "Tables of Integral Transforms," Vol. 1, McGraw-Hill, N.Y., 1954.

26. Watson, G.N., "A Treatise on the Theory of Bessel Function," 2nd ed., Cambridge Univ. Press, 1944.

M∞⇨

kutta
condition

z

x

L.E.

T.E.

PLENUM CHAMBER
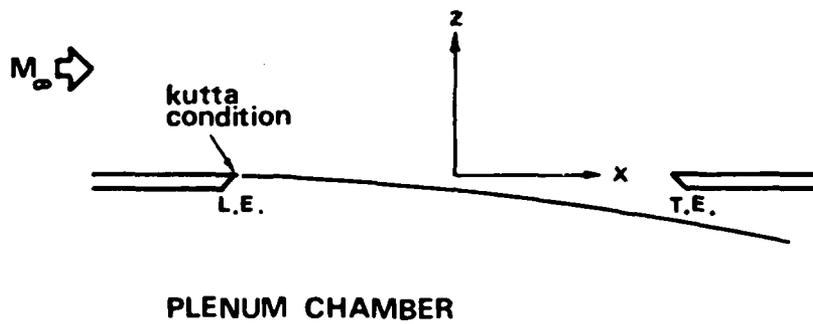
Fig.(3-1a) Two-dimensional slot flow.

LIFTING PROBLEM

M∞⇨

z

L.E.

x T.E.

p = 0

w = known

p = 0

kutta
condition

SLOT PROBLEM

M∞⇨

z

L.E.

x T.E.

w = 0

P = known

w = 0

kutta
condition
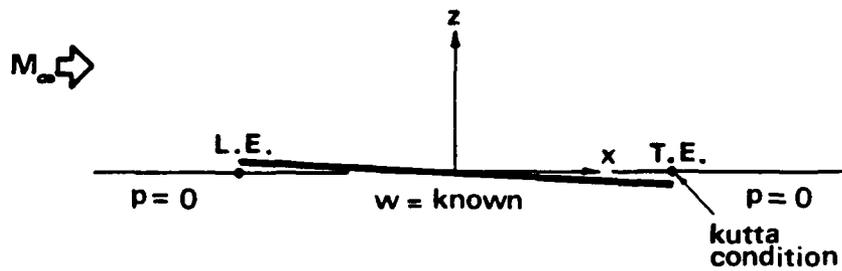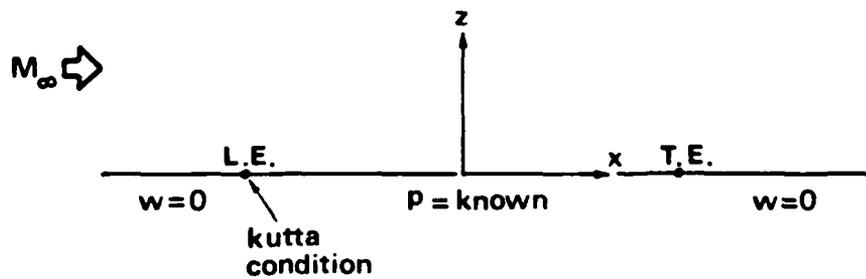
Fig.(3-1b) Schematic illustration of the analogy between the 2D lifting
and slot flows.
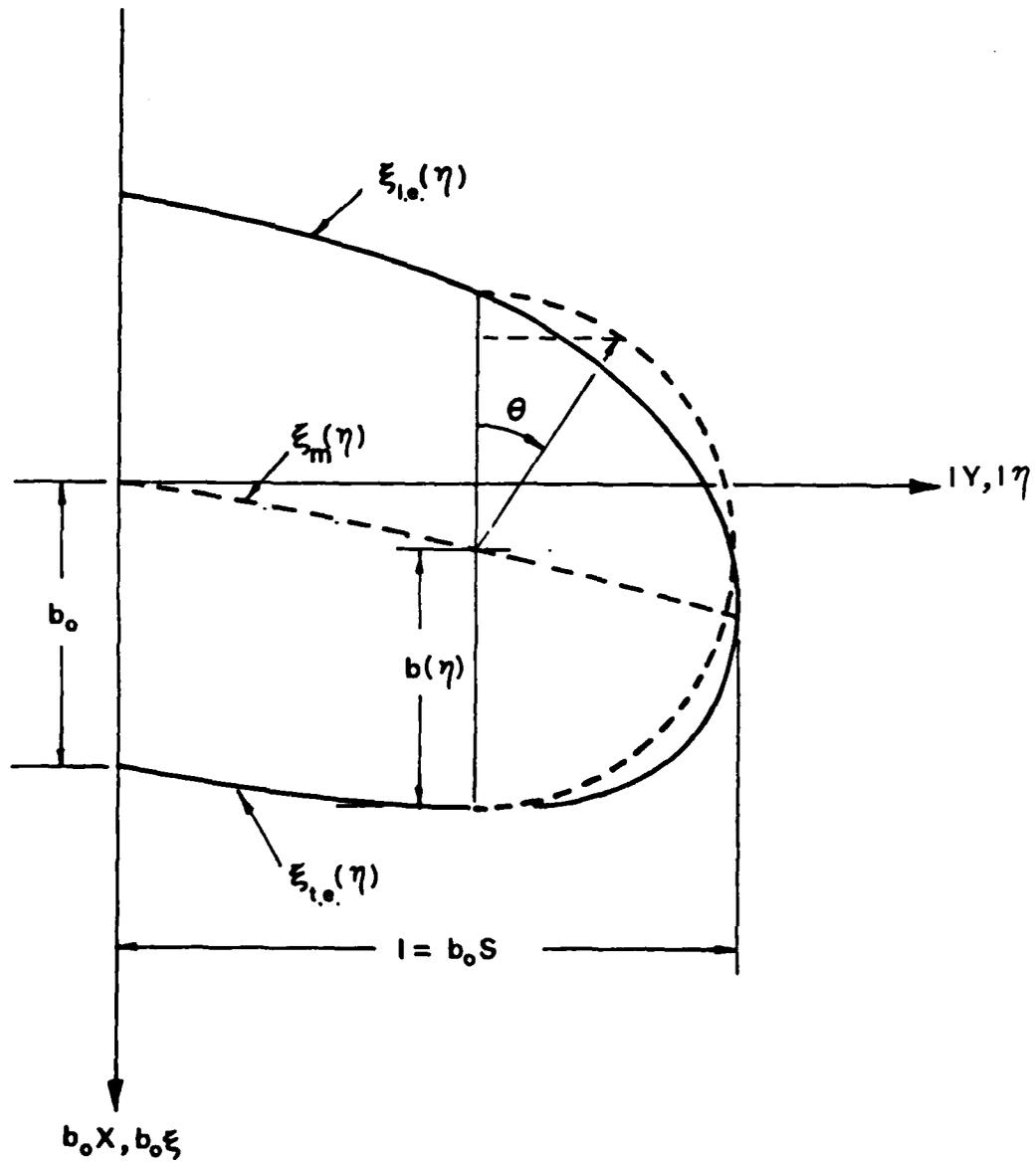
Fig.(3-2) The coordinate system and non-dimensional notation used in Watkin's kernel function method.
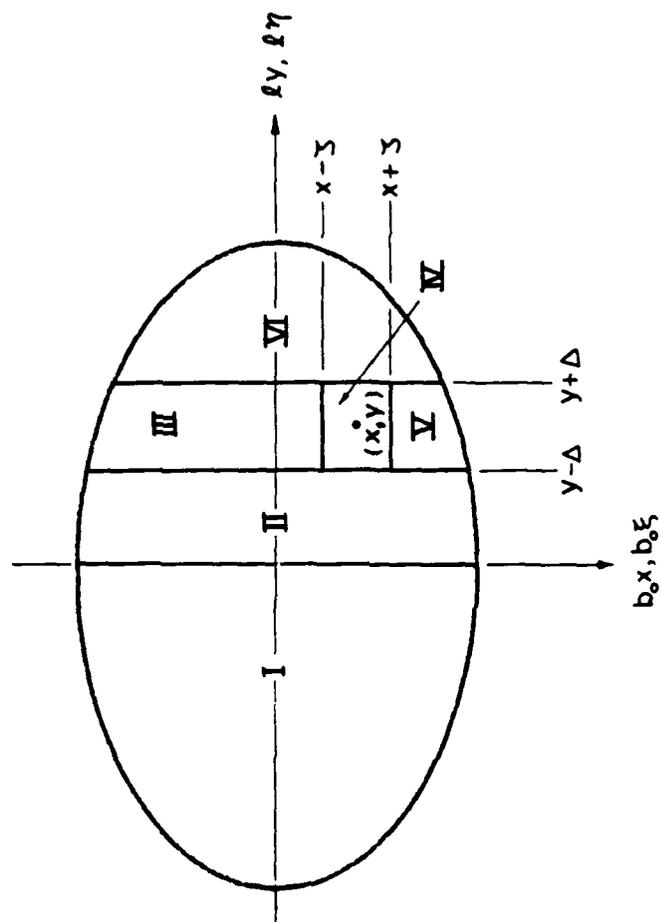
Fig. (3-3) Sub-regions of the planform used in the numerical scheme for the leaking-hole theory.
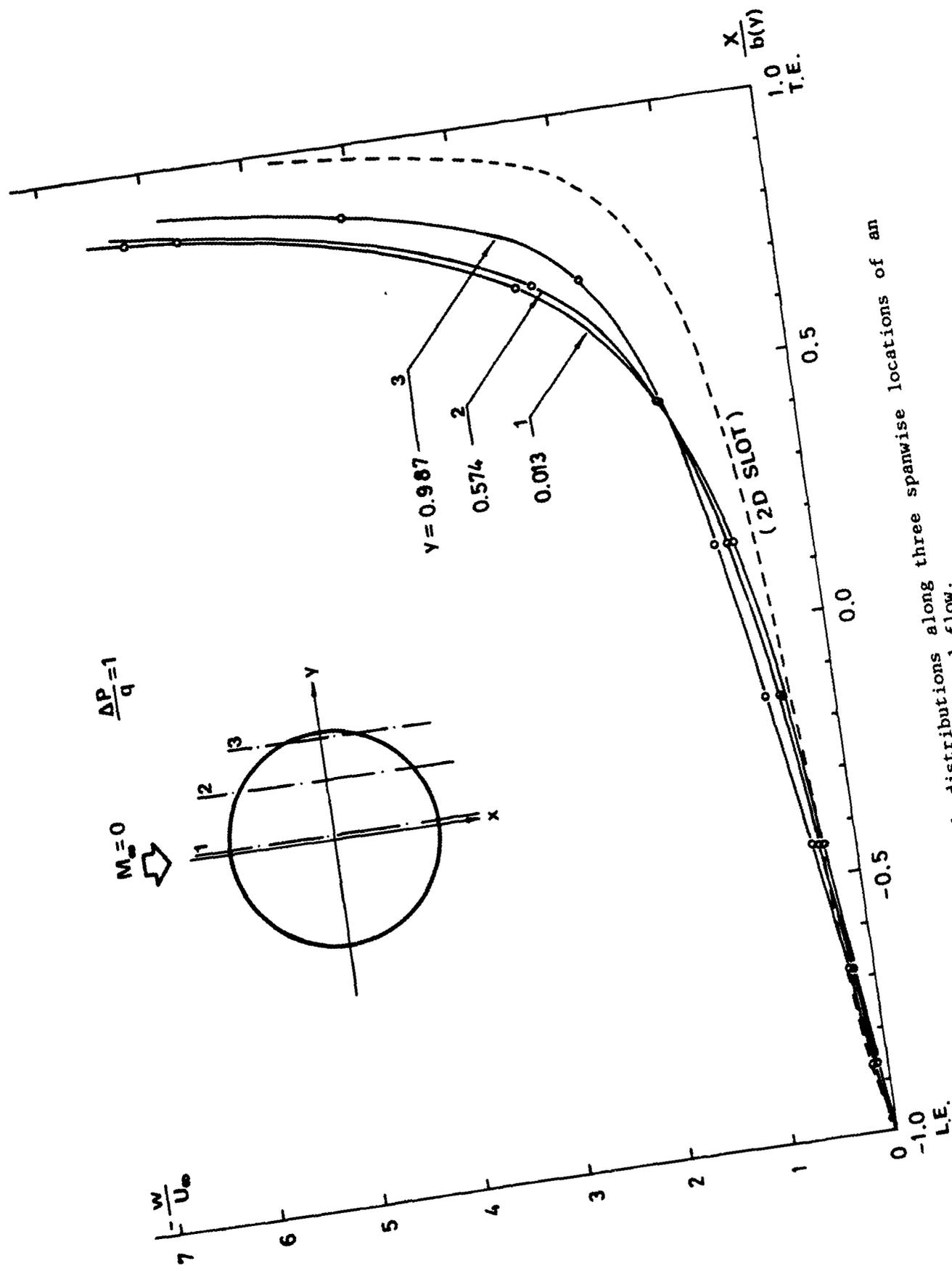
Fig. (3-4) Downwash distributions along three spanwise locations of an isolated round hole in the tunnel flow.
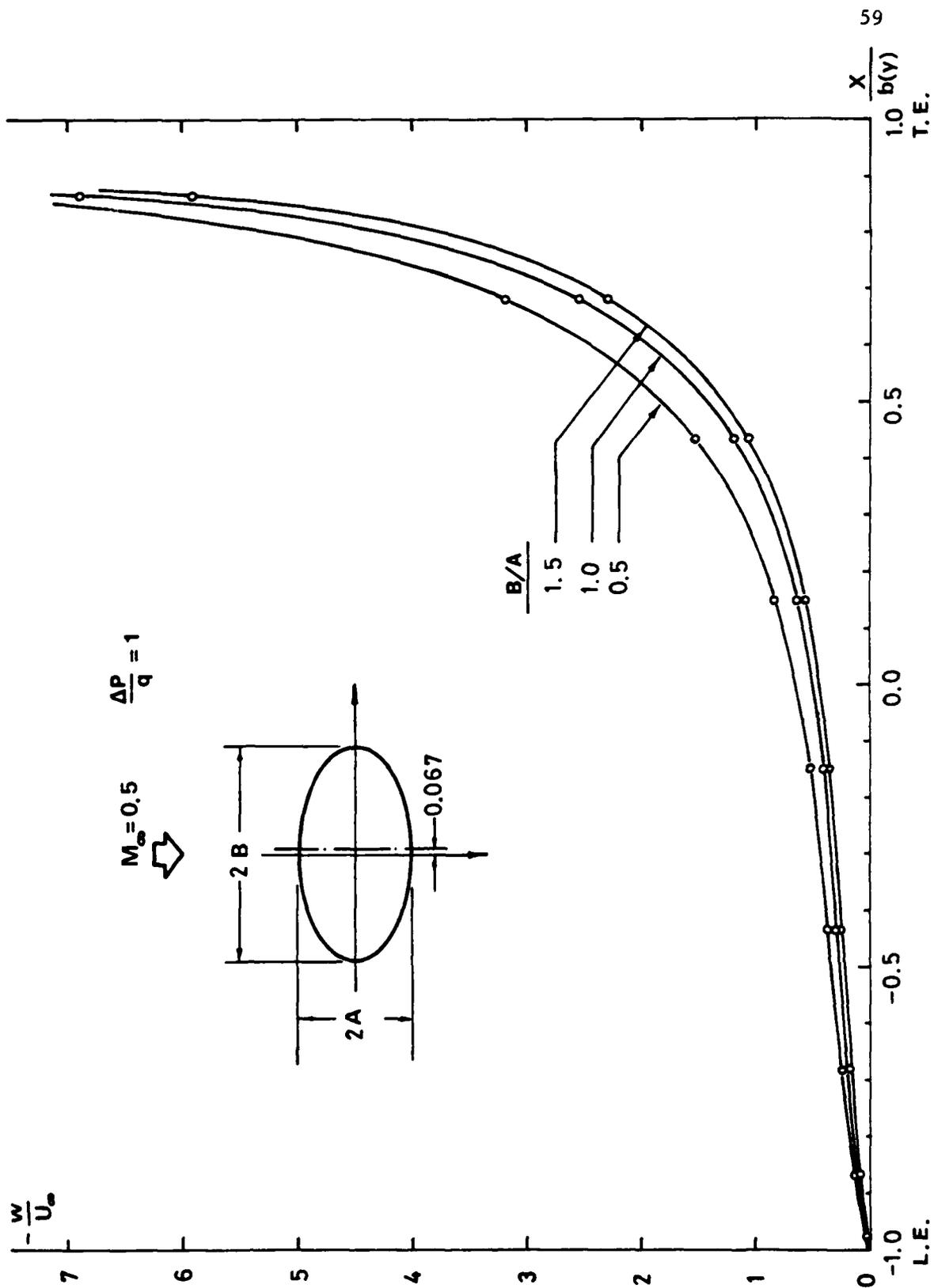
Fig.(3-5) Downwash distributions near the central region of the cross-
flow over three elliptic holes.
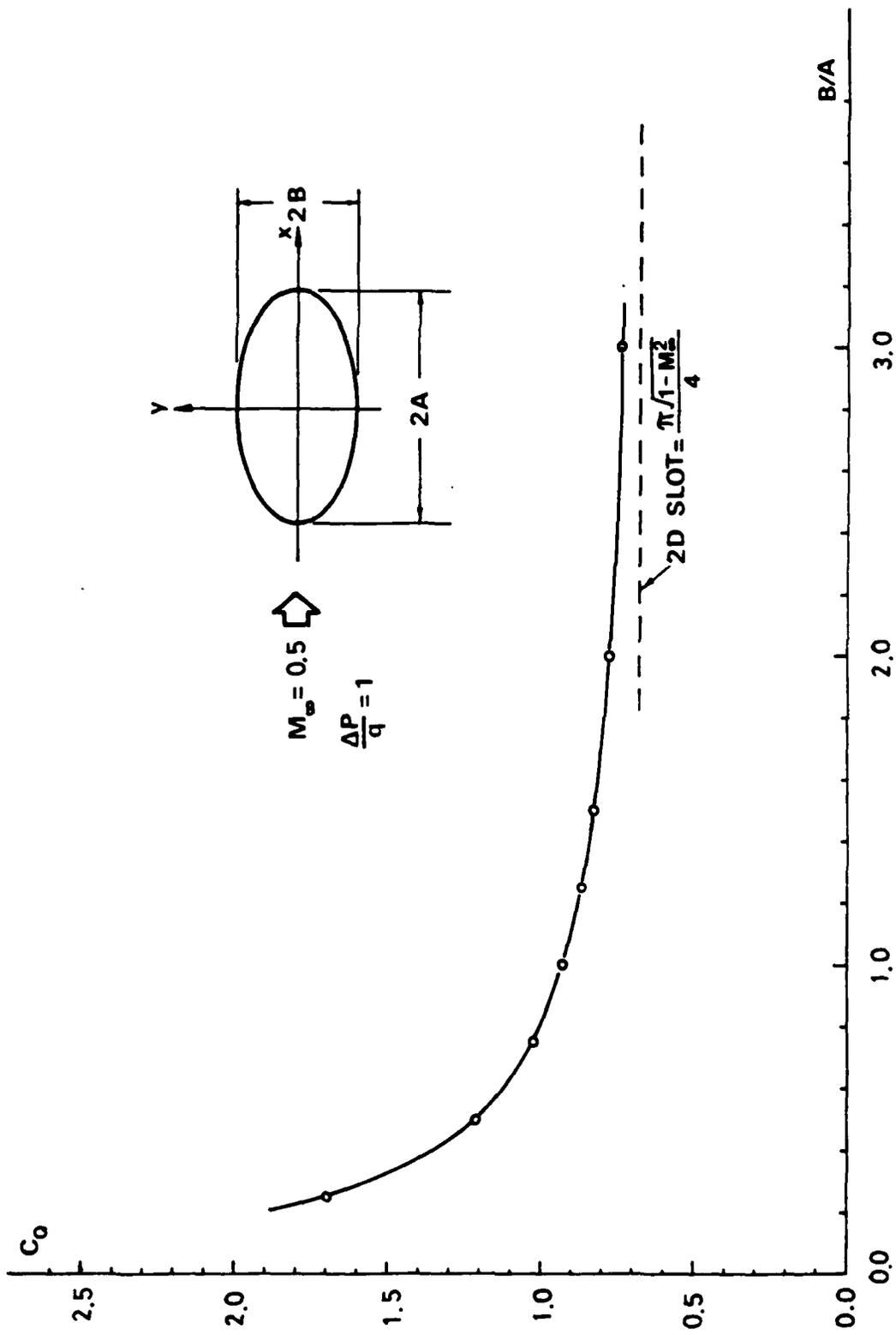
Fig.(3-6) Volume flowrate versus aspect ratio obtained from the numerical leading-hole theory.
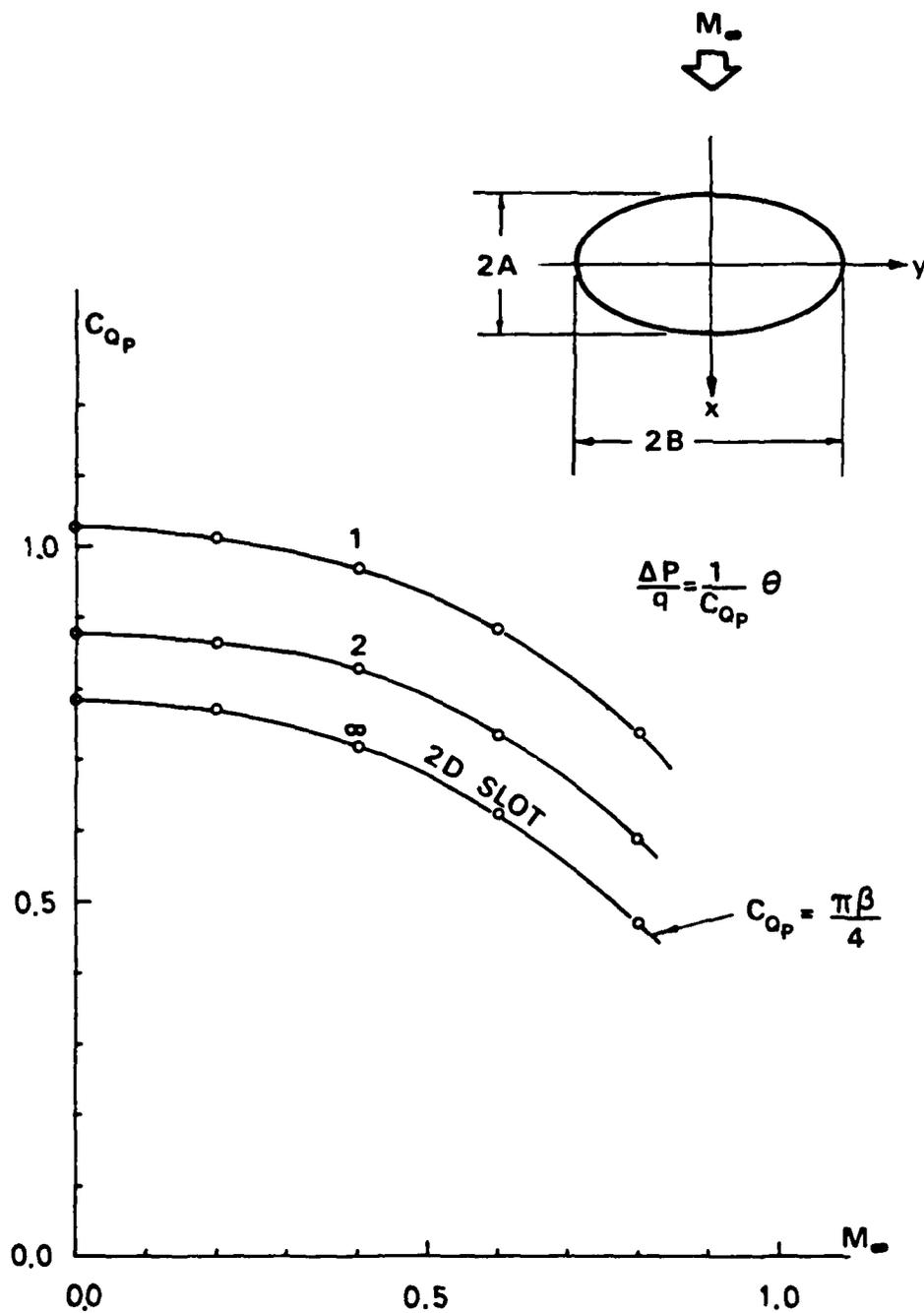
Fig.(3-7) Volume flowrate versus free-stream Mach number relationship obtained from the numerical leaking-hole theory.
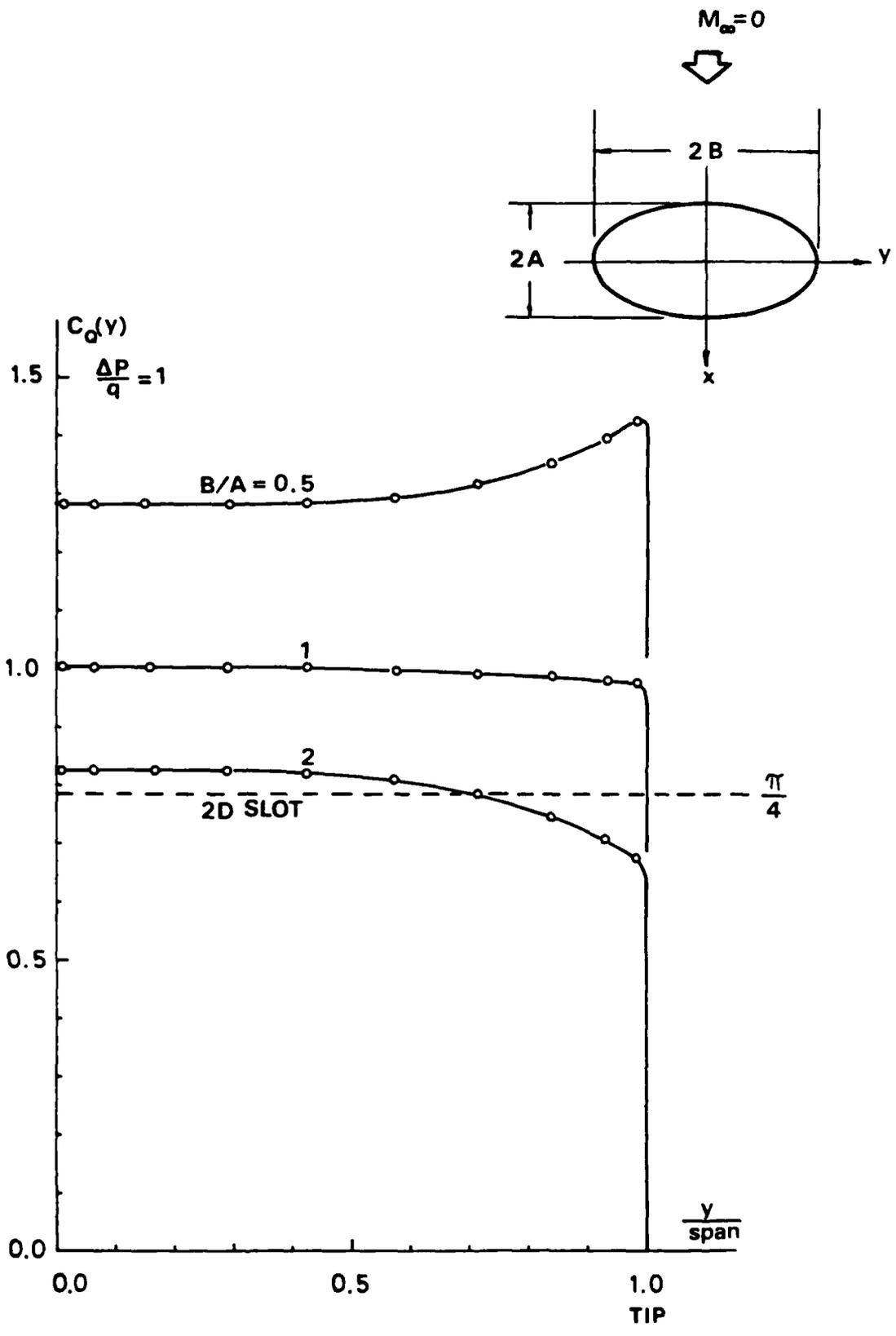
Fig.(3-8) Sectional volume flowrate distributions over finite-holes with aspect ratios 0.5,1.0, and 2.0.

63
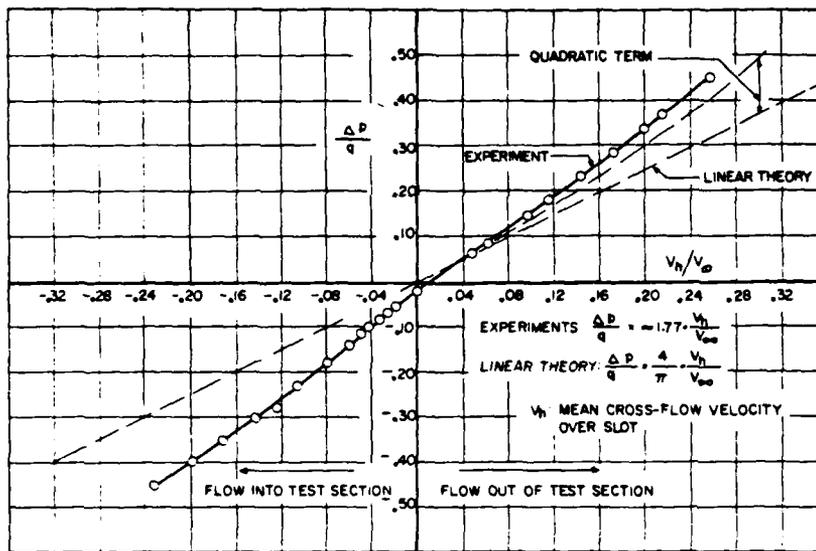
(a) Cross-flow characteristics of single transverse slot. (M∞=0.05)
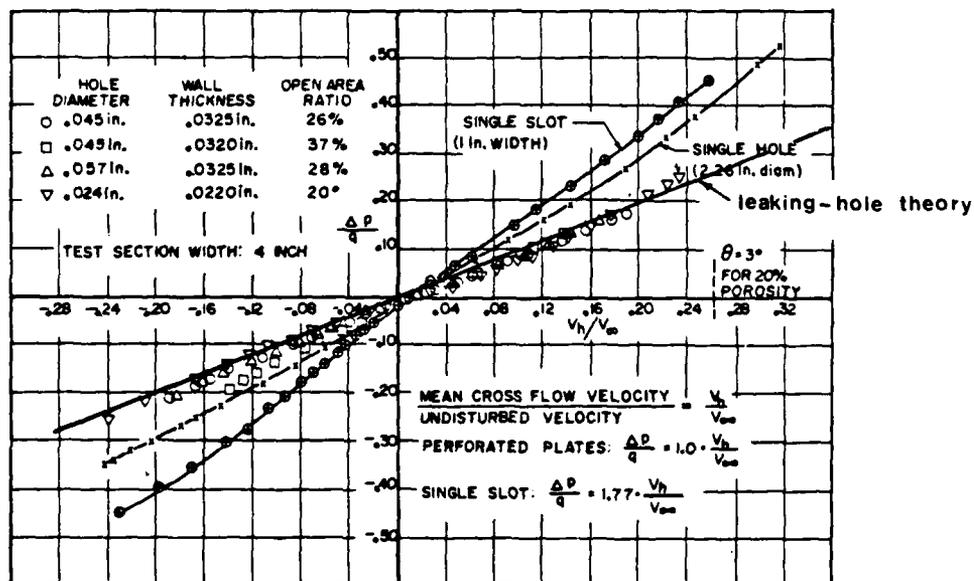
(b) Cross-flow characteristics of various perforated walls. (M∞=0.05)

Fig.(3-9) Comparisons of the cross-flow characteristics obtained from the present theory and experiment (Ref. 1)
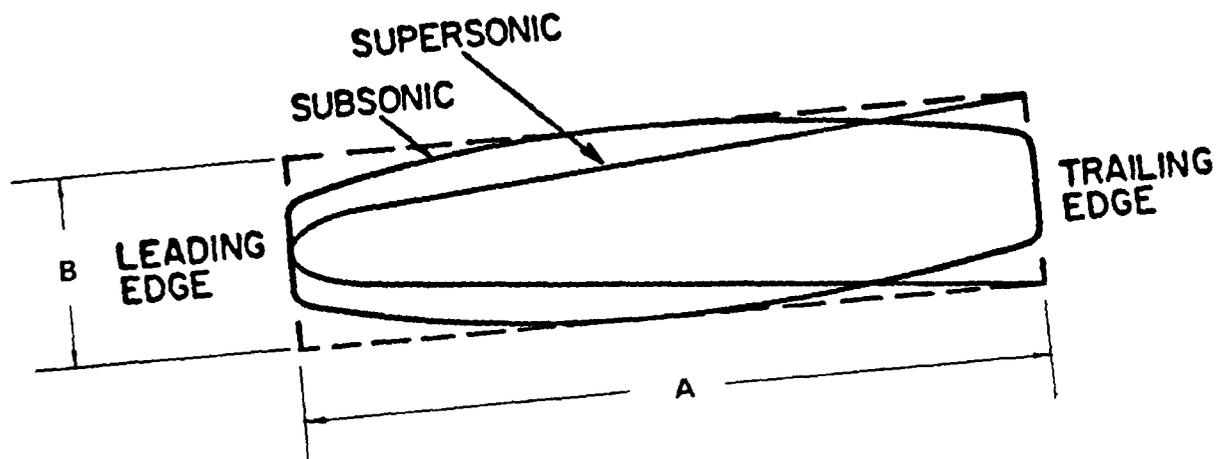
Fig. (3-10) Slot planforms for analytical solutions. (Ref. 12)
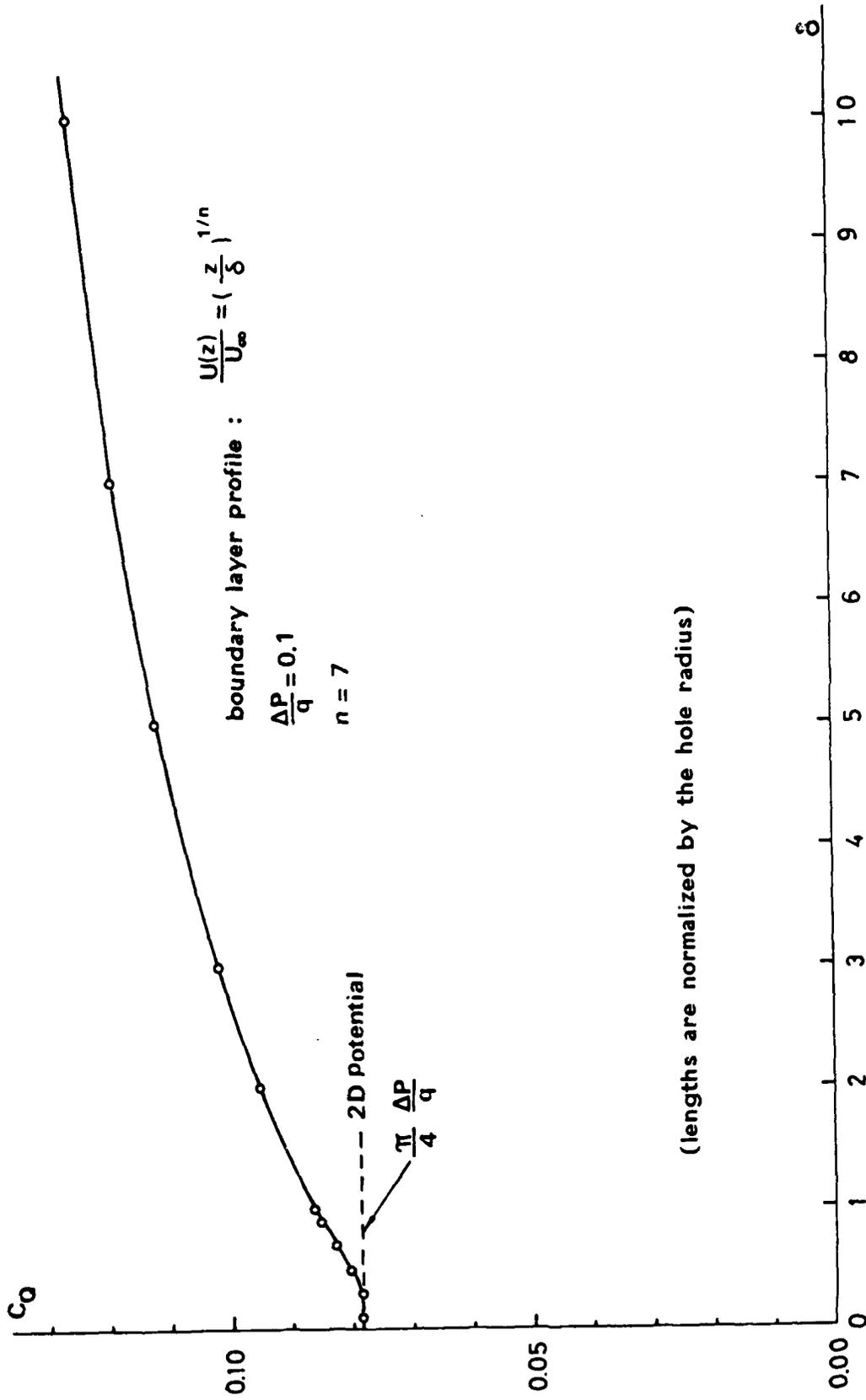
Fig. (3-24) Volume flowrate versus boundary layer thickness for a 1/7 power-law shear flow over a transverse slot.

78

boundary layer profile : $\frac{U(z)}{U_\infty} = (\frac{z}{\delta})^{1/n}$

n=7

$\frac{\Delta P}{q} = 0.1$

(lengths are normalized by the half slot width)
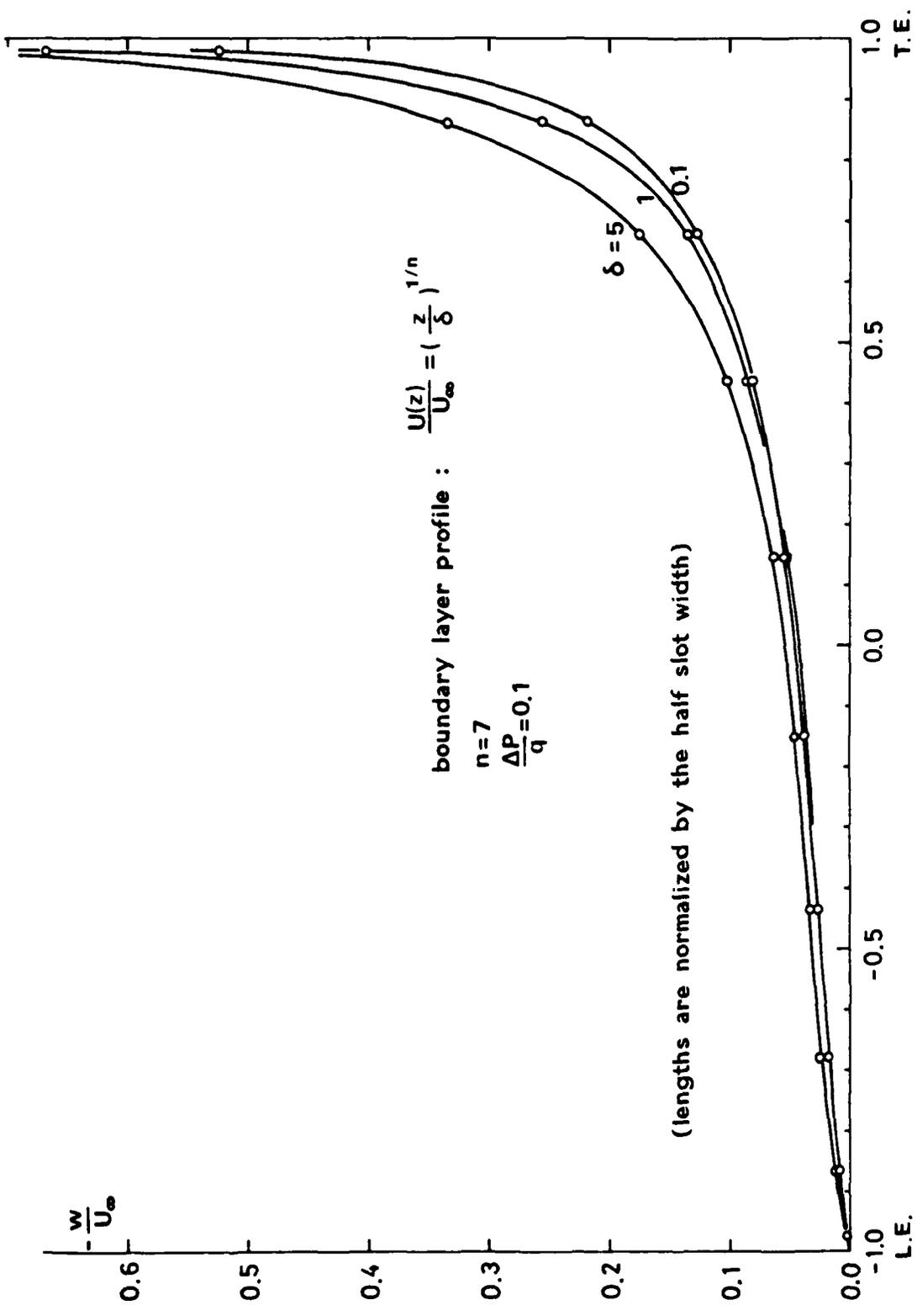
Fig.(3-23) Downwash distributions for a shear flow over a transverse slot with different boundary layer thicknesses.

df/dx : free surface slope distribution

boundary layer profile : $\dfrac{U(z)}{U_\infty} = \left(\dfrac{z}{\delta}\right)^{1/n}$

$n = 7$

$\dfrac{\Delta P}{q} = 0.1$

(lengths are normalized by the half slot width)
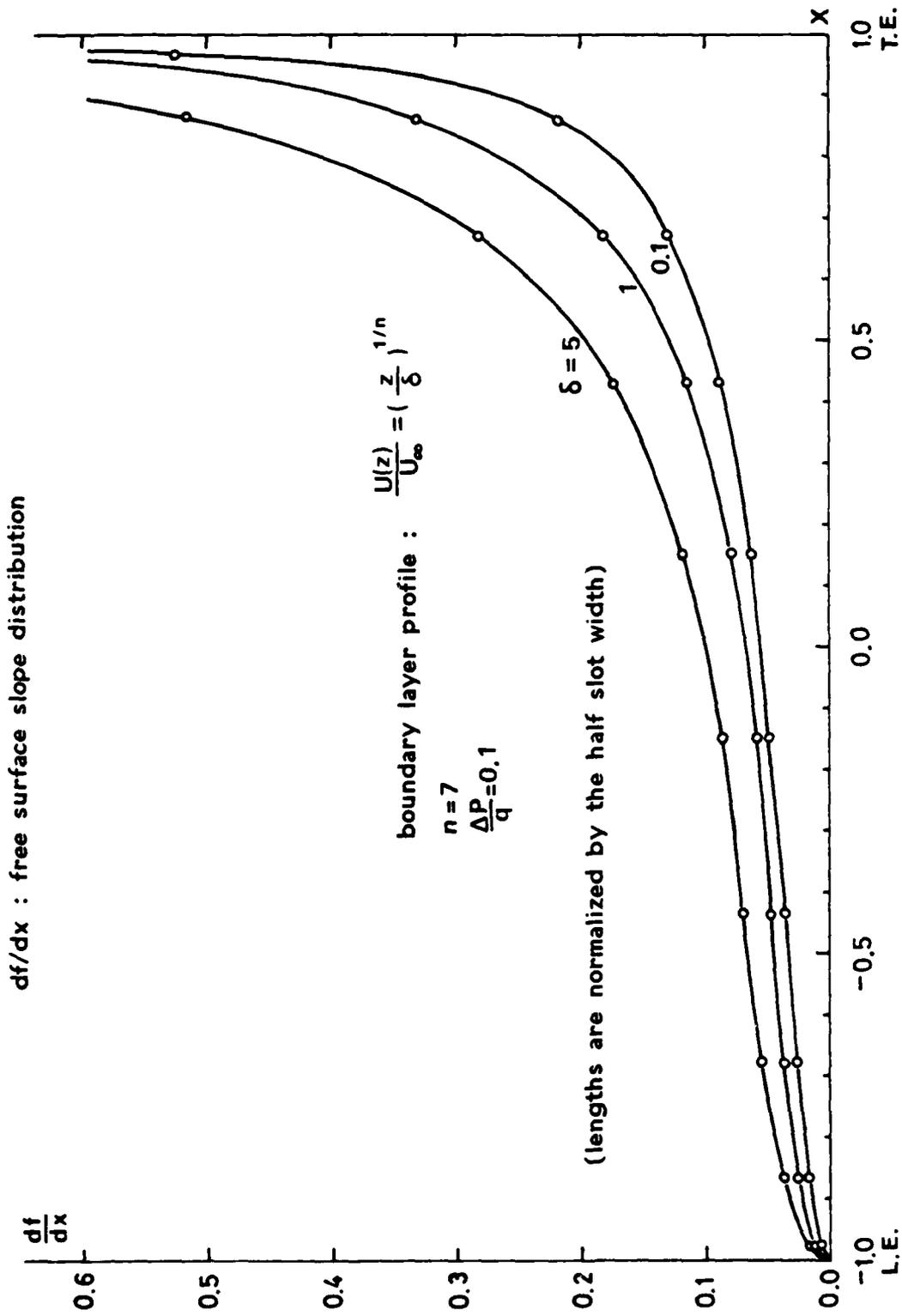
Fig.(3-22) Free surface slope distributions for a shear flow over a transverse slot with different boundary layer thicknesses.
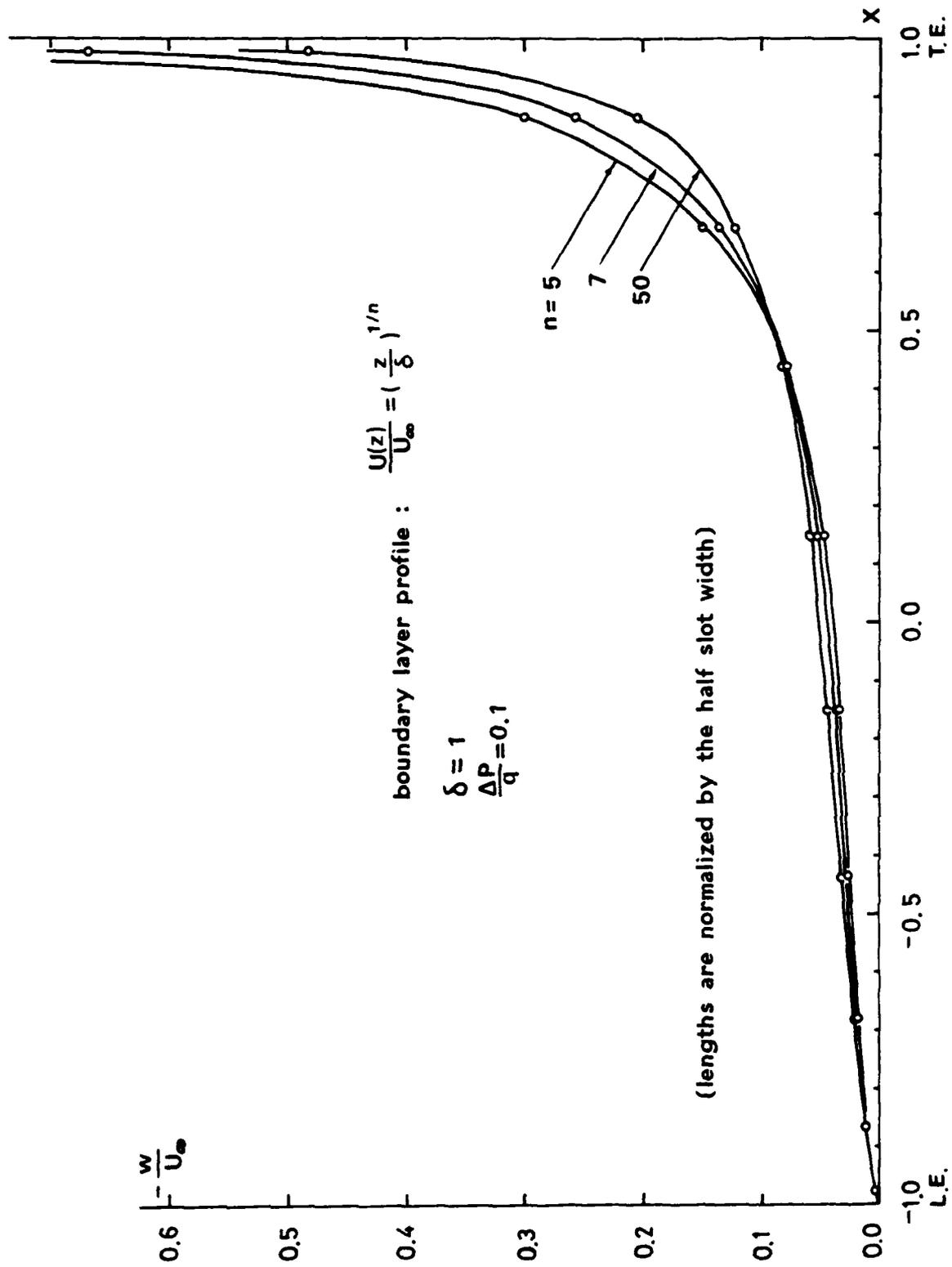
Fig.(3-21) Downwash distributions for a shear flow over a transverse slot with different boundary layer profiles.

df/dx : free surface slope distribution

boundary layer profile : $\frac{U(z)}{U_\infty} = (\frac{z}{\delta})^{1/n}$

$\delta = 1$

$\frac{\Delta P}{q} = 0.1$

(lengths are normalized by the half slot width)

$\frac{df}{dx}$
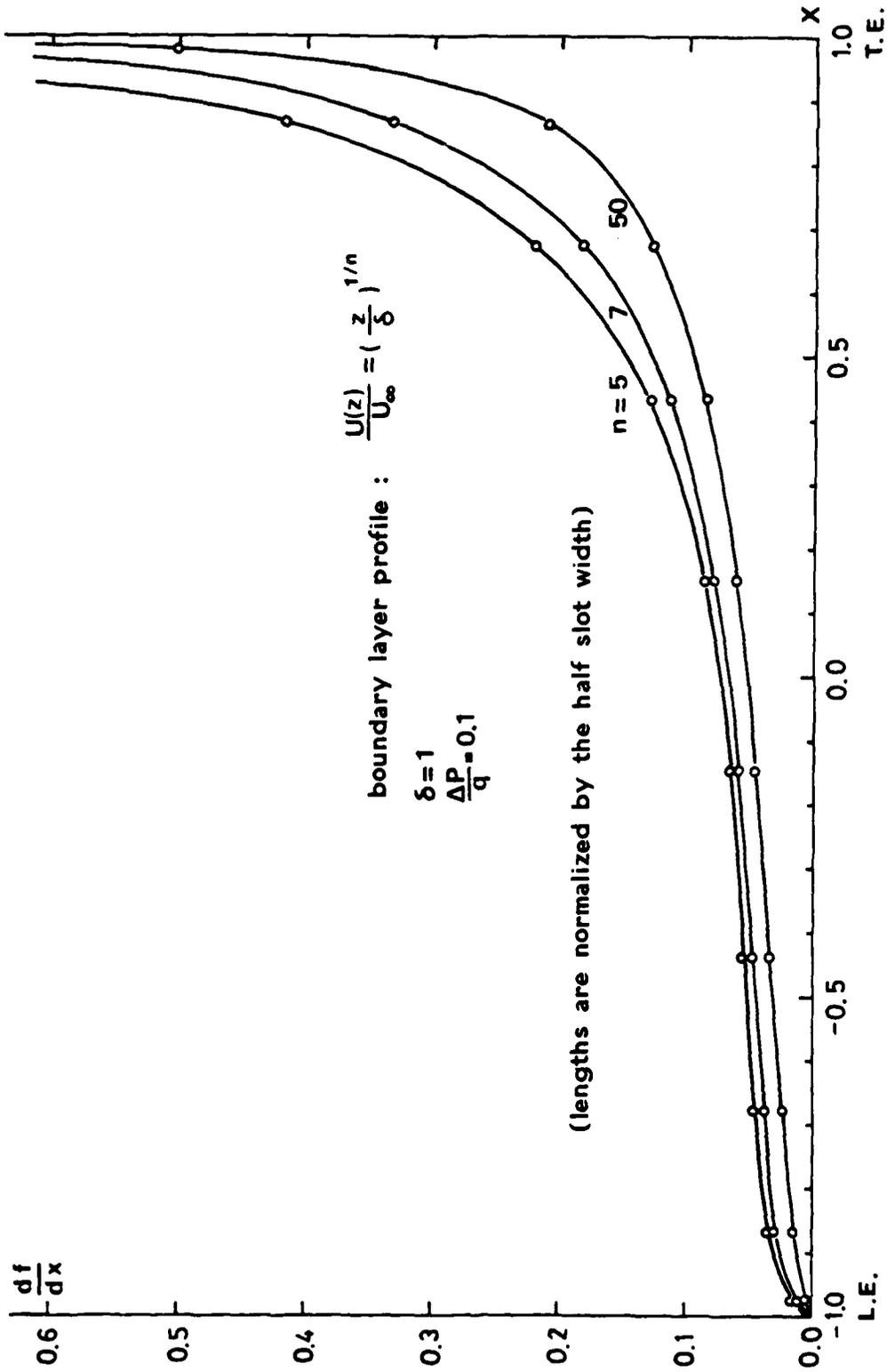
Fig.(3-20) Free surface slope distributions for a shear flow over a transverse slot with different boundary layer profiles.

boundary layer profile : $\frac{U(z)}{U_\infty} = (\frac{z}{\delta})^{1/n}$

n = 7

2D potential

$\beta = 0.1$

1.0

5.

(lengths are normalized by the half slot width)

$\frac{\Delta P}{q}$

$\frac{w_m}{U_\infty}$
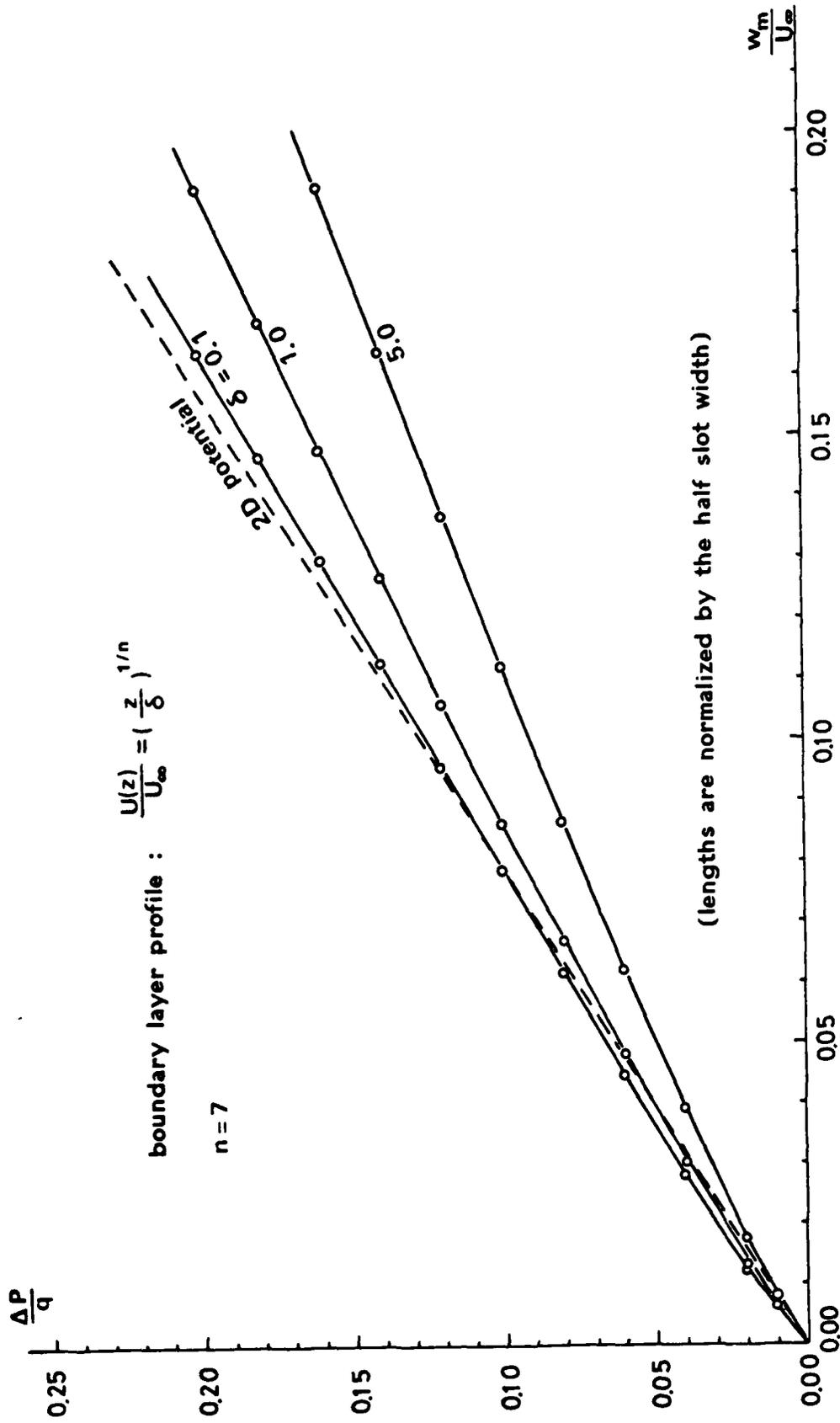
Fig.(3-19) Pressure differential versus average flow deflection angle for a transverse slot in shear flows with different boundary layer thicknesses.

boundary layer profile : $\frac{U(z)}{U_\infty} = (\frac{z}{\delta})^{1/n}$

$\frac{\Delta P}{q} = 0.1$

$\delta = 1$

(lengths are normalized by the half slot width)

$\frac{\pi}{4} \frac{\Delta P}{q}$

(potential)
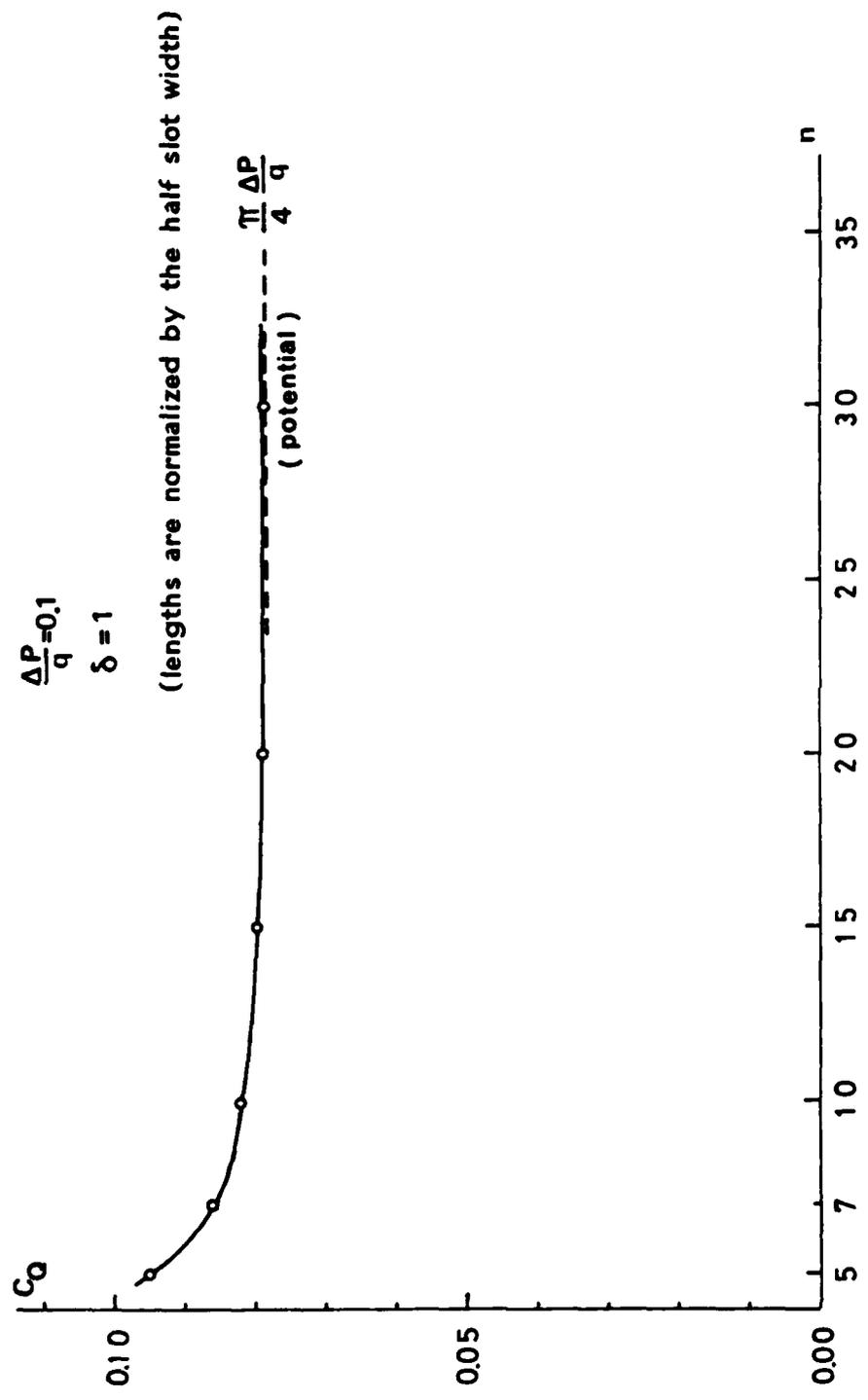
Fig.(3-18) Volume flowrate across a tranverse slot in a power-law profile shear flow.

TUNNEL FLOW

$$\frac{U(z)}{U_\infty} = \left(\frac{z}{\delta}\right)^{1/n}$$

δ

w Δx

f(x)

f(x) + $\frac{\partial f}{\partial x}\Delta$x

PLENUM CHAMBER

Δx
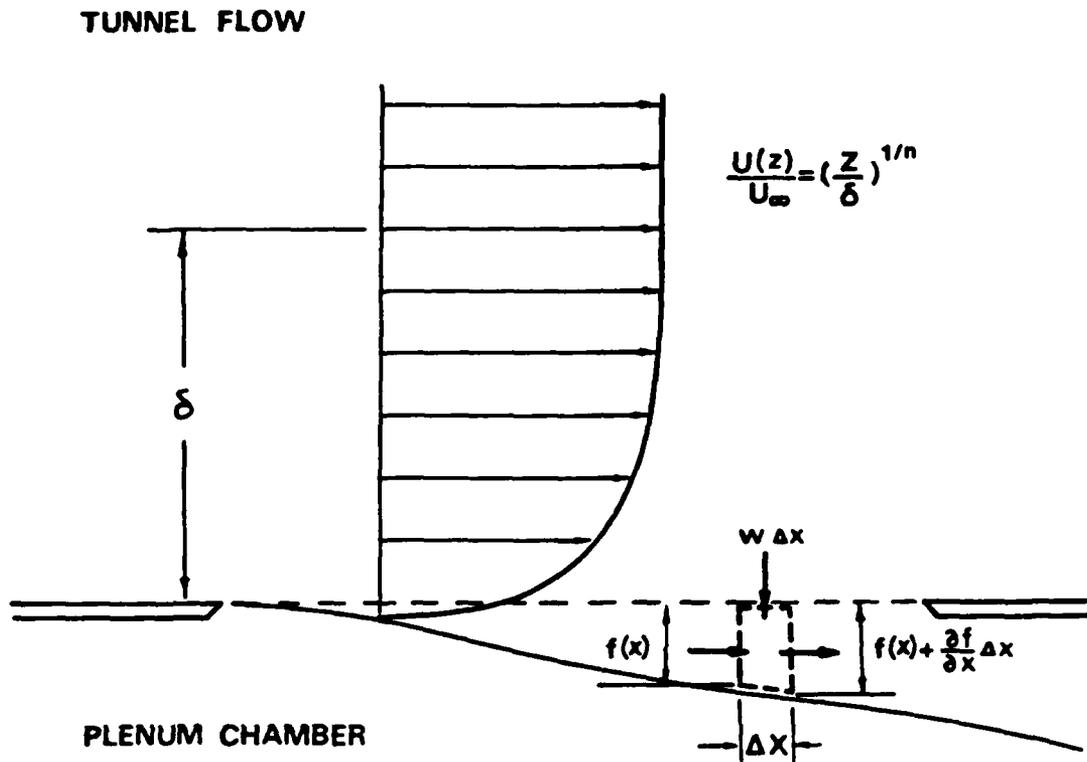
Fig.(3-17) Sketch of the control volume for the relation between entrance plane downwash and free surface slope distributions of a shear flow over a slot or hole.
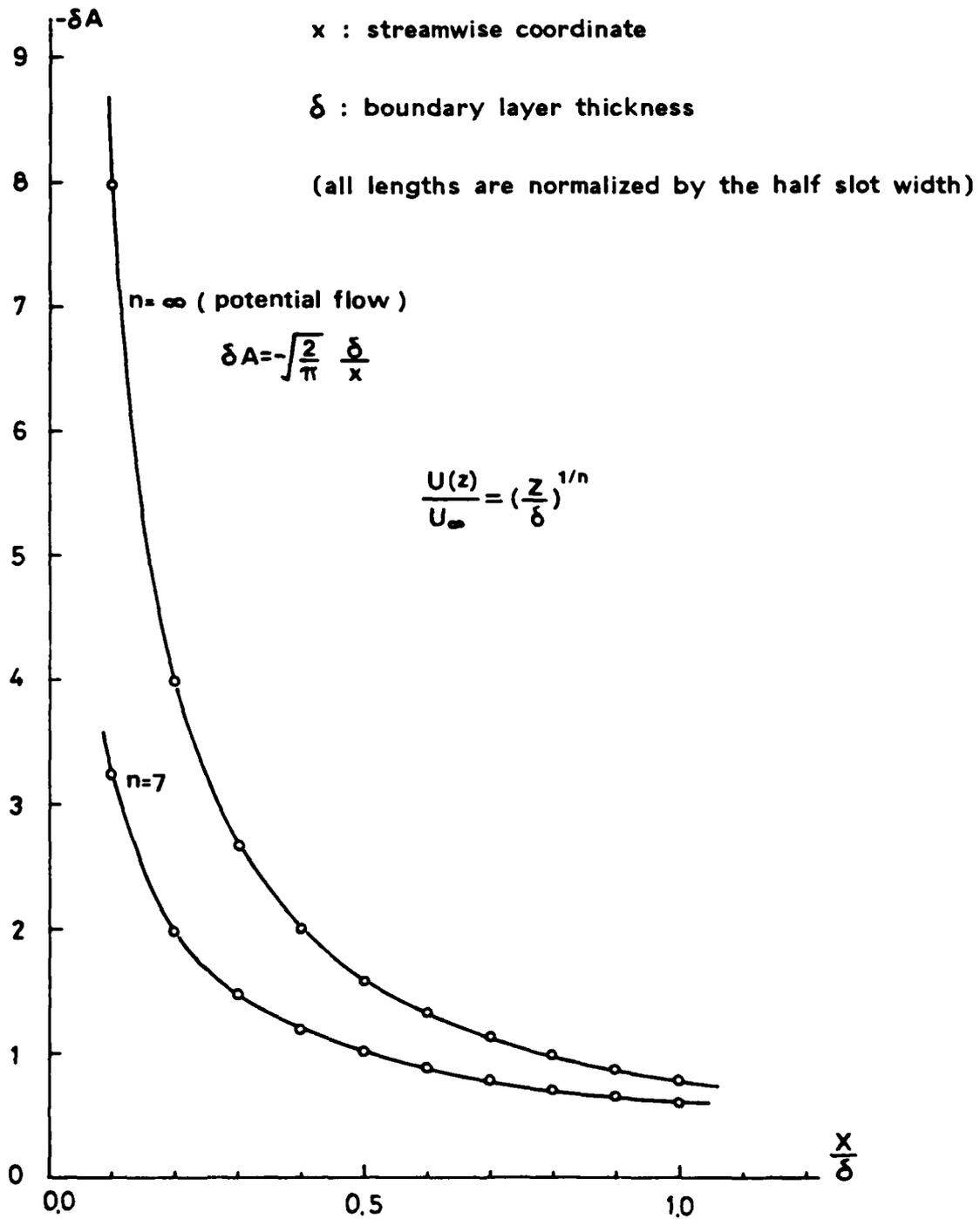
Fig.(3-16) Kernel function for a parallel shear flow over a 2D transverse slot.
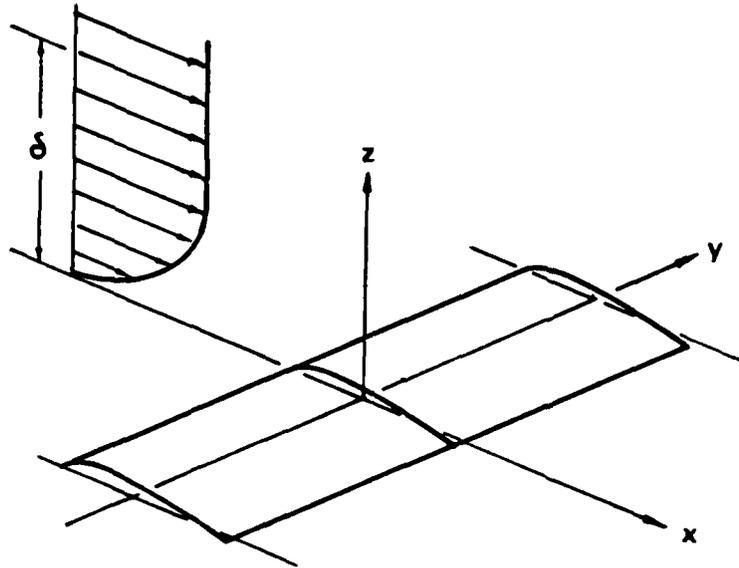
(a) Shear flow over a wing
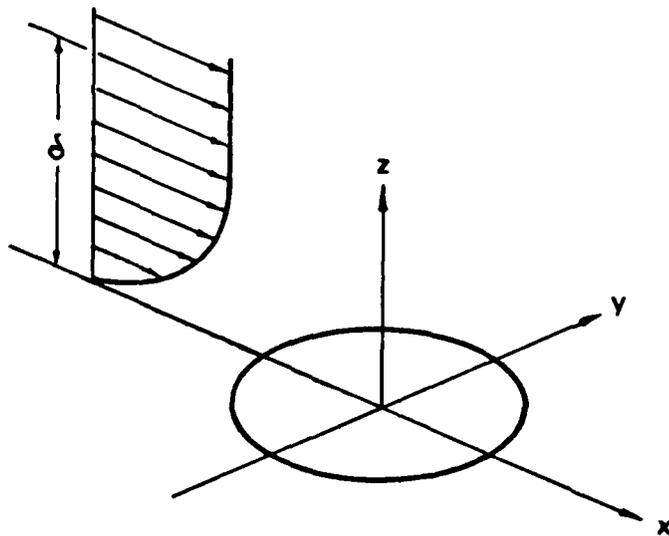
(b) Shear flow over a hole on a wall.

Fig.(3-15) Shear flow aerodynamics.
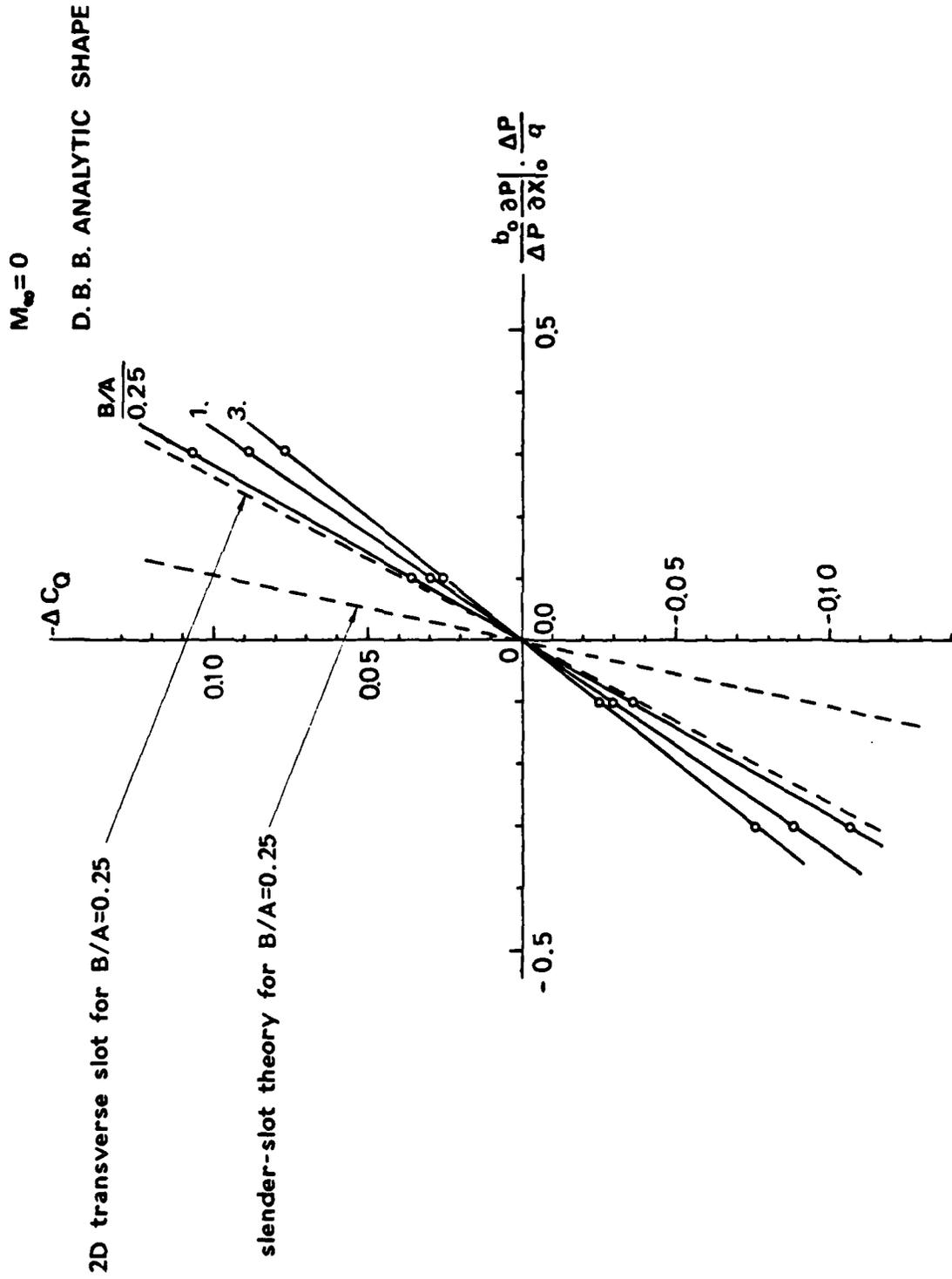
Fig. (3-14) Influence of the pressure gradient effect on the total volume flowrate across holes obtained by the slender-slot, leaking-hole, and leaking-slot theories.
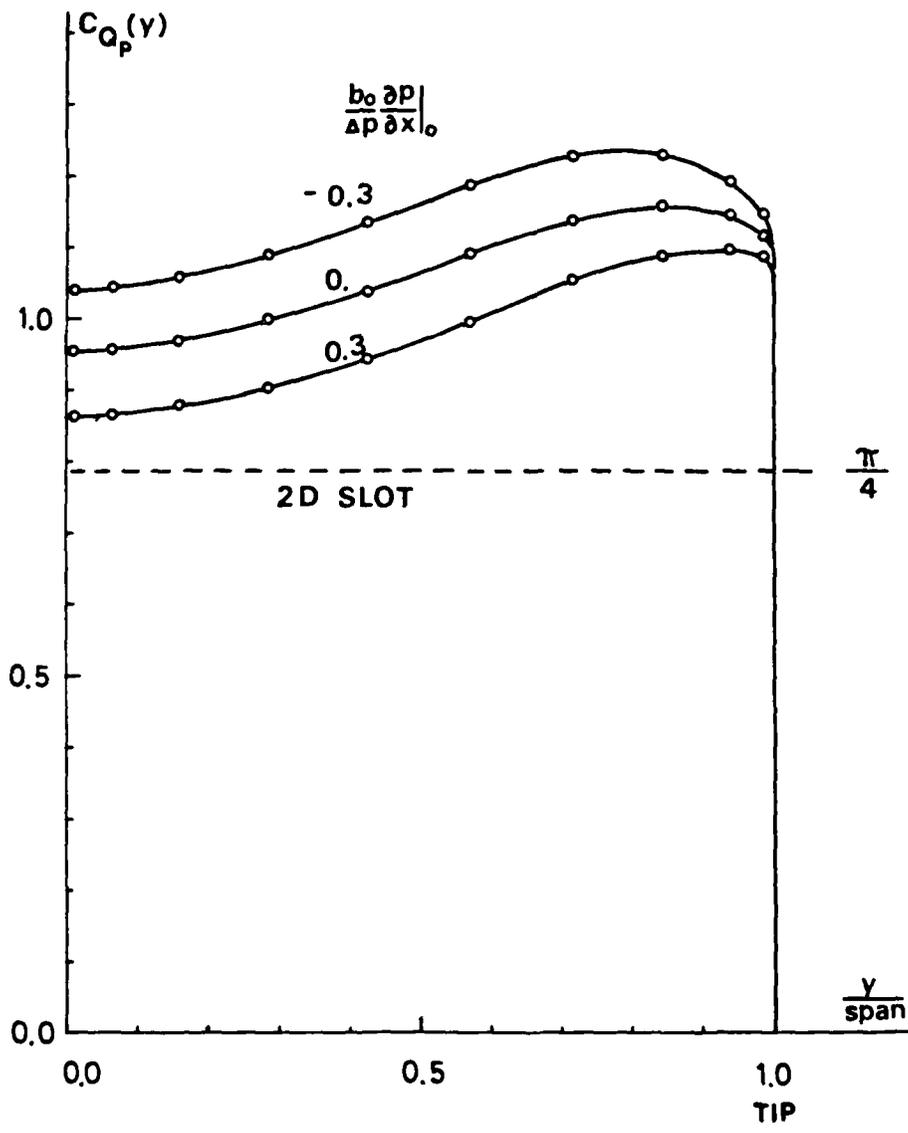
Fig.(3-13) Sectional volume flowrate distributions of the cross-flow over a finite-hole with imposed pressure gradients.
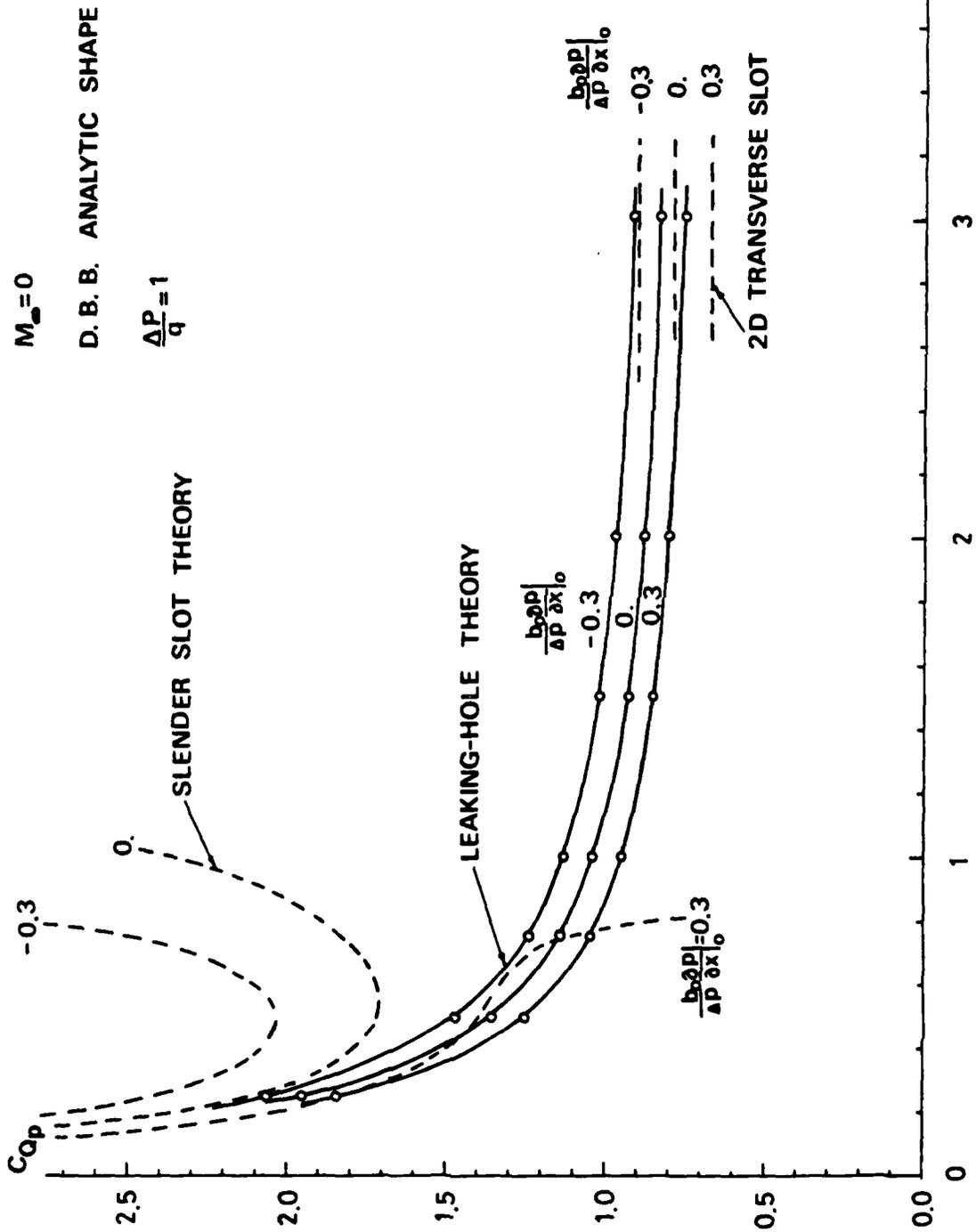
Fig. (3-12) Volume flowrate versus aspect ratio obtained from the slender-slot, leaking-hole, and leaking-slot theories with imposed pressure gradient effect considered.
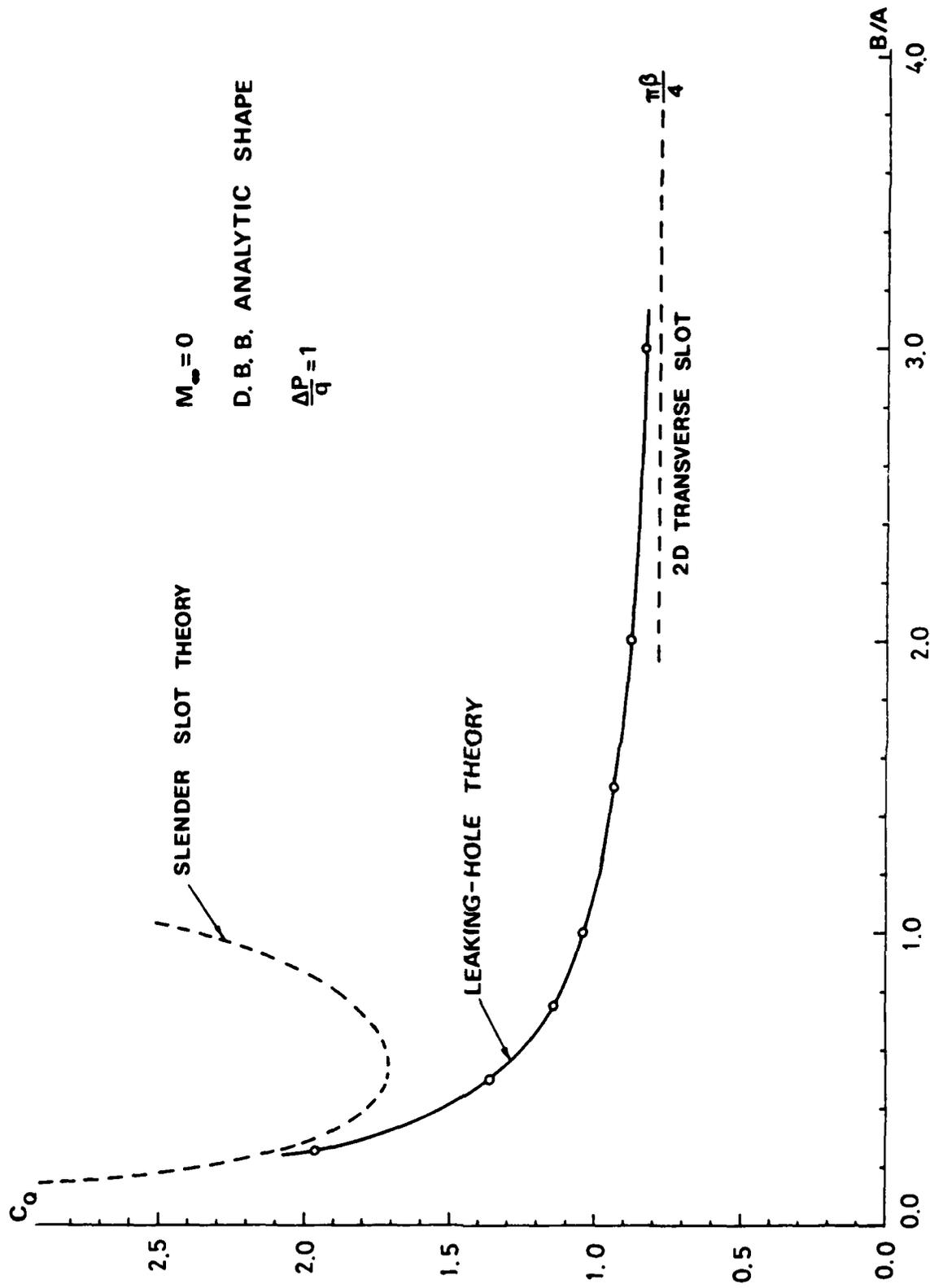
Fig.(3-11) Volume flowrate versus aspect ratio obtained from the slender-slot, leaking-hole, and leaking-slot(transverse) theories.
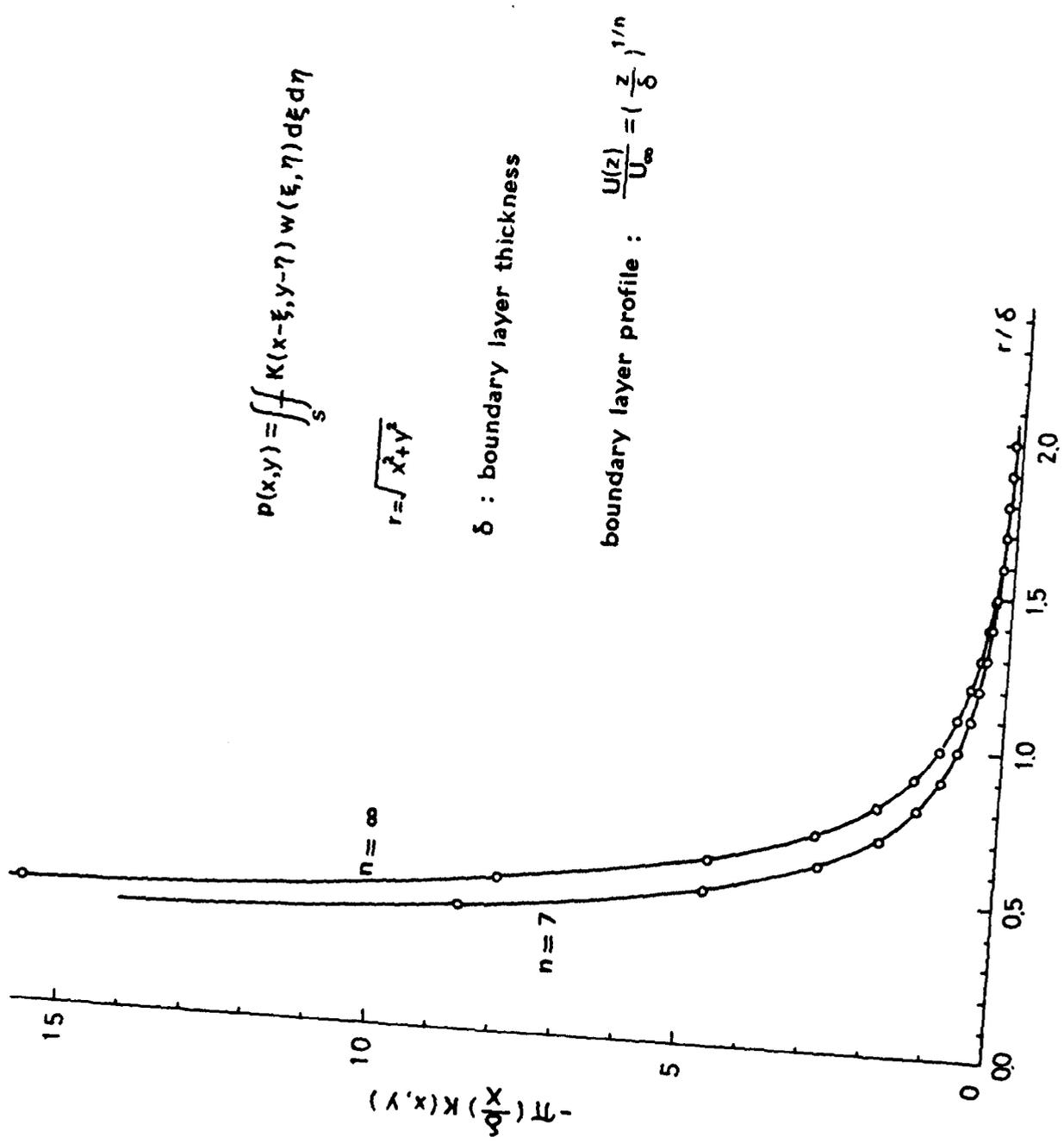
$$p(x,y) = \iint_S K(x-\xi, y-\eta) w(\xi,\eta) d\xi d\eta$$

$$r = \sqrt{x^2 + y^2}$$

δ : boundary layer thickness

boundary layer profile : $\dfrac{U(z)}{U_\infty} = (\dfrac{z}{\delta})^{1/n}$
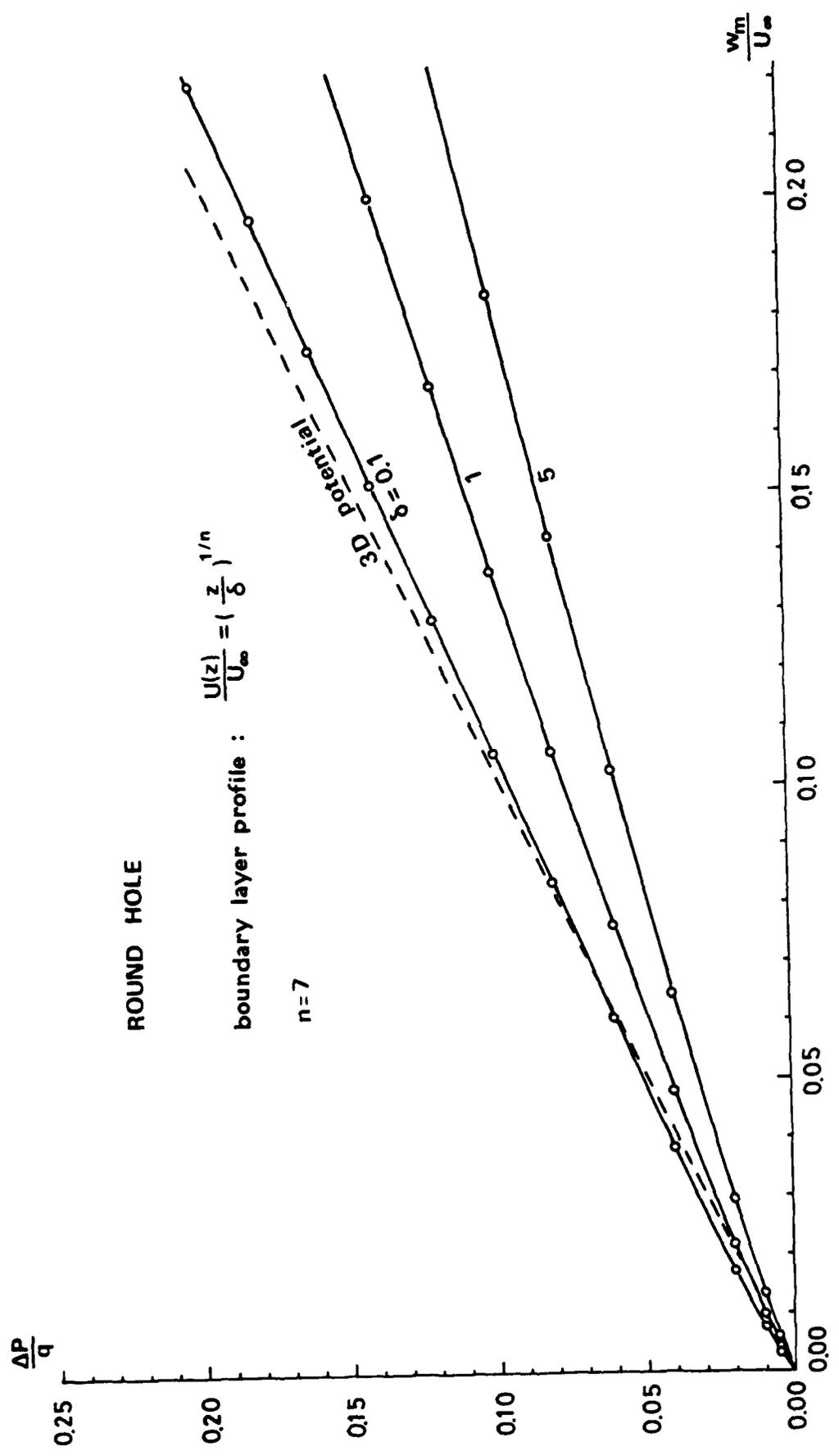
Fig. (3-25) Kernel functions for a parallel shear flow over a 3-D finite hole.

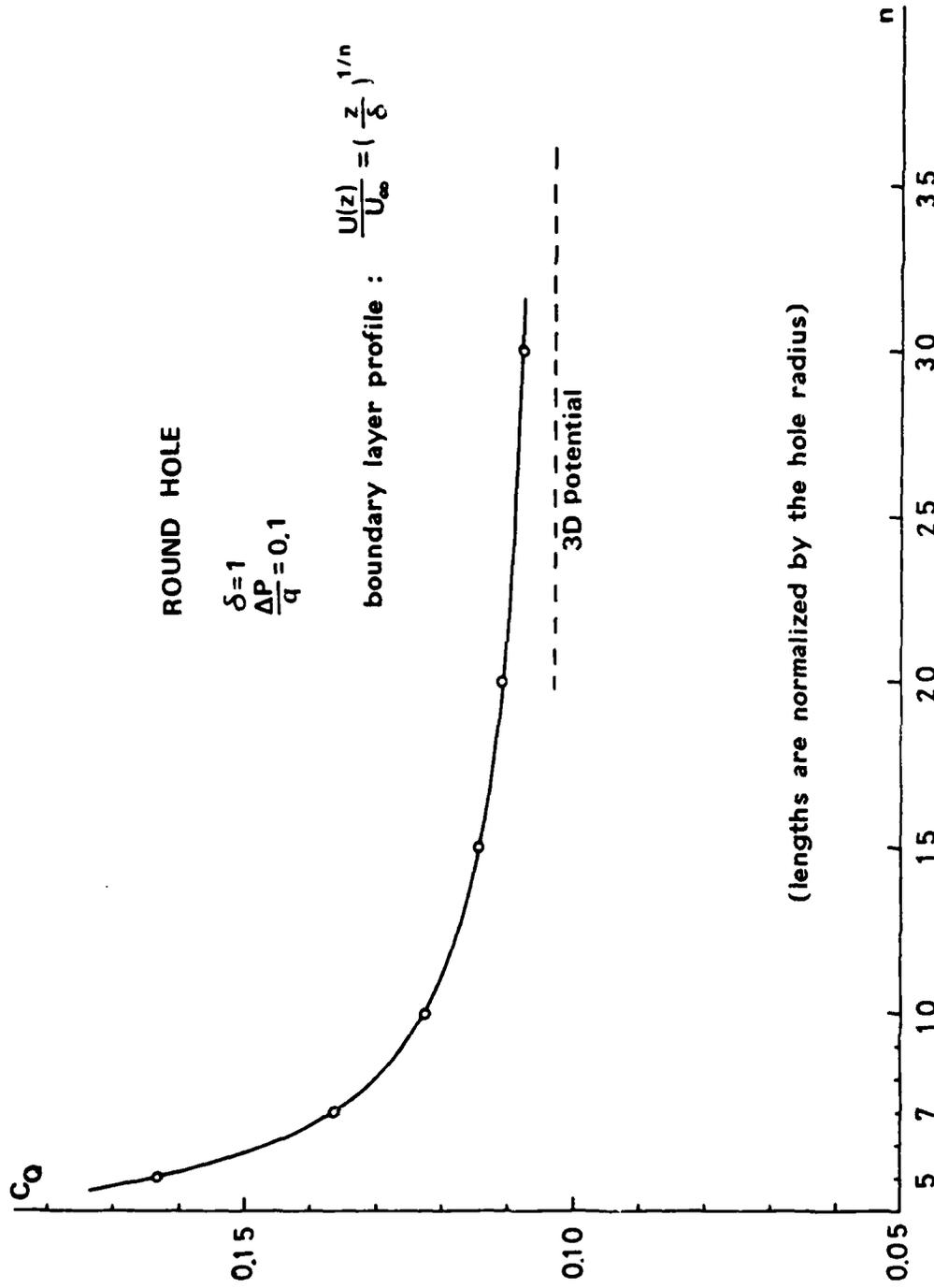Fig.(3-26) Cross-flow characteristics of a shear flow over a round hole with different boundary layer thicknesses.

80

ROUND HOLE

$\delta = 1$
$\frac{\Delta P}{q} = 0.1$

boundary layer profile : $\frac{U(z)}{U_\infty} = \left(\frac{z}{\delta}\right)^{1/n}$

— — — 3D Potential

(lengths are normalized by the hole radius)

Fig.(3-27) Volume flowrate across a round hole in shear flows with power-law profiles.

ROUND HOLE

$\delta = 1$

$\frac{\Delta P}{q} = 0.1$

boundary layer profile : $\frac{U(z)}{U_\infty} = \left(\frac{z}{\delta}\right)^{1/n}$

$C_Q(y)$

0.15

n = 7

10

30

0.10

Potential

0.05

(lengths are normalized by the hole radius)

$\frac{y}{span}$
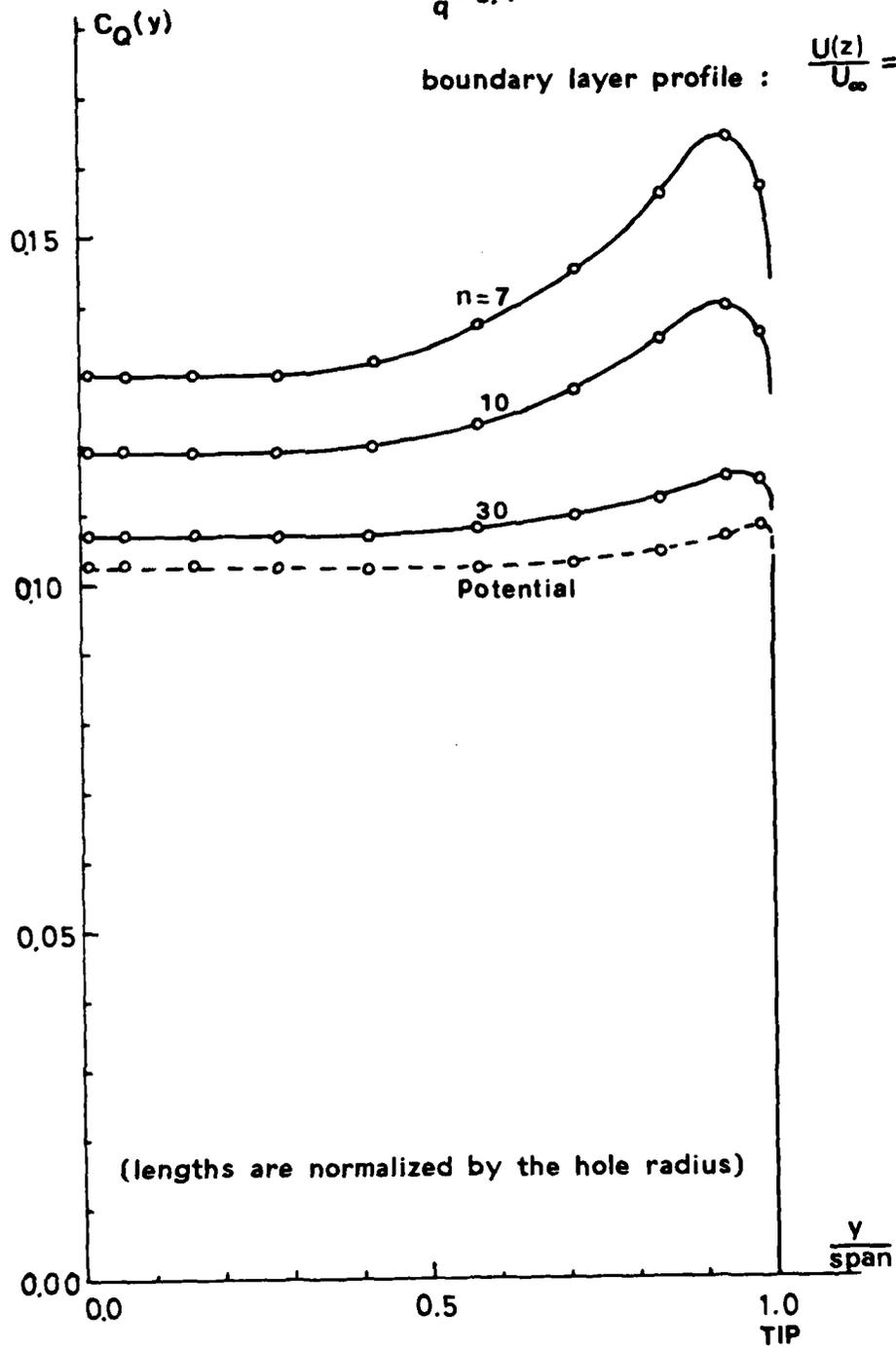
0.00

0.0   0.5   1.0

TIP

Fig.(3-28) Sectional volume flowrate distributions for a round hole in a
power-law profile shear flow.

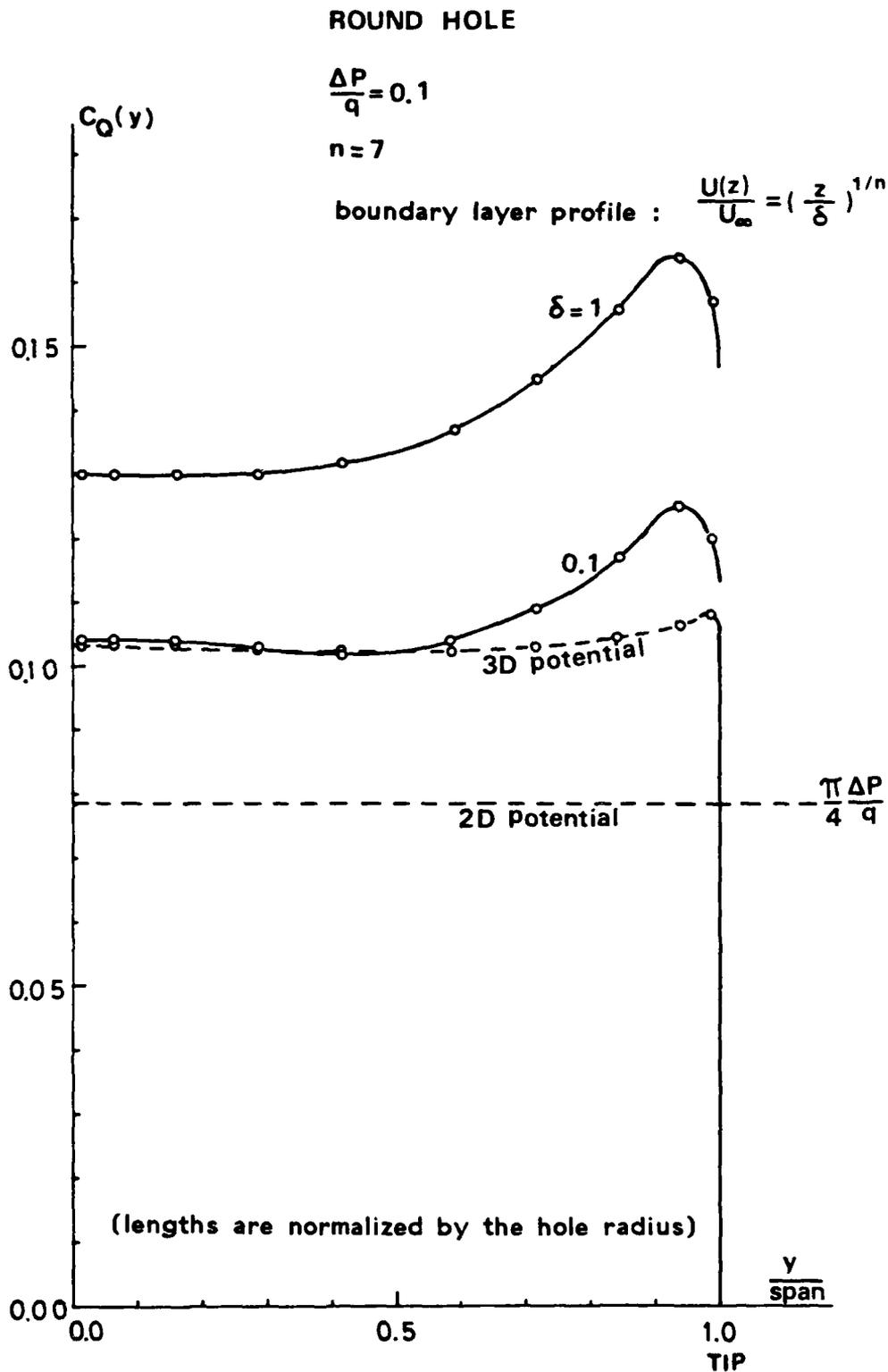Fig.(3-29) Sectional volume flowrate distributions for a round hole in shear flows with different boundary layer thicknesses.
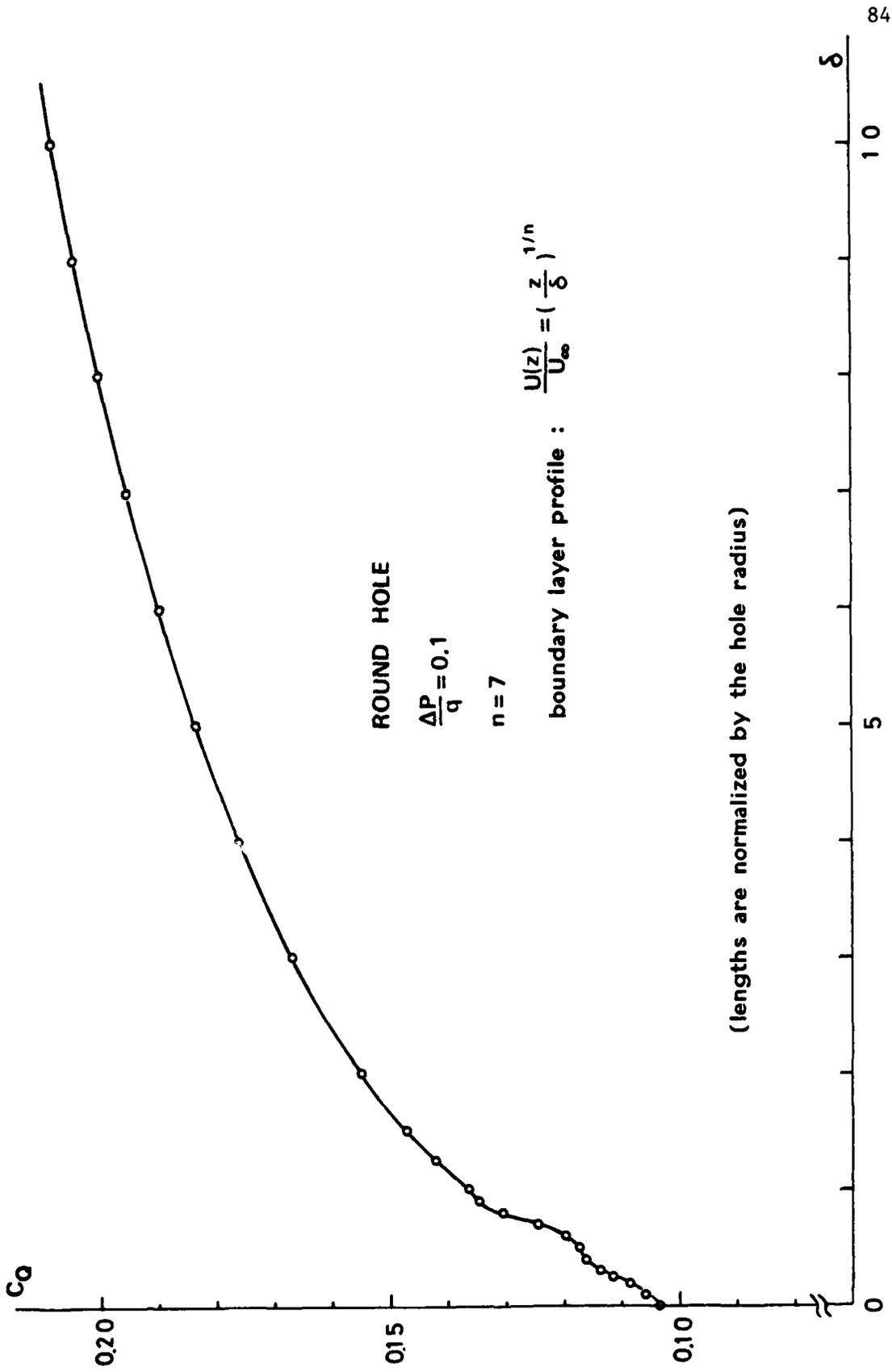
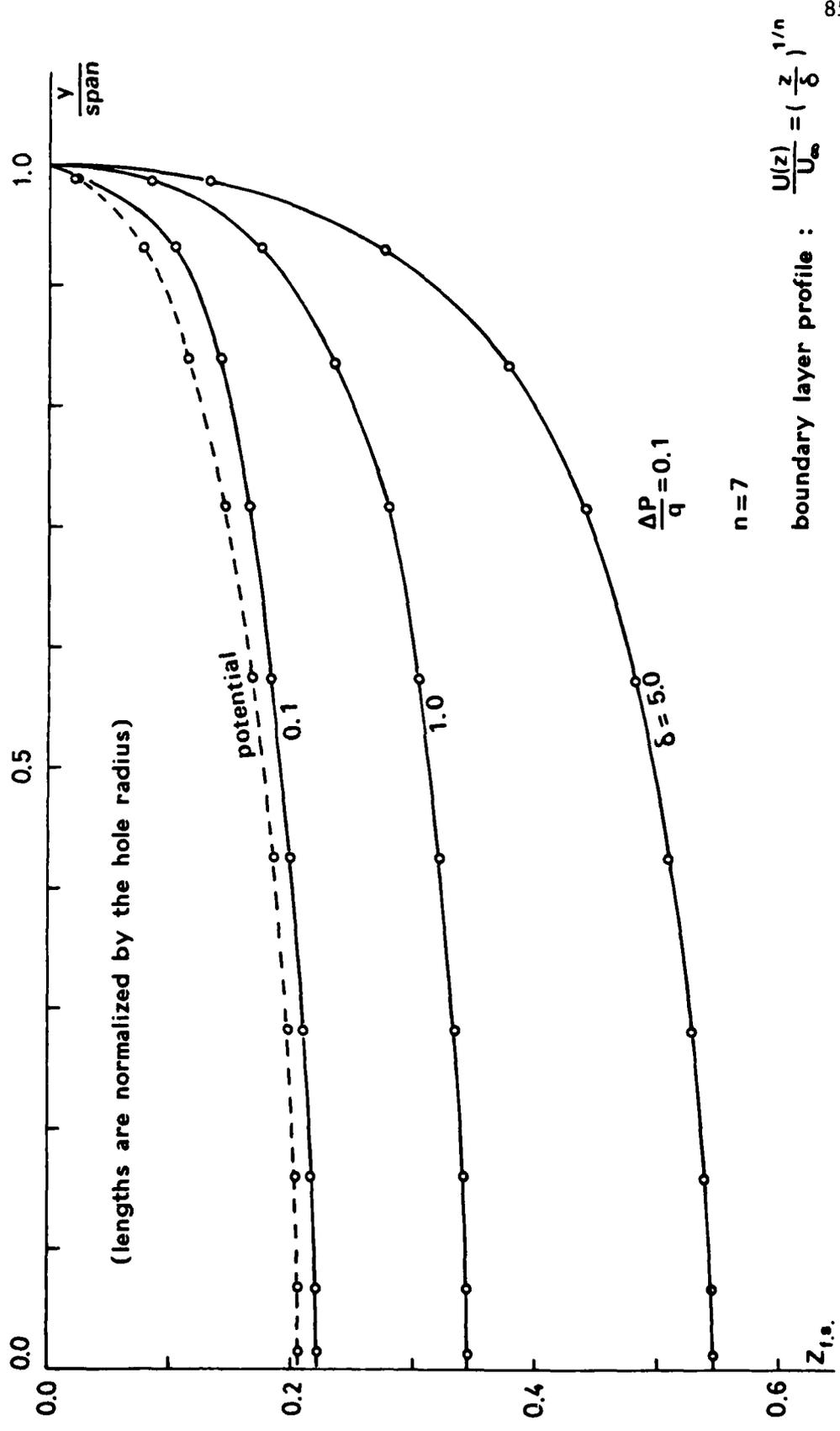Fig.(3-30) Volume flowrate versus boundary layer thickness for a round hole in a shear flow.

$$\frac{U(z)}{U_\infty} = \left(\frac{z}{\delta}\right)^{1/n}$$

boundary layer profile :

$\frac{\Delta P}{q} = 0.1$

$n = 7$

$\delta = 5.0$

1.0

0.1

potential

(lengths are normalized by the hole radius)

Fig.(3-31) Free surface deflection height along the trailing edge of a round hole in a shear flow.

ROUND HOLE

$\dfrac{\Delta P}{q} = 1$

$n = 7$

boundary layer profile : $\quad \dfrac{U(z)}{U_{\infty}} = \left(\dfrac{z}{\delta}\right)^{1/n}$

$Z_{f.s._{max}}$

δ

(lengths are normalized by the hole radius)
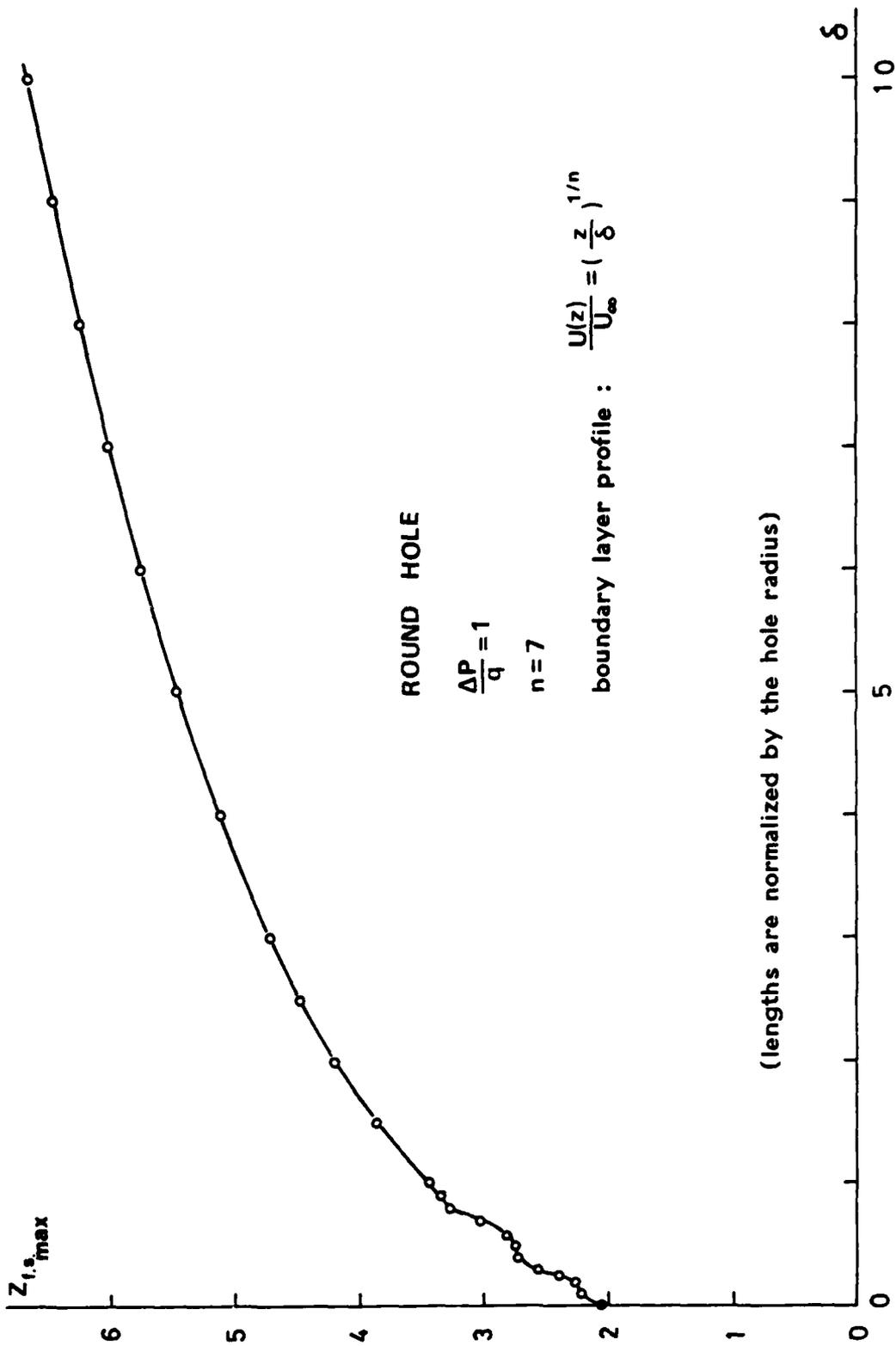
Fig.(3-32) Maximum free surface deflection of a shear flow over a round hole.

D.B.B. ANALYTICAL SHAPE (B/A=1)

boundary layer profile : $\dfrac{U(z)}{U_\infty} = (\dfrac{z}{\delta})^{1/n}$

n = 7

3D potential

$\delta = 0.1$
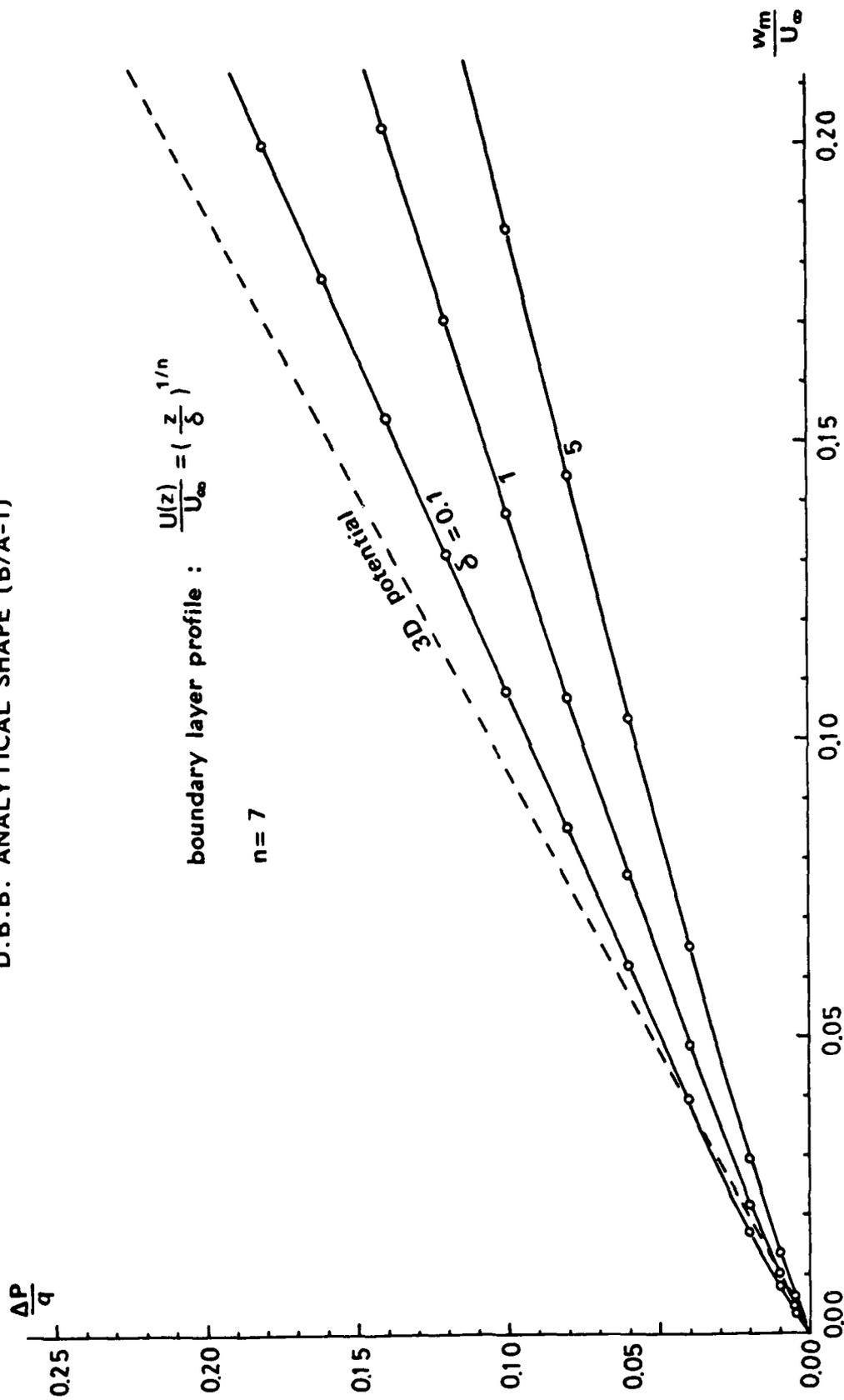
1

5

$\dfrac{w_m}{U_\infty}$

$\dfrac{\Delta P}{q}$

Fig.(3-33) Cross-flow characteristics of a shear flow over a D.B.B. hole with different boundary layer thicknesses.
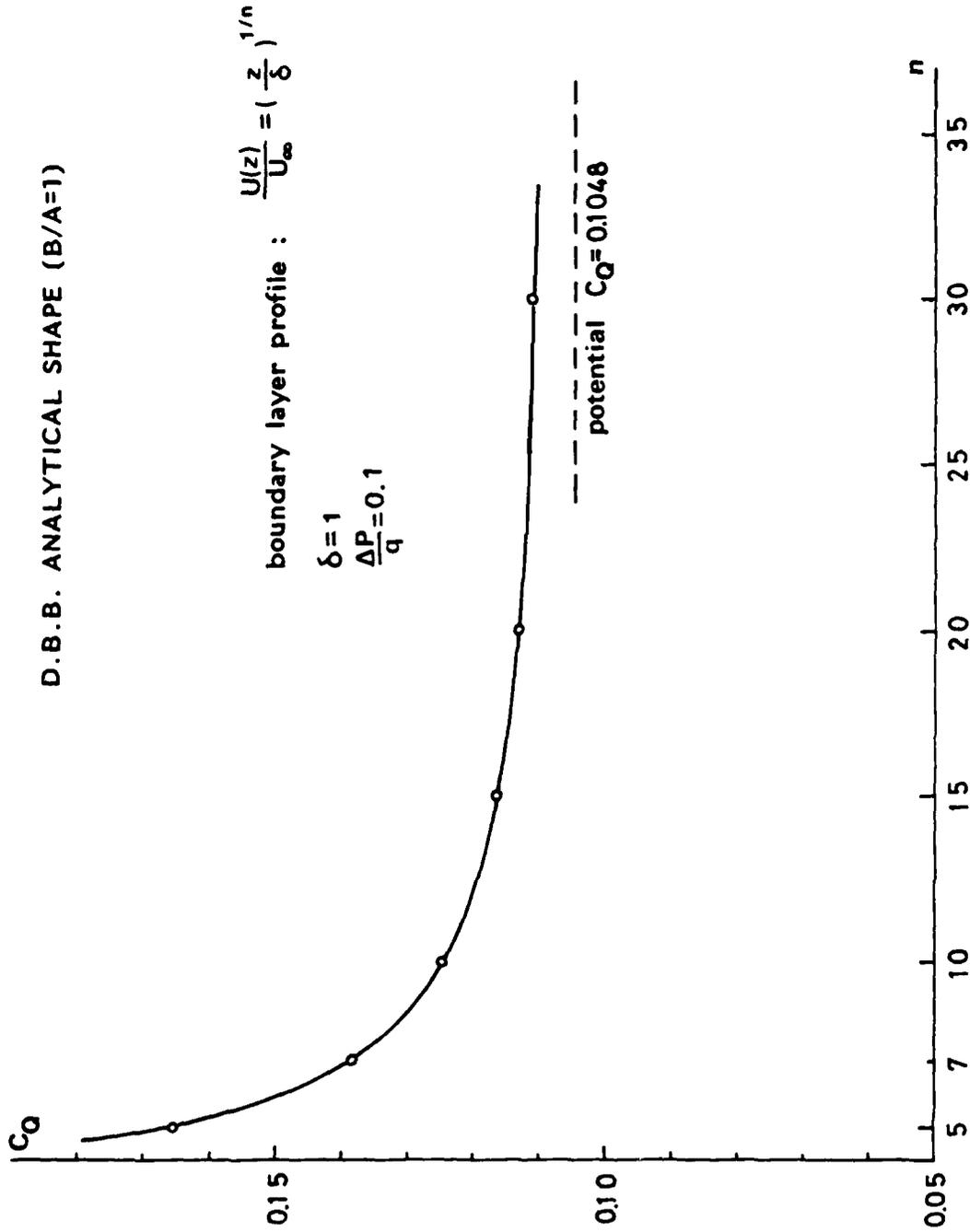
D.B.B. ANALYTICAL SHAPE (B/A=1)

boundary layer profile : $\frac{U(z)}{U_\infty} = \left(\frac{z}{\delta}\right)^{1/n}$

$\delta = 1$

$\frac{\Delta P}{q} = 0.1$

— — — potential $C_Q = 0.1048$

C_Q

0.15

0.10

0.05

5   7   10   15   20   25   30   35 n

Fig.(3-34) Volume flowrate across a D.B.B. hole in a power-law profile shear flow.

D.B.B. ANALYTICAL SHAPE (B/A=1)

boundary layer profile : $\dfrac{U(z)}{U_\infty} = (\dfrac{z}{\delta})^{1/n}$
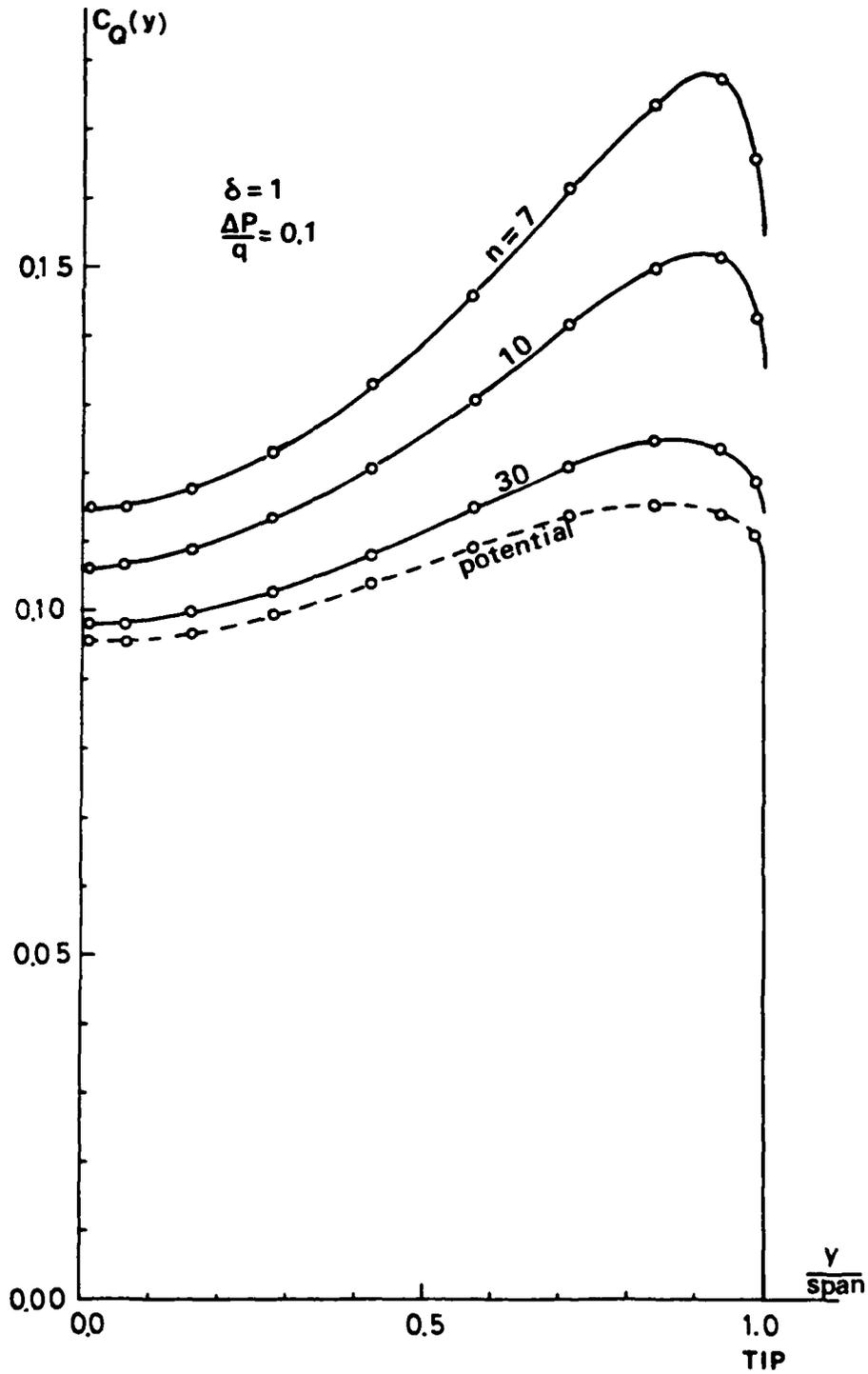

Fig.(3-35) Sectional volume flowrate distributions for a D.B.B. hole in shear flows.
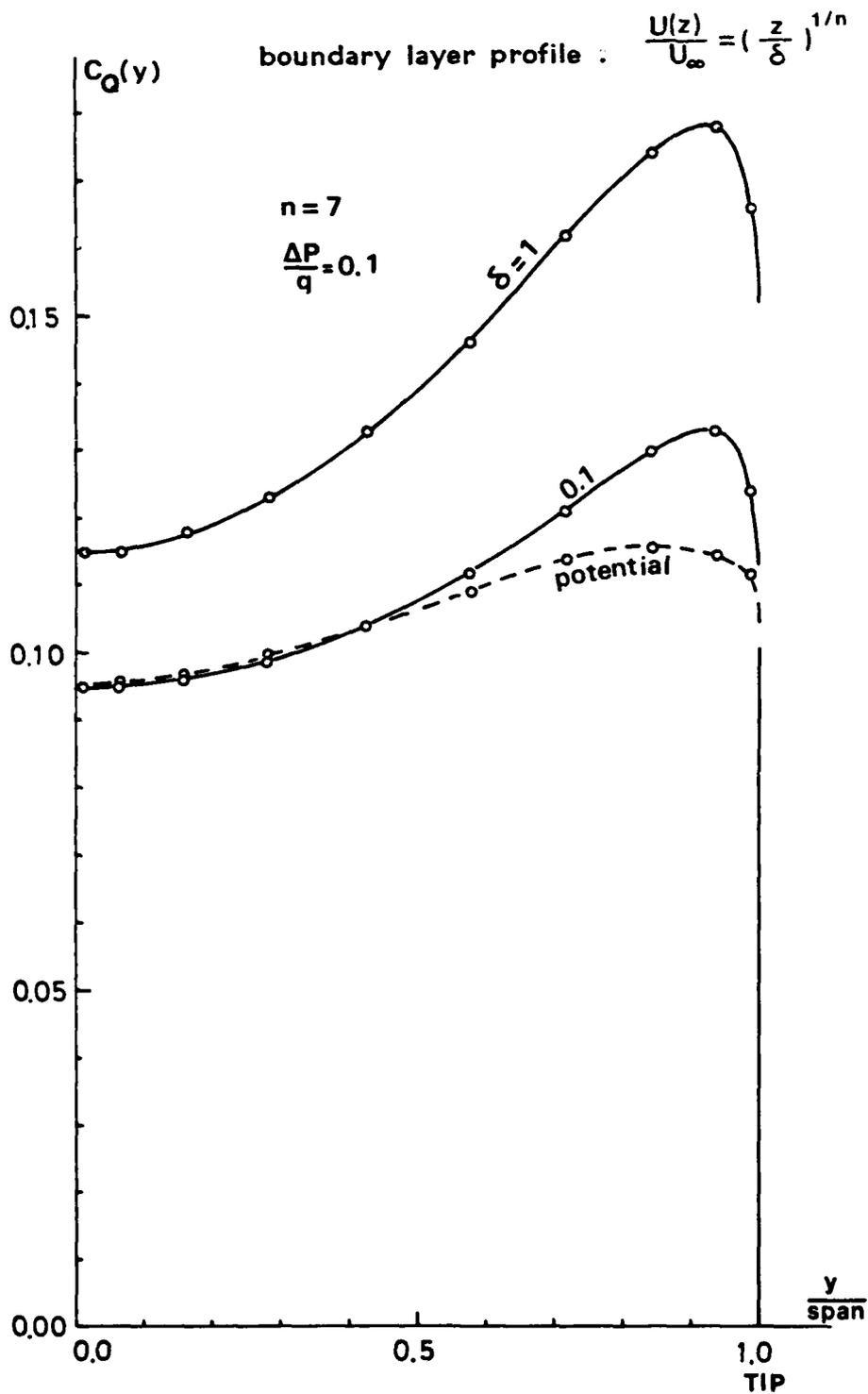
D.B.B. ANALYTICAL SHAPE (B/A=1)

boundary layer profile : $\dfrac{U(z)}{U_\infty} = (\dfrac{z}{\delta})^{1/n}$

$C_Q(y)$

$n = 7$

$\dfrac{\Delta P}{q} = 0.1$

$\delta = 1$

0.1

potential

0.15

0.10

0.05

0.00

$\dfrac{y}{span}$

0.0   0.5   1.0
TIP

Fig.(3-36) Sectional volume flowrate distributions for a D.B.B. hole in shear flows with different boundary layer thicknesses.

D.B.B. ANALYTICAL SHAPE (B/A=1)

n=7

$\frac{\Delta P}{q}=0.1$

boundary layer profile : $\frac{U(z)}{U_\infty} = \left(\frac{z}{\delta} \right)^{1/n}$
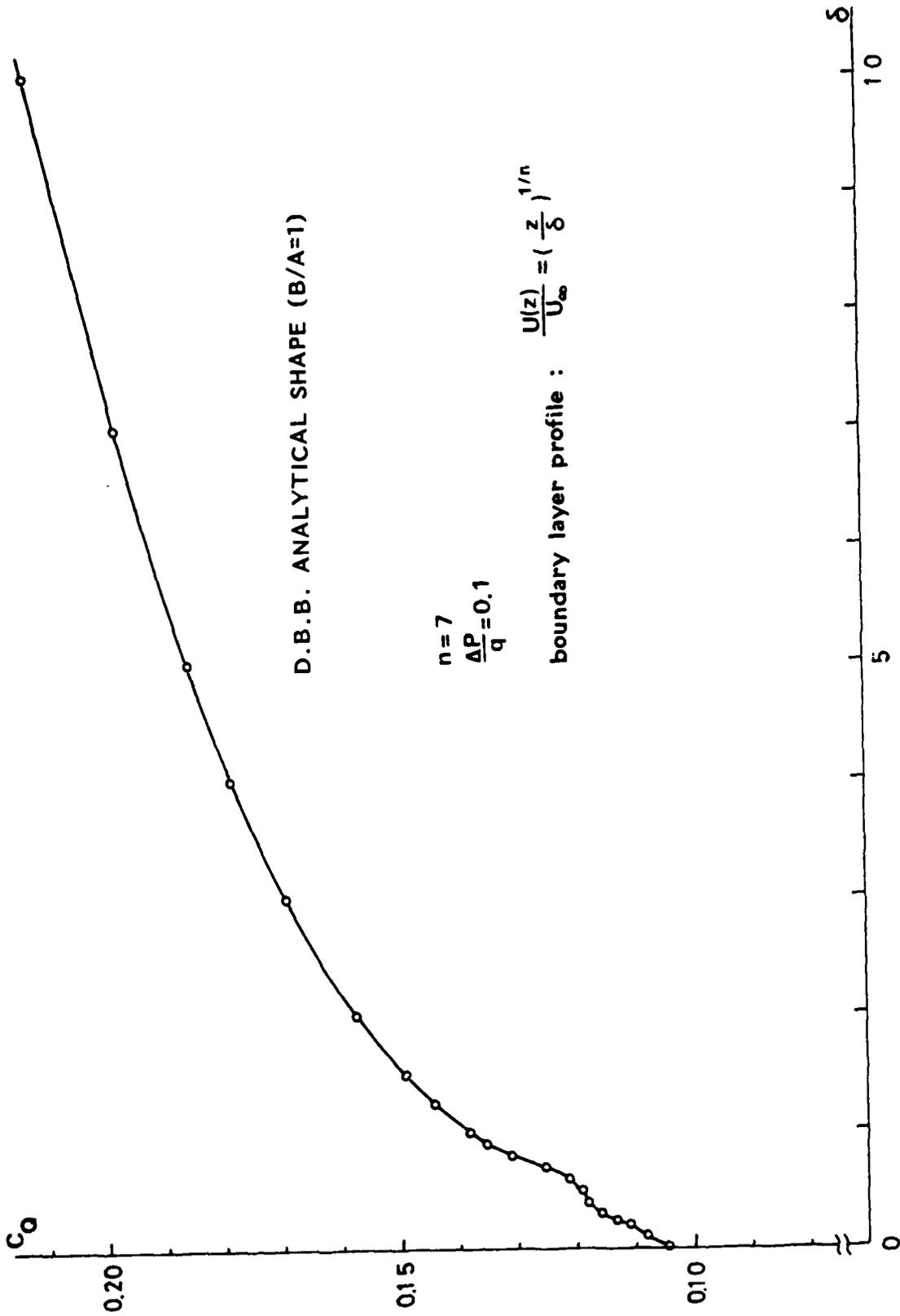
Fig.(3-37) Volume flowrate versus boundary layer thickness for a D.B.B. hole in shear flow.

END

FILMED

4-85

DTIC